AD-A071 029 O'DONNELL AND ASSOCIATES INC PITTSBURGH PA F/G 13/7
HYPERVELOCITY WIND TUNNEL COMPONENTS STRUCTURAL EVALUATION, VOL--ETC(U)
MAY 79 D PETERSON, E WESTERMANN N60921-78-C-0013
UNCLASSIFIED ODAI-1270-8-79-VOL-1 NL

1 OF 2
AD A071029

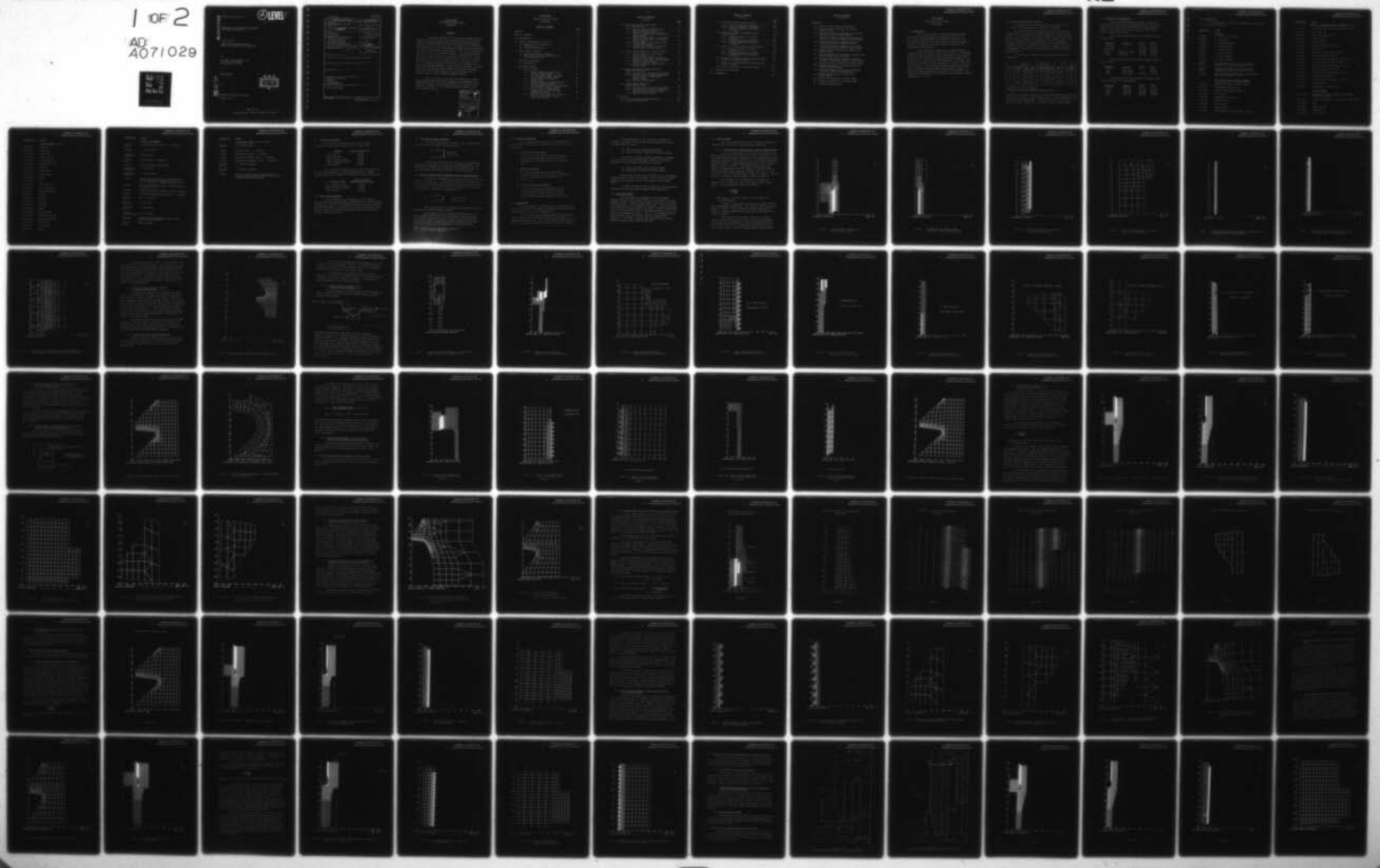

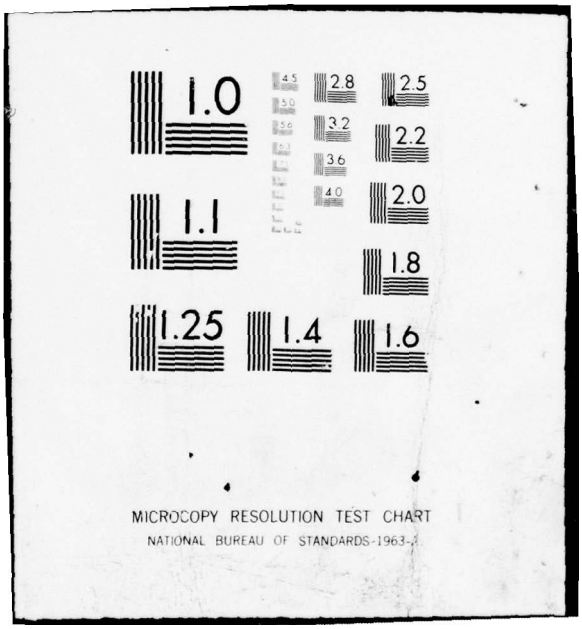
1.0
1.1
1.25
1.4
1.6
2.8
2.5
3.2
2.2
3.6
2.0
4.0
1.8
MICROCOPY RESOLUTION TEST CHART
NATIONAL BUREAU OF STANDARDS-1963-A

REPORT ODAI-1270-8-79

(2) LEVEL II

HYPERVELOCITY WIND TUNNEL COMPONENTS STRUCTURAL EVALUATION

Prepared for:

NAVAL SURFACE WEAPONS CENTER
WHITE OAK, SILVER SPRING, MARYLAND

By

O'DONNELL & ASSOCIATES, INC.
241 Curry Hollow Road
Pittsburgh, PA. 15236

FINAL REPORT

on

CONTRACT NO. N60921-78-C-0013

Volume 1 of 2

(May 1979)

SECURITY CLASSIFICATION OF THIS PAGE (When Data Entered)

REPORT DOCUMENTATION PAGE

READ INSTRUCTIONS BEFORE COMPLETING FORM

1 REPORT NUMBER: ODAI-1270-8-79 Vol-I	2 GOVT ACCESSION NO.
3 RECIPIENT'S CATALOG NUMBER: --	
4 TITLE (and Subtitle): Hypervelocity Wind Tunnel Components Structural Evaluation. Volume I.	5 TYPE OF REPORT & PERIOD COVERED: Final rept.
	6 PERFORMING ORG. REPORT NUMBER: --
7 AUTHOR(s): D. Peterson, E. Westermann	8 CONTRACT OR GRANT NUMBER(s): N60921-78-C-0013
9 PERFORMING ORGANIZATION NAME AND ADDRESS: O'Donnell & Associates, Inc. 241 Curry Hollow Road Pittsburgh, PA 15236	10 PROGRAM ELEMENT, PROJECT, TASK AREA & WORK UNIT NUMBERS: NIF
11 CONTROLLING OFFICE NAME AND ADDRESS: Naval Surface Weapons Center White Oak, Silver Spring, Md. 20910 Attn: Code CA-41	12 REPORT DATE: May 1979
	13 NUMBER OF PAGES: 540 (2 volumes)
14 MONITORING AGENCY NAME & ADDRESS (if different from Controlling Office): -- (12) 153 p.	15 SECURITY CLASS (of this report): Unclassified
	15a DECLASSIFICATION/DOWNGRADING SCHEDULE

16 DISTRIBUTION STATEMENT (of this Report)

Approved for public release; distribution unlimited

17 DISTRIBUTION STATEMENT (of the abstract entered in Block 20, if different from Report)

--

18 SUPPLEMENTARY NOTES

--

19 KEY WORDS (Continue on reverse side if necessary and identify by block number)

Wind Tunnel Components
Fatigue
High Pressure
Crack Propagation

20 ABSTRACT (Continue on reverse side if necessary and identify by block number)

See following page.

DD FORM 1 JAN 73 1473 EDITION OF 1 NOV 65 IS OBSOLETE

FINAL REPORT
HYPERVELOCITY WIND TUNNEL
COMPONENTS

ABSTRACT

A structural evaluation of the large threaded Pressure Vessels in the wind tunnel facility was performed using finite element techniques coupled with fatigue and fracture mechanics analyses of the critical locations. The results of this evaluation show that these threaded pressure vessels have limited fatigue life due to high stress concentrations at the root of the thread root radii in the threaded end closures. Design modifications were made to the most critical end closures (Bottom End of Mach 14/18 Heater Vessel and Inlet End of Driver Vessel) to increase the design life of these pressure vessels. The design life of all of the threaded pressure vessels was also increased by reducing the maximum pressure at which they are operated. Periodic inspection requirements which account for variable pressure cycling and mean stress effects were also developed for the critical areas of these threaded pressure vessels.

The net result of the design modifications, reduced operating pressures and periodic inspection requirements is to increase the design life and confidence in the safety related structural integrity of the threaded pressure vessels in the wind tunnel facility.

FINAL REPORT

HYPERVELOCITY WIND TUNNEL

COMPONENTS

TABLE OF CONTENTS

TABLE OF CONTENTS

(cont'd)

TABLE OF CONTENTS

(cont'd)

TABLE OF CONTENTS

(cont'd)

APPENDICES

FINAL REPORT

HYPERVELOCITY WIND TUNNEL COMPONENTS

1.0 INTRODUCTION

This report presents a safety-related structural evaluation of the Hypersonic Wind Tunnel facility at the U. S. Naval Ordnance Laboratory, White Oak, Maryland. The evaluation, based entirely upon pressure loading, consists of ductile bursting safety margins, fracture mechanics, and fatigue life computations.

Since the service conditions of the Wind Tunnel Components fall outside the range of applicability of the ASME Boiler and Pressure Vessel Code, determination of the adequacy of the design is based upon sound engineering judgment while maintaining the basic intent and methodology of the ASME Code. A detailed discussion of this procedure is covered in Section 3 of this report. The fatigue and fracture mechanics analyses were carried out using the ANSYS Finite Element Program. The bursting strength analysis was performed in accordance with guidelines established by the Pressure Vessel Research Committee (References 6, 7 & 8).

2.0 GENERAL DESCRIPTION OF FACILITY

The Hypersonic Wind Tunnel facility is located at the U. S. Naval Ordnance Laboratory in White Oak, Maryland.

The Wind Tunnel is a blowdown type using high pressure Nitrogen gas to achieve high Reynolds number flow. The facility consists of high pressure lines, boost compressor, storage vessel, heater vessel and valves. The heater vessel is used to bring the gas up to the final pressure requirements prior to blowdown. At the downstream end of the heater vessel is the diaphram/nozzle assembly. Flow is initiated in the system by rupture of a series of diaphrams. The flow rate is controlled by a bank of remotely operated valves.

The facility is designed for the following operating conditions:

Mach No.	Pressure			Mass Flow			Temp. °R	Re	Run Time Sec
	Design** ATM	Max. ATM	Min. ATM	Design PPS	Max. PPS	Min. PPS		Design* $x10^6$	
10	430	1000	100	337	780	80	1900	46	1.0
15	2365	3110	250	180	240	20	3300	30	1.0
20	3110	3110	500	27	27	4.5	5000	6.5	4.0

*Based on nozzle exit diameter

**Pressure used for aerodynamic design of nozzles

Presently, the facility consists of two test legs (Mach 10 and Mach 15). The test legs utilize a common storage vessel system, compressors, control valves and vacuum sphere. Each test leg has its own heater vessel and nozzle combination to achieve the desired Mach Number.

2.1 MATERIALS OF CONSTRUCTION

The heavy-walled threaded pressure vessels were constructed of high strength forged materials. Most of the forged vessel bodies and forged heads were constructed of modified AISI 4340 or "gun steel" similar to what is now known as ASTM A-723 material.

The material specifications for the manifolds are listed below:

Component	Material	S_u,psi	S_y,psi
Inlet Body	--	143,000	131,000
Exit Body	--	142,000	129,500
Studs	ASTM A193, GRB-7	125,000	105,000
Flange	AISI 4340	135,000	120,000

The material data for the MACH 10 Heater Vessel is listed below:

Component	Material	S_u,psi	S_y,psi
Nuts	Alloy Steel	--	100,000
Body	Alloy Steel	135,000	120,000

The material data for the MACH 14/18 Heater Vessel and Driver Vessel are listed below:

Component	Material	S_u,psi	S_y,psi
Covers	CR-NI-MO	145,000	130,000
Liner	CR-NI-MO	160,000	150,000
Body	CR-NI-MO	145,000	130,000

2.2 DRAWING LIST

The Hypervelocity Wind Tunnel components are described by the following drawings:

DRAWING NO.	TITLE
	MANIFOLD
4-01518	2 - Heater Inlet Pipes
4-01514	2 - Exit Nuts
4-01518	4 - Threaded Flanges
4-01511	4 - Blind Flanges
4-01511	4 - Blind Flanges
4-01514	1 - Exit Manifold
4-01513	4 - Inlet Closures
4-01515	1 - Inlet Manifold
4-01513, Rev. C	High Pressure Manifolds, Inlet Manifold - Assembly and Details, Sheet No. 3 of 9
4-01514, Rev. A	High Pressure Manifolds, Exit Manifold - Assembly and Details, Sheet No. 4 of 9
4-01518	High Pressure Manifolds, Mach 15 & 20 Heater Inlet Pipe, Sheet No. 8 of 9
	MACH 10 DIAPHRAGM & THROAT ASSEMBLY
77-F-1131	Diaphragm & Throat Assembly, Mach 10
77-B-1164	Thermocouple Tube, Mach 10
77-B-1163	Collar, Blowdown Pipe, Mach 10
77-B-1161	Pin, Mach 10
77-B-1160	Diaphragm Stud, Mach 10
77-B-1147	Bushing, Mach 10
77-B-1146	Stud, Mach 10
77-B-1145	Runner, Mach 10
77-C-1121	Flow Restrictor (Front Plate), Mach 10

DRAWING NO.	TITLE
	MACH 10 DIAPHRAGM & THROAT ASSEMBLY (cont'd)
77-C-1125	Butt Plate, Ring Particle Separator, Mach 10
77-C-1133	Elbow, Mach 10
77-C-1135	Burst Diaphragm, Mach 10
77-C-1148	Washer, Mach 10
77-C-1149	Spacer, Mach 10
77-C-1152	Triangle Backup Seal, Mach 10
77-C-1162	Plug, Mach 10
77-D-1110	Template, Nozzle Throat, Mach 10
77-D-1120	Thermocouple Ring, Mach 10
77-D-1122	Flow Restrictor (Backup Plate), Mach 10
77-D-1123	Separator Body (Upstream), Mach 10
77-D-1124	Separator Body (Downstream), Mach 10
77-D-1126	Particle Separator, Mach 10
77-D-1128	Housing Particle Separator, Mach 10
77-D-1129	Nozzle Throat, Mach 10
77-D-1139	Housing Particle Separator, Mach 10
77-D-1150	Tray, Mach 10
77-E-1130	Nozzle Throat Insert Carrier
	MACH 10 HEATER
E-PV-1793-6	Navy Mach 10 Vessel <494036>, Arrangement Drawing B-PV-1408-1
B-PV-1408-1	General Arrangement of Mach 10 Gas Heater Vessel
B-PV-1409	Body
B-PV-1411-1	Right End Head
B-PV-1420-1	Piston Block
B-PV-1422-1	Outer Housing

DRAWING NO.	TITLE
	MACH 10 HEATER (cont'd)
B-PV-1437	Support
E-PV-1426	Stop Block
E-PV-1427	Index Block
F-PV-1414-1	Gasket Carrier
F-PV-1415	Gasket Retainer
F-PV-1417-1	Nozzle Liner - M9
F-PV-1418	Flange
F-PV-1421-1	Bronze Shoe
F-PV-1424-4	Filler Piece
F-PV-1425-1	Spacer
F-PV-1428	Pin
F-PV-1429	Locating Block
F-PV-1430	Drive Sprocket #1
F-PV-1431	Drive Sprocket #5
F-PV-1432	Shim #2
F-PV-1433	Shim #7
F-PV-1434	Shim #8
F-PV-1435	Retainer
F-PV-1436-1	Wiper
C-PV-1410-2	Left End Head
C-PV-1412-1	Left End Main Nut
C-PV-1413	Right End Main Nut
C-PV-1416-1	Nozzle Tube
C-PV-1419	Nozzle Block
C-PV-1423	Piston

DRAWING NO.	TITLE
	MACH 14 & 18 HEATER
4-01266, Rev. H	Pressure Vessel Assembly, 2 - Required
4-01266, Rev. C	2 - Bottom Nuts
4-01266-E & 4-01424-D	Bottom Covers
4-01181, Ref. F	Vessel Body, 2 - Required
1-01155	Round Bar Upset Threaded Rods
4-00673-H & 4-01135-C	3 - Top Covers
4-00673-H & 4-01136-A	3 - Bottom Covers
I-3110	Grayloc Flanged Applications, Schematic of 16-3/8" O.D. Thrd. Flange Conn. for 7-1/4" O.D. x 2-11/16" I.D. Tube with Size 27 G.S.R.
Q-4964	Grayloc Ring Seat Fittings, Machining Details for Size 27 G.R.S.
1-01440	Connector Tube Modification, Item 05, 2 Tubes
1-01425	2" Diameter 8UN-2A Hex Head Bolt, 8 - Required
1-01031, Rev. A	Nut, 2 - Required
4-00673, Rev. H	3 - Top Nuts
4-00673-A, Rev. H	3 - Bottom Nuts
4-01359 Sht.1B&4-01360	2 - Top Covers
4-01424, Rev. D	Electrode & Thermocouple Locations & BTM Cover, Machining Details
4-01359, Rev. G	Elbow Assembly

DRAWING NO.	TITLE
	GAS STORAGE VESSEL (Driver Vessel)
4-00673, Rev. I	Gas Storage Vessel
1-00691	Top Outer Ring, 3 - Required
1-00690	Bottom Outer Ring, 3 - Required
4-01135	Top Cover Assembly, West, 3 - Required
4-01136	Bottom Cover Assembly, East, 3 - Required
4-01136, Rev. E	3 - Liners & Sleeves
4-01135, Rev. F	3 - Liners & Sleeves
4-00766	Detail of Final Undercut Machining for 1" Pitch N Buttress Internal Thd. (Also applies to MACH 14/18 Heater Vessel)

2.3 OPERATING CONDITIONS

The Internal Design Pressures for the original Hypervelocity Wind Tunnel Components are listed below:

Component	Design Pressure, psi
Exit Manifold	46,000
Inlet Manifold	60,000
MACH 10 Heater Vessel	15,000
MACH 14/18 Heater Vessel	46,000
Driver Vessel	60,000

The structural evaluation given herein indicates that the operating pressure for these threaded pressure vessels should be reduced and limited to the maximum values listed below:

Pressure Vessel	Maximum Internal Operating Pressure, psi
MACH 10 Heater Vessel	12,000
MACH 14/18 Heater Vessel	22,000
Driver Vessel	40,000

3.0 BASIC STRESS CRITERIA

In its present form, the ASME Boiler and Pressure Vessel Code contains disclaimers for application to high pressures. In addition, only Code-listed materials may be used in conjunction with the Code Rules. This material list does not include a small group of materials which are extensively used in high pressure design, such as gun steels.

3.1 CODE DESIGN STRESS INTENSITY

The basic design stress intensity, S_m, is specified by the Code to be the lesser of the following:

$$\left.\begin{array}{l} S_m \leq \text{UTS}^*/3 \\ \text{or} \\ S_m \leq 2/3\ \text{YS}^* \end{array}\right\} \text{ASME Code Limits on } S_m$$

For the gun steels UTS is on the order of 140,000 psi, and YS is on the order of 125,000 psi at room temperature. The Code Rules on design stress intensity would therefore limit S_m to on the order of 45,000 psi (UTS/3) for the gun steels.

3.2 MODIFIED DESIGN STRESS INTENSITY FOR HIGH YIELD MATERIALS

Reference 4 recommends that only the limit, $S_m \leq 2/3$ YS, be used to define S_m. In keeping with the basic intent of the Code, in particular the Code-intended safety margins under hydrotest conditions the following limits on design stress intensity are suggested by O'Donnell & Associates, Inc.

$$\left.\begin{array}{l} S_m \leq \text{UTS}/2 \\ \text{or} \\ S_m \leq 2/3\ \text{YS} \end{array}\right\} \text{ODAI Suggested Limits on } S_m$$

These limits result in a design stress intensity for the gun steels of about 70,000 psi (UTS/2).

The suggested limits on design stress intensity, S_m, are considered justifiable for high pressure vessels operated under safety conditions typically observed during hydrotesting of pressure vessels, subjected to detailed fatigue and fracture mechanics evaluations, and inspected at suitable intervals.

---

*UTS = ultimate tensile strength of material.
YS = yield strength of material.

4.0 EVALUATION PROCEDURE

The evaluation was performed in accordance with state-of-the-art technology as described in the criteria outlined below:

(a) Primary Stress Evaluation

The basic wall thicknesses and primary stress values were evaluated by the design criteria established by the ASME as given in References 1 and 2.

(b) Fatigue Evaluation

The fatigue design life was determined in accordance with the rules as given in Reference 3. Material fatigue data was obtained from Reference 4.

(c) Fracture Mechanics Evaluation

The cyclic life of the threaded portion of these pressure vessels for various initial defect depths and cyclic stress levels was evaluated using fracture mechanics techniques.

4.1 ASSUMPTIONS

The technology is well developed for evaluating the safe operating life of threaded closures where the materials of construction have been well characterized.

The friction forces between mating threads have been found to dissipate as threaded closures are subjected to repeated pressurizations. Thus, the effects of such friction forces are quite small after the first few cycles of operation.

The acceptability of the following threaded end closures was based on calculations which assumed there was no friction between threads:

(a) MACH 10 Heater Vessel End Closures
(b) Top End Closure on MACH 14/18 Heater Closure

The effect of friction between threads was included in the typical detailed thread model without an elliptical undercut for the following threaded end closures:

(a) Inlet and Outlet Ends of Driver Vessel
(b) Bottom End of MACH 14/18 Heater Vessel

Notice that friction was included only in the detailed thread models for these end closures. No friction was assumed between mating threads in all of the overall finite element models.

No thermal conditions were considered in the structural evaluation of the wind tunnel components (See Appendix 9).

5.0 ANALYTICAL MODELS

For the purpose of analysis by digital computer methods, several finite element models were developed for these pressure vessels. Overall closure models were used to calculate the thread loads in the threaded end closures. A detailed model of one thread was then prepared and used to calculate the maximum stress in the thread root due to the maximum thread load on each particular threaded end closure. Most of the computer analyses were performed using the digital computer program ANSYS, Reference 5. The other analyses were performed using special computer programs and/or hand calculations.

5.1 MACH 10 MODELS

The finite element models used to analyze the MACH 10 components are described in the following subsections.

5.1.1 OVERALL MODEL FOR RIGHT END OF MACH 10 HEATER VESSEL

A finite element model of the right end closure on the MACH 10 Heater Vessel was prepared and used in conjunction with the ANSYS computer program, Reference 5, to calculate the maximum loads and stresses in this closure due to the internal operating pressure loading. A computer-drawn scale plot of this overall model is shown in Figure 1. This model contains many axi-symmetric Isoparametric (STIF42) elements. The model consists of three separate parts--the main cylinder body, the nut, and the cover. The main cylinder body is shown in Figure 2. The nut is shown in Figure 3, and the cover is shown in Figure 4.

The cylinder part was modeled to a distance of approximately $\pi\lambda$ beyond the end of the taper on the cylinder, where λ is the attenuation length (see Figure 2):

$$\lambda = \frac{\sqrt{R_{mean}\, t}}{1.285}$$

where R_{mean} is the mean radius of the cylinder, and
t is the thickness.

As shown in the Figures, the nut and cylinder threads have been modeled individually. The cylinder threads alone are shown in Figure 5. The nut threads are shown separately in Figure 6. Typical meshing of the nut and cylinder threads is shown in Figure 7.

The mating pairs of nodes at the nut to cylinder thread interface are specified to have the same displacements in the direction perpendicular to the thread tooth surface. This allows the load to be transmitted from one thread tooth to the other with no sliding friction between mating threads.

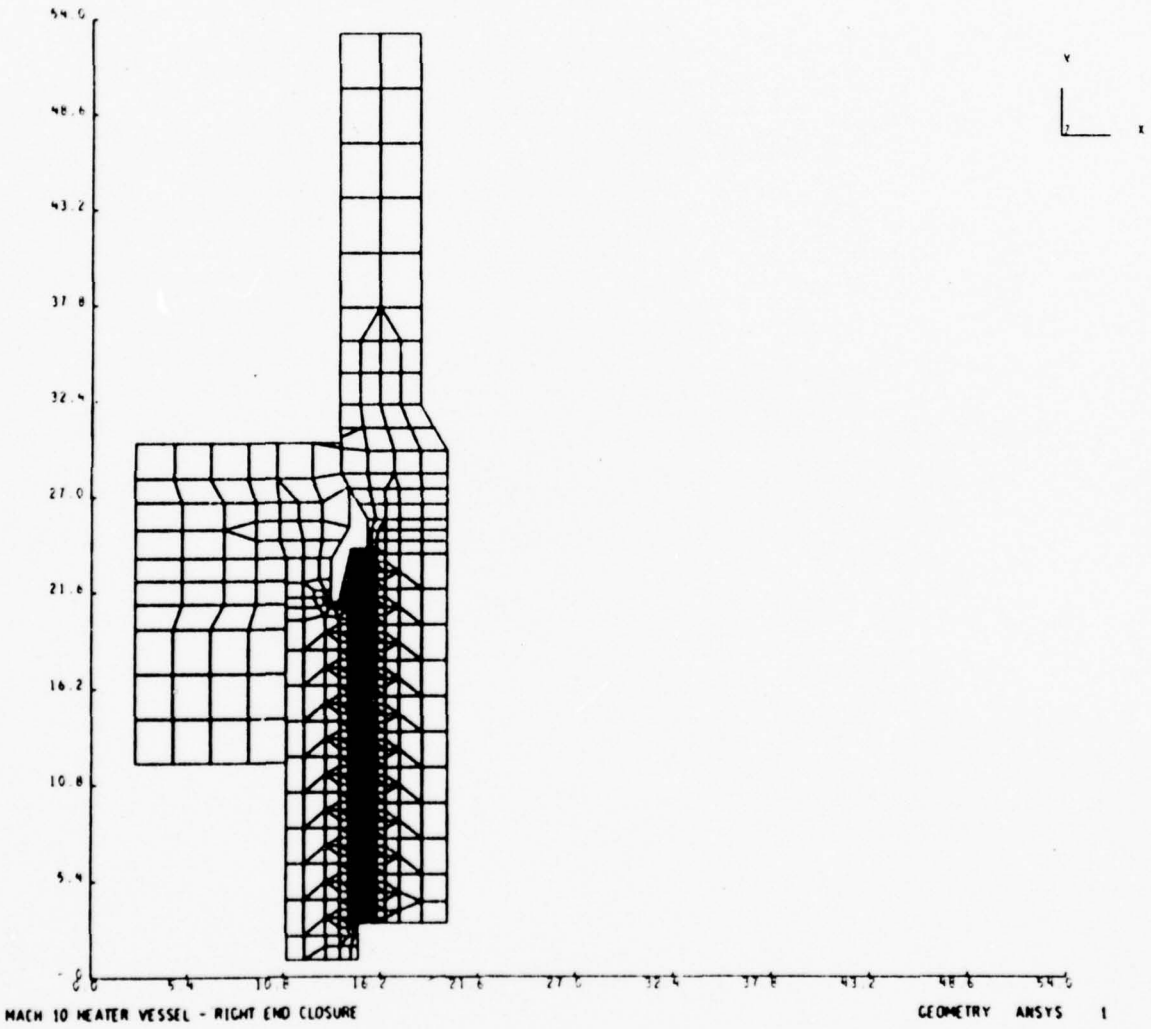

FIGURE 1 - OVERALL MODEL - RIGHT END OF MACH 10 HEATER VESSEL

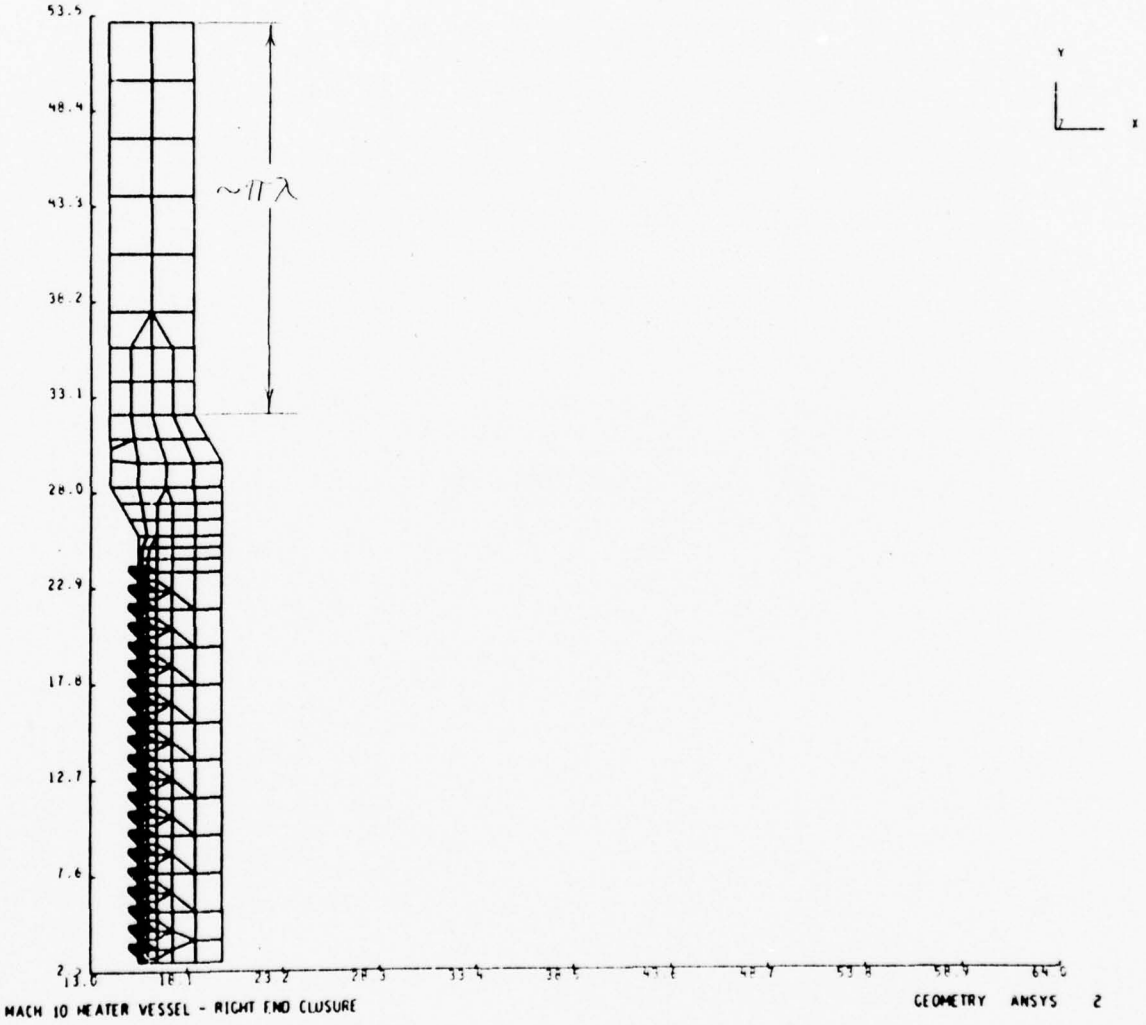

FIGURE 2 - CYLINDER PART OF OVERALL MODEL - RIGHT END OF MACH 10 HEATER VESSEL

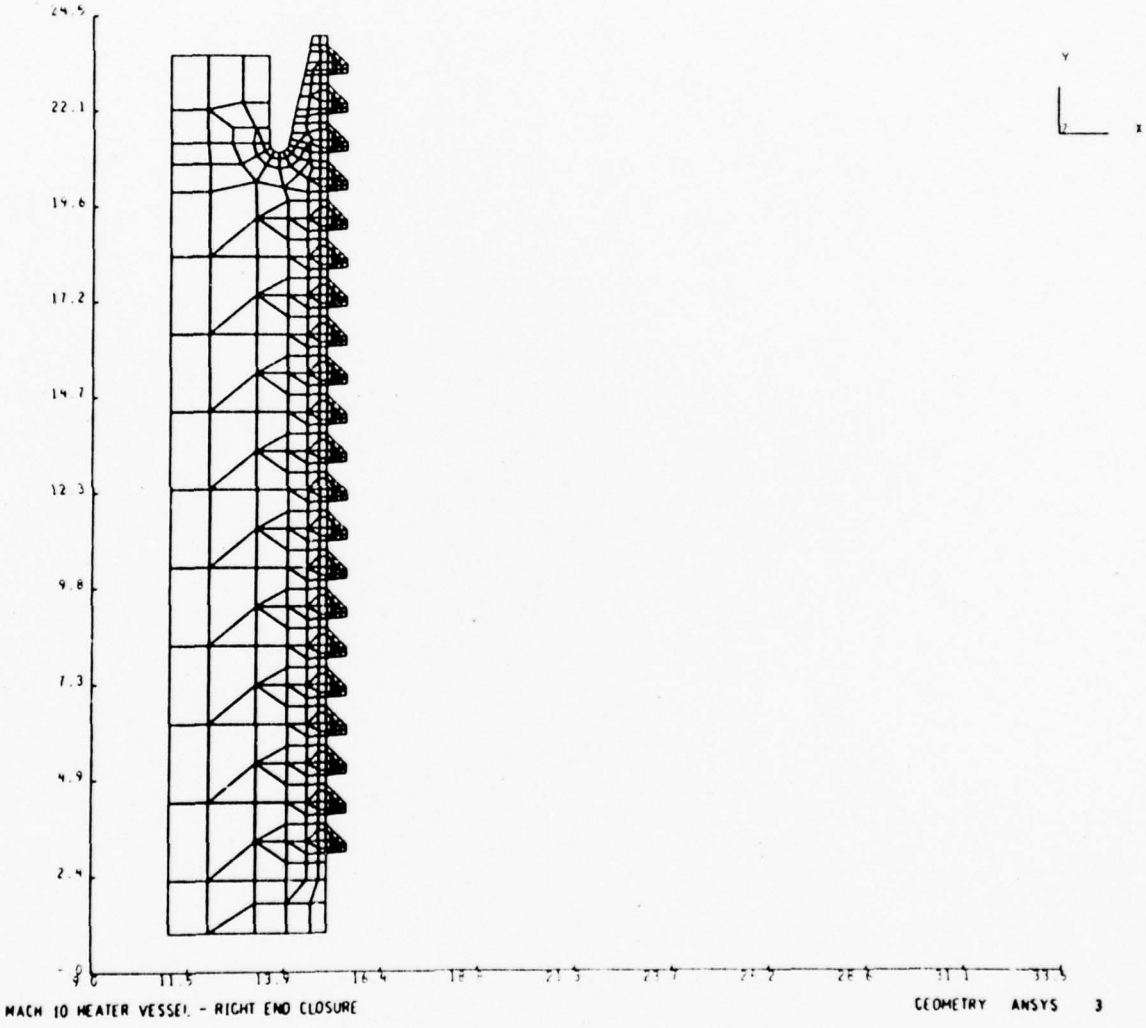

FIGURE 3 - NUT ON OVERALL MODEL - RIGHT END OF MACH 10 HEATER VESSEL

FIGURE 4 - COVER ON OVERALL MODEL - RIGHT END OF MACH 10 HEATER VESSEL

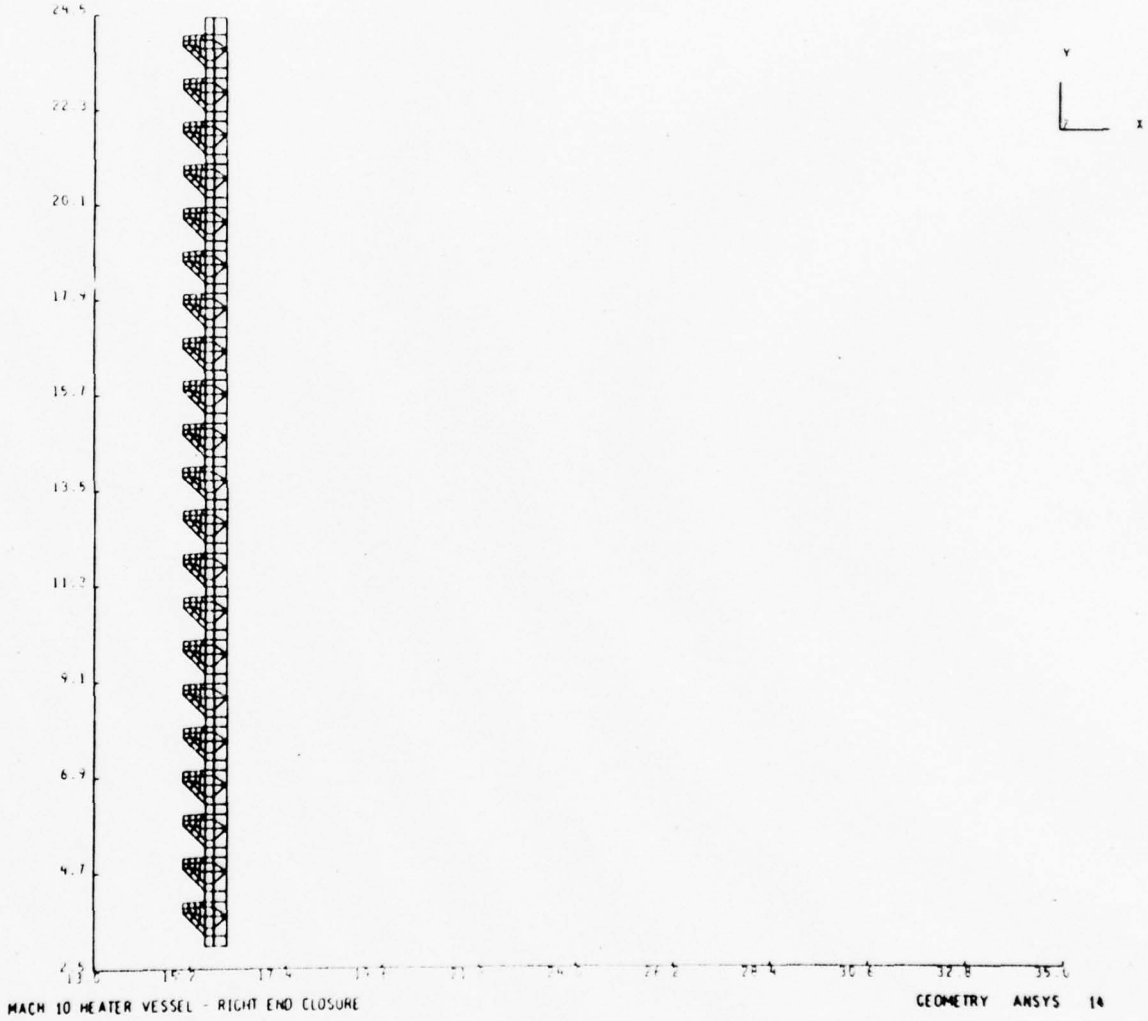

FIGURE 5 - THREADED PORTION OF MAIN CYLINDER ON OVERALL MODEL - RIGHT END OF MACH 10 HEATER VESSEL

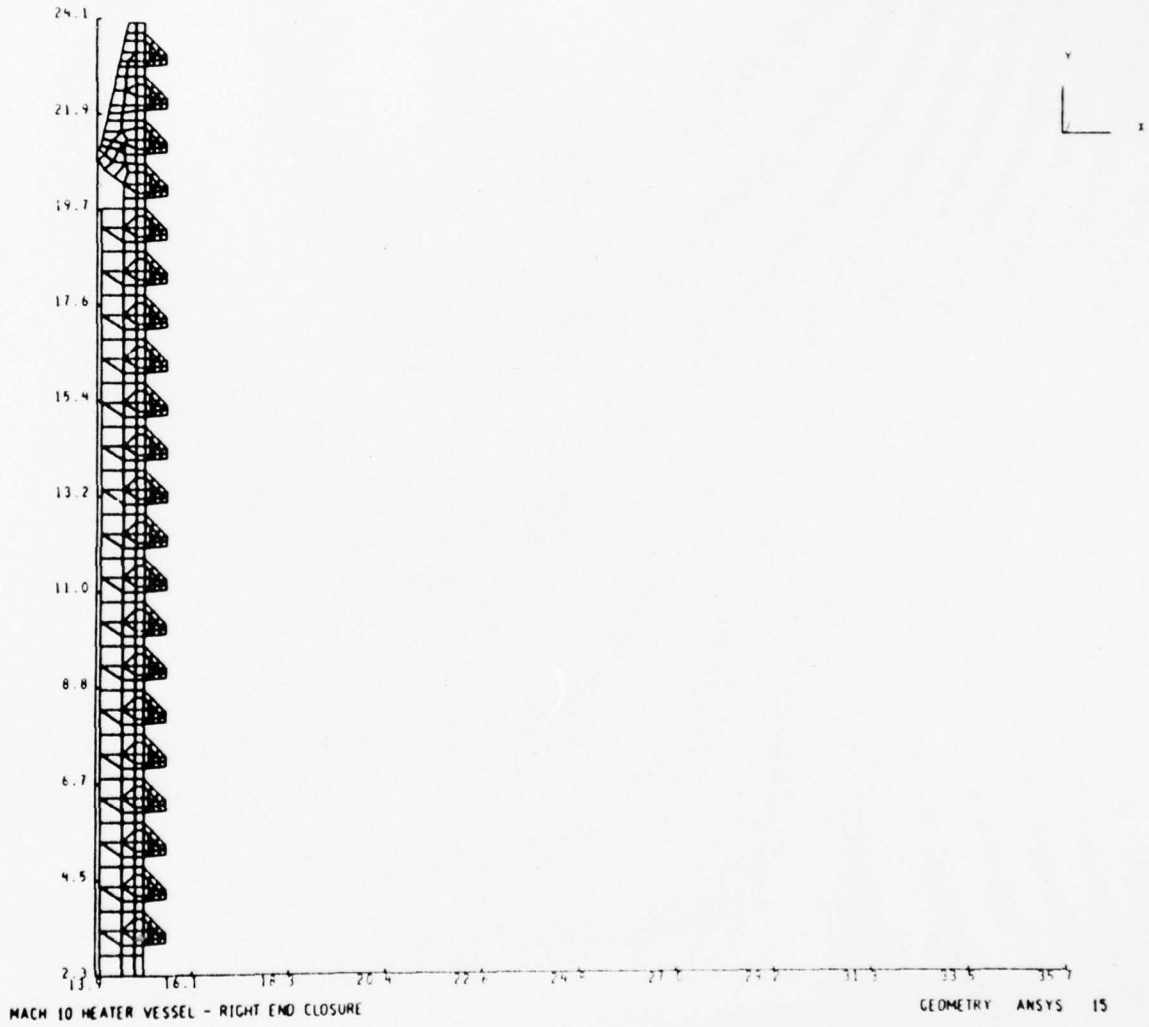

FIGURE 6 - THREADED PORTION OF NUT ON OVERALL MODEL - RIGHT END OF MACH 10 HEATER VESSEL

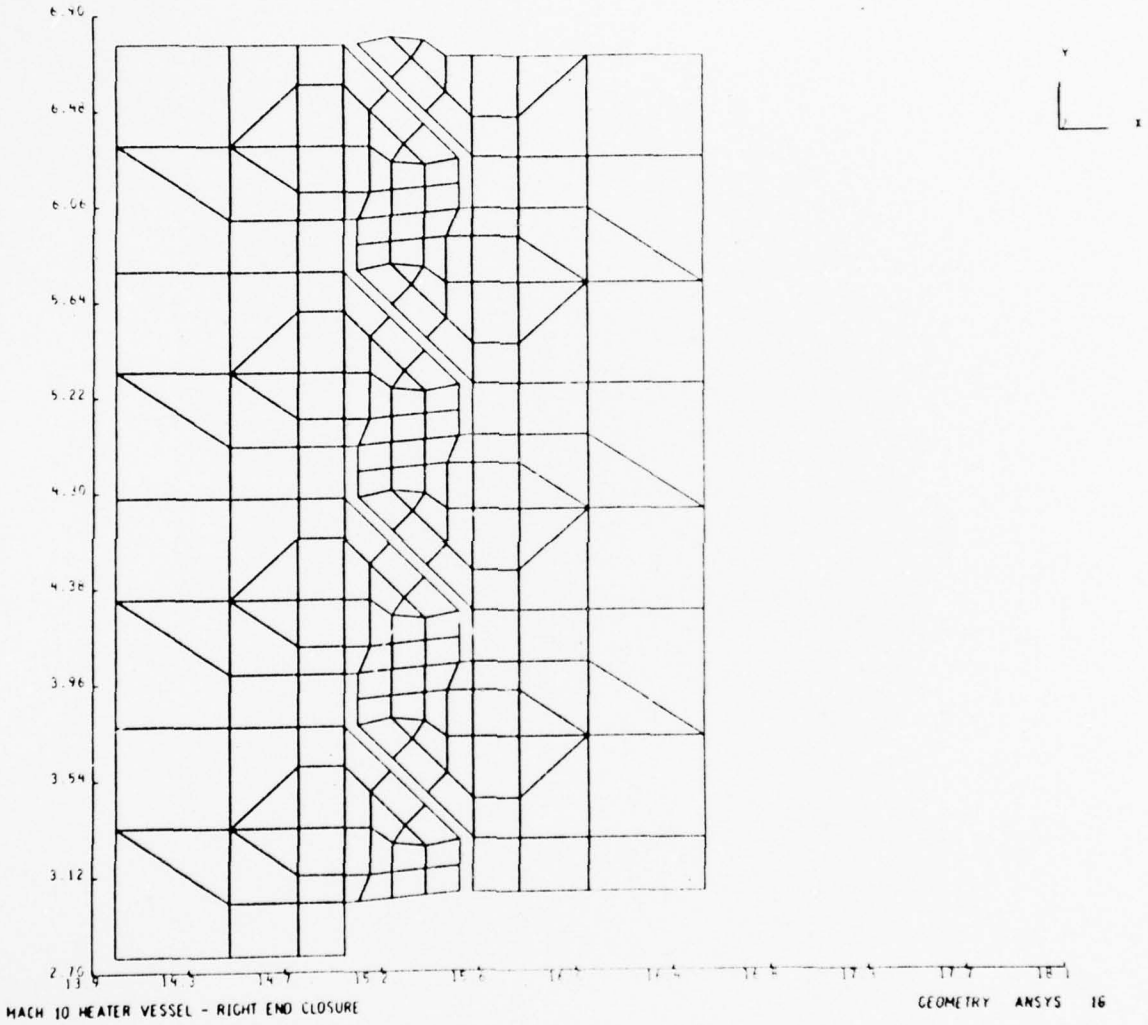

FIGURE 7 - MESHING OF FIRST THREE NUT AND CYLINDER THREADS ON OVERALL MODEL - RIGHT END OF MACH 10 HEATER VESSEL

An internal pressure of 15,000 psi was applied to the inside surfaces of the overall model. The load on each of the individual threads was then obtained from the computer results. The resulting maximum thread load was then converted into an equivalent uniform load and applied to the tooth surface on the detailed thread model. In addition, displacements from the overall model in the vicinity of the thread where the maximum thread load occurs were applied as boundary conditions on the edges of the detailed model.

5.1.2 DETAILED THREAD MODEL FOR RIGHT END OF MACH 10 HEATER VESSEL

A computer-drawn scale plot of the detailed thread model for the threads on the right end closure of the MACH 10 Heater Vessel is shown in Figure 8. This model is made up of many axisymmetric Isoparametric (STIF42) elements. The maximum thread load on the overall model was converted into an equivalent pressure load and applied to the tooth surface on the detailed thread model (see Appendix 2B). The displacements from the overall model in the vicinity of the thread where the maximum thread load occurs were applied as boundary conditions on the edges of this detailed model.

This detailed model was used to calculate the maximum stresses in the thread root for the right end closure. The maximum thread load on the right end closure was applied to this model, and the resulting maximum stress at the thread root was calculated using the ANSYS computer program.

5.1.3 OVERALL MODEL FOR MACH 10 NOZZLE AREA

The MACH 10 Nozzle assembly consists of three major threaded closures. These are: (1) Heater Body/Left End Main Nut, (2) Heater Body/Outer Housing, and (3) Nozzle Block/ Piston Block.

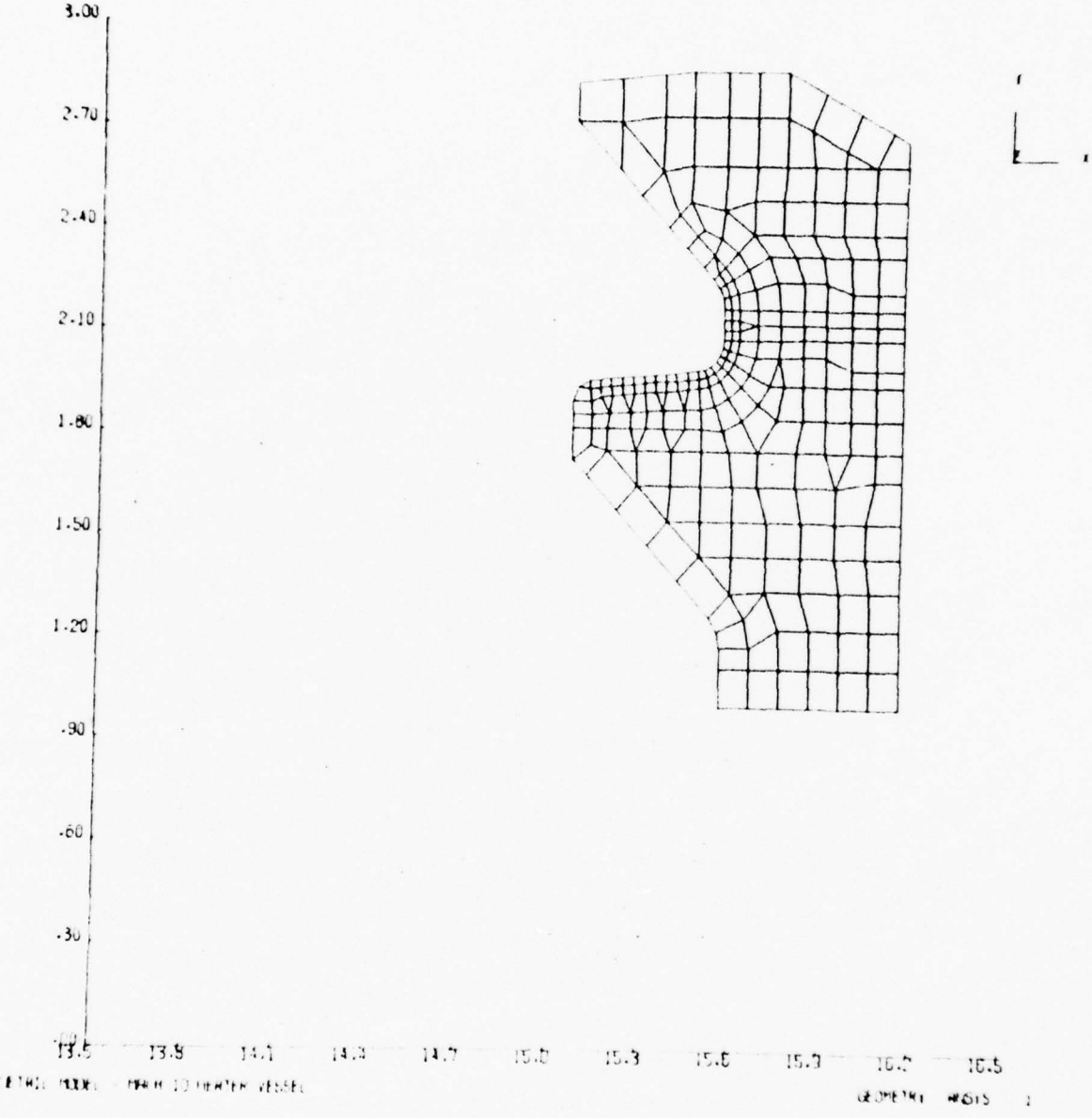

FIGURE 8 - DETAILED THREAD MODEL FOR MACH 10 HEATER VESSEL

The worst loading condition was determined to be prior to rupture of the diaphragms. At this time, the closures are loaded by 15,000 psi internal pressure, as well as a 4,000 psi preload pressure applied by the piston block.

To determine the load paths through the various components, a course finite element model of the entire area was utilized. This model is shown in Figure 9. It includes the major components of the M10 Nozzle Assembly.

5.1.4 OVERALL MODEL FOR DOWNSTREAM END OF MACH 10 HEATER VESSEL

The configuration of the downstream end of the MACH 10 Heater is shown below along with the imposed loading obtained from the overall model.

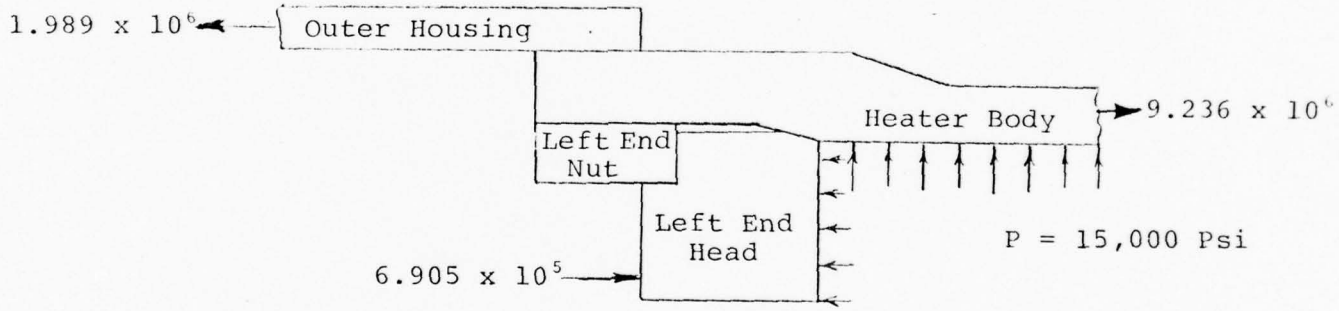

Before Rupture

The ANSYS finite element model for this area is shown in Figures 10 through 18. The model consists of 1985 Isoparametric (STIF42) elements. The threaded connections between the Heater Body and Outer Housing and between the Heater Body and Left End Nut are modeled by 27 element teeth shown in Figures 10 through 18. The nodes common between mating threads were coupled together if they were found to be in compression and let free if they were in tension. Only the normal direction was coupled, and the nodes were free to slide tangentially. No friction was assumed between threads.

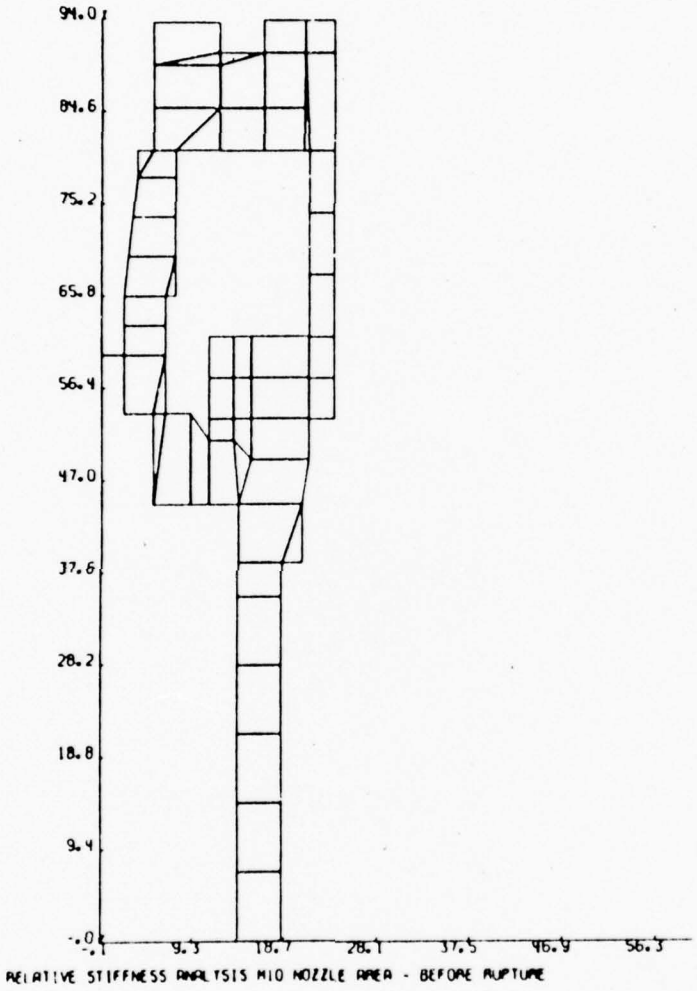

FIGURE 9 - ANSYS FINITE ELEMENT MODEL - M10 NOZZLE AREA
COARSE MODEL OF ENTIRE NOZZLE AREA

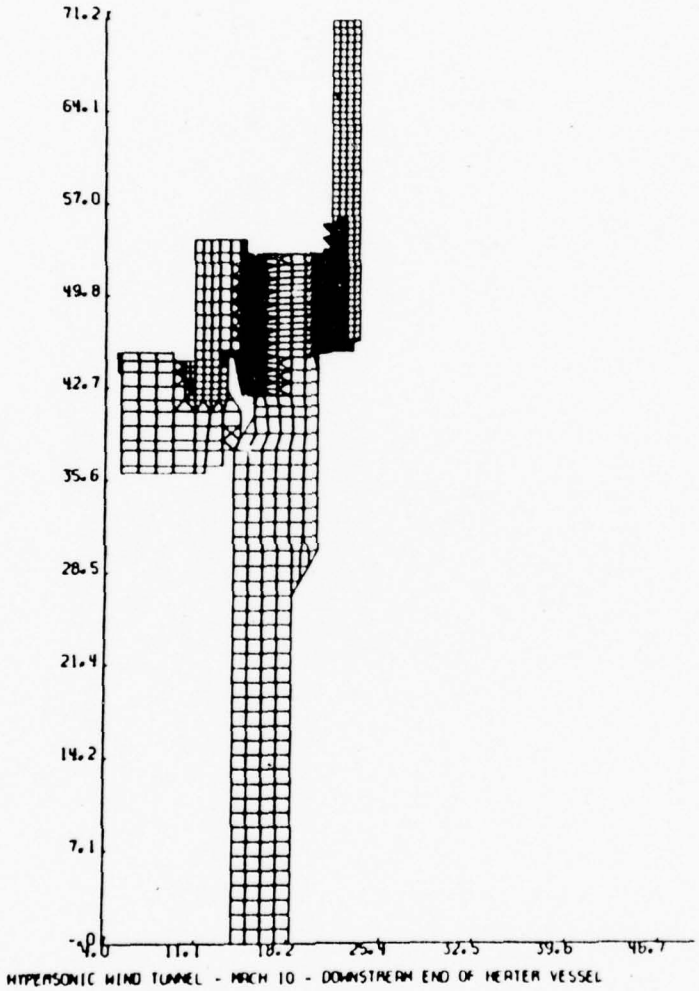

FIGURE 10 - ANSYS FINITE ELEMENT MODEL - DOWNSTREAM END OF HEATER VESSEL

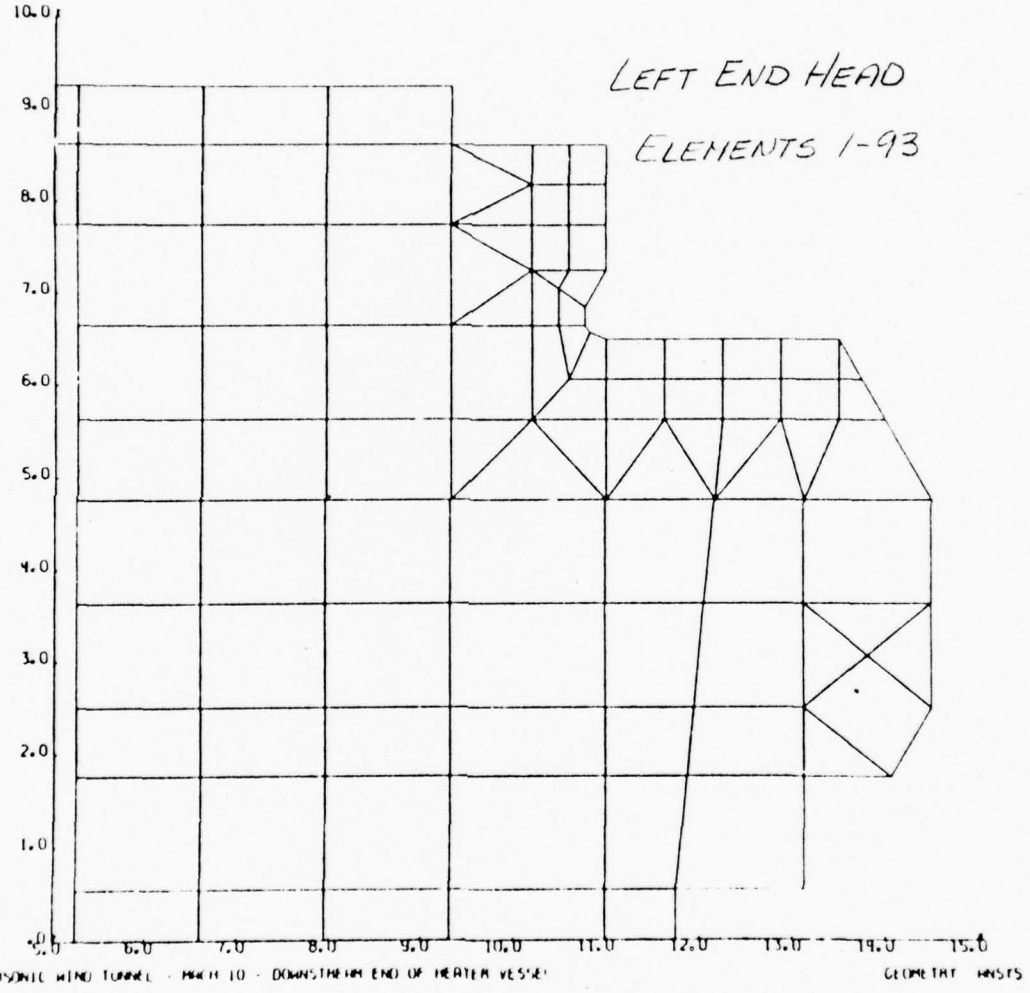

FIGURE 11 - ANSYS FINITE ELEMENT MODEL -
DOWNSTREAM END OF HEATER VESSEL

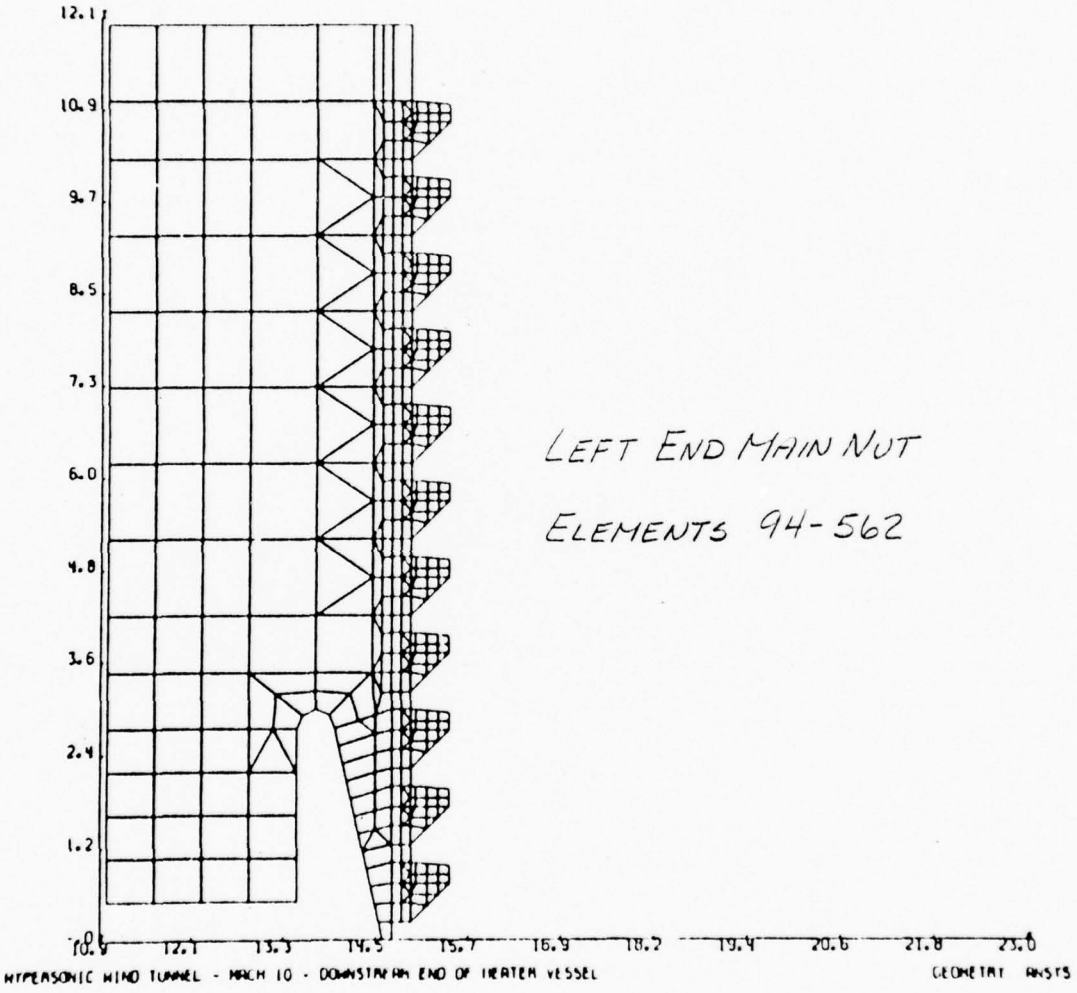

FIGURE 12 - ANSYS FINITE ELEMENT MODEL -
DOWNSTREAM END OF HEATER VESSEL

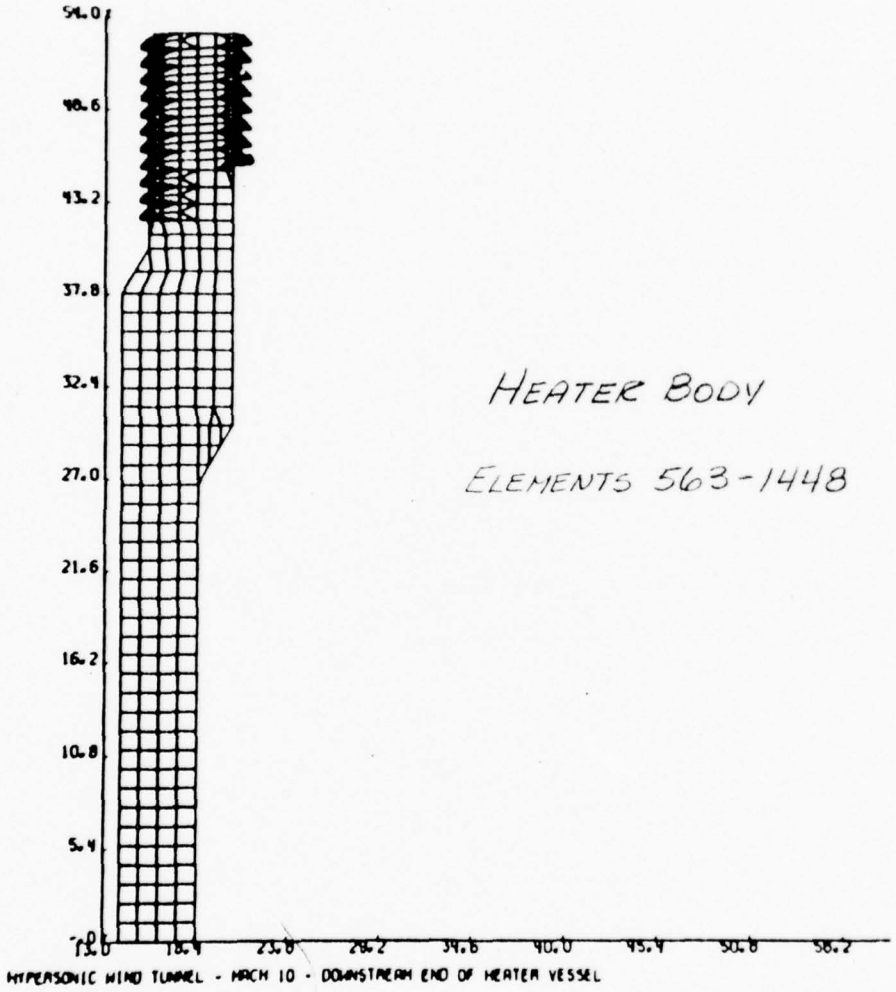

HEATER BODY

ELEMENTS 563-1448

FIGURE 13 - ANSYS FINITE ELEMENT MODEL - DOWNSTREAM END OF HEATER VESSEL

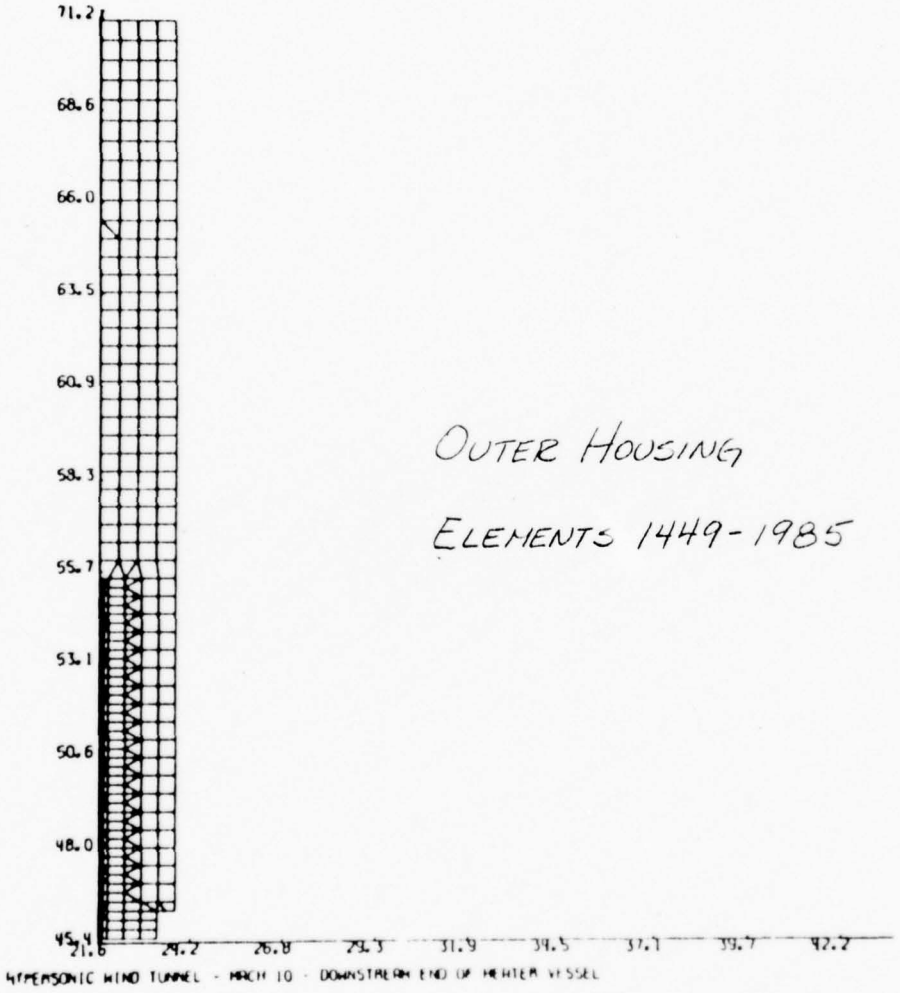

FIGURE 14 - ANSYS FINITE ELEMENT MODEL -
DOWNSTREAM END OF HEATER VESSEL

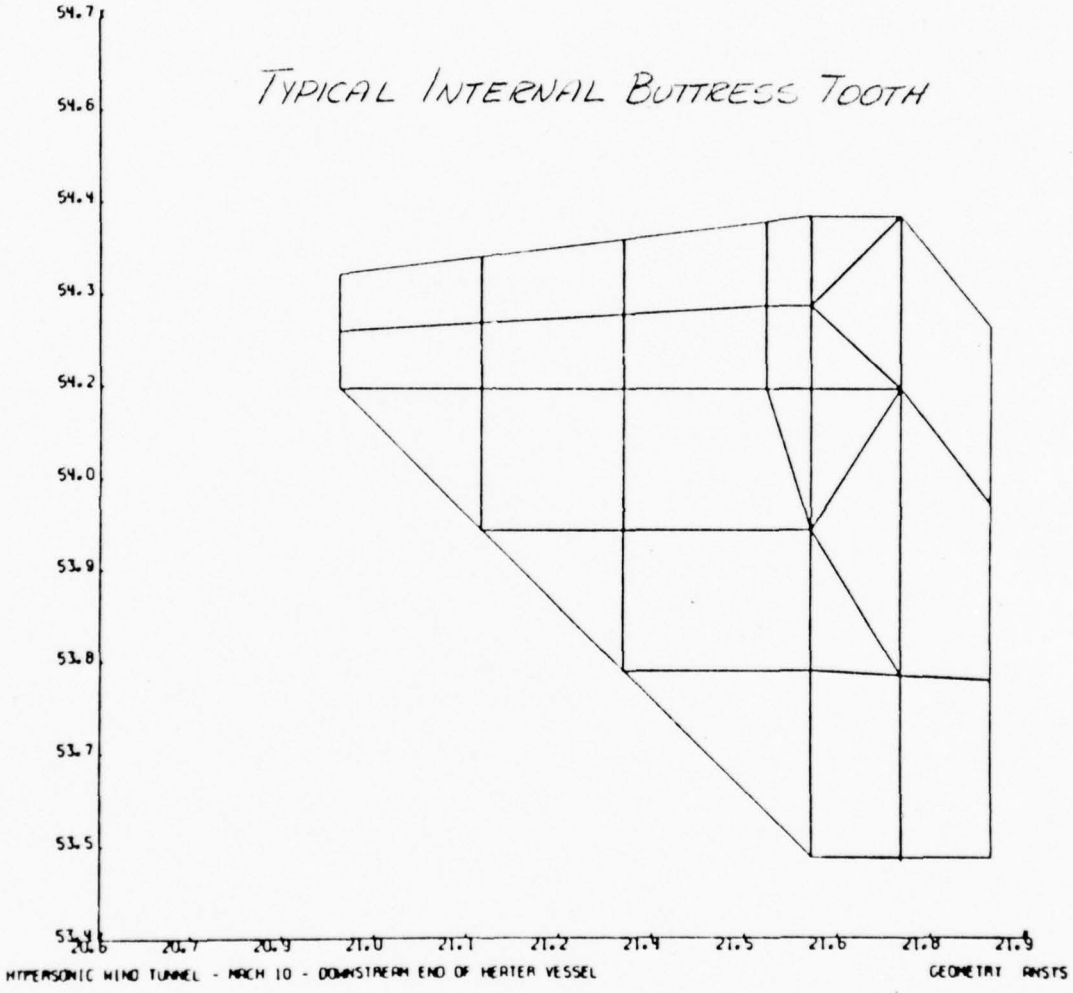

FIGURE 15 - ANSYS FINITE ELEMENT MODEL - DOWNSTREAM END OF HEATER VESSEL

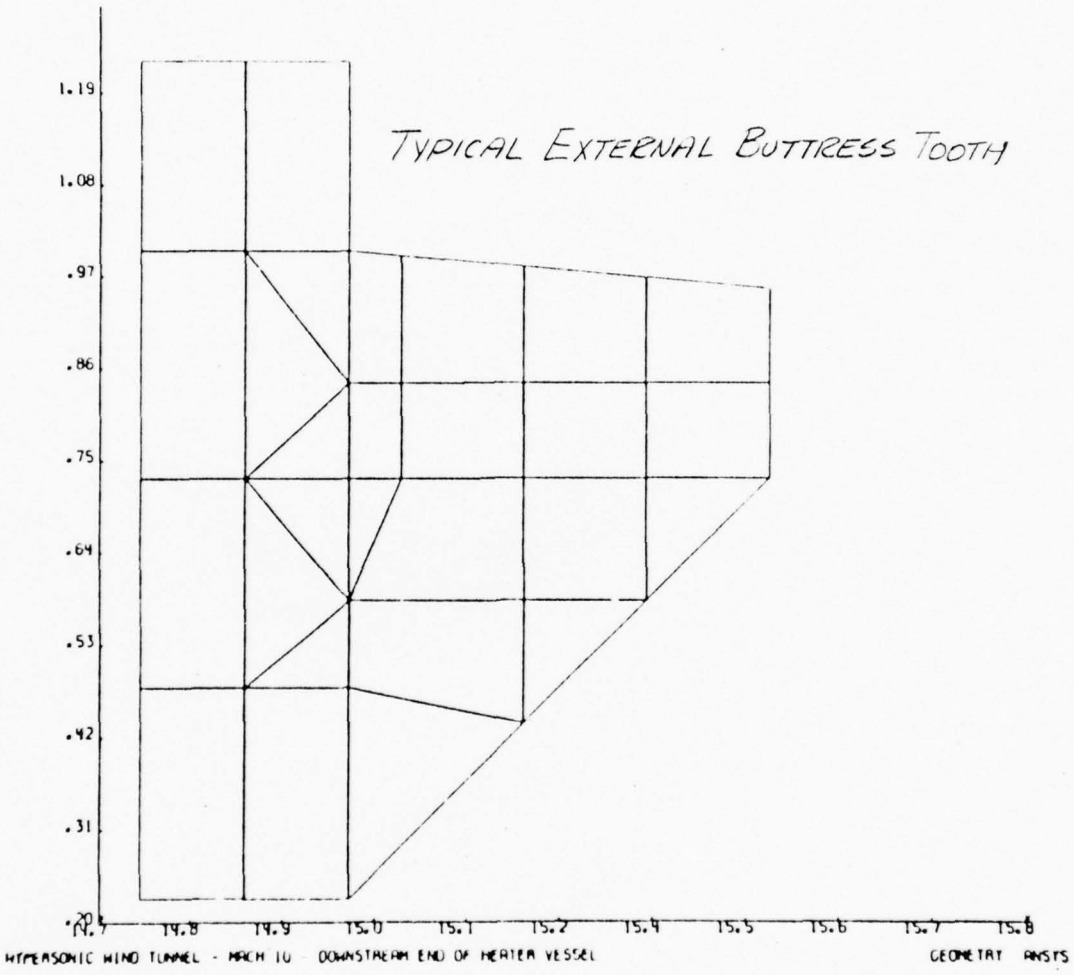

FIGURE 16 - ANSYS FINITE ELEMENT MODEL - DOWNSTREAM END OF HEATER VESSEL

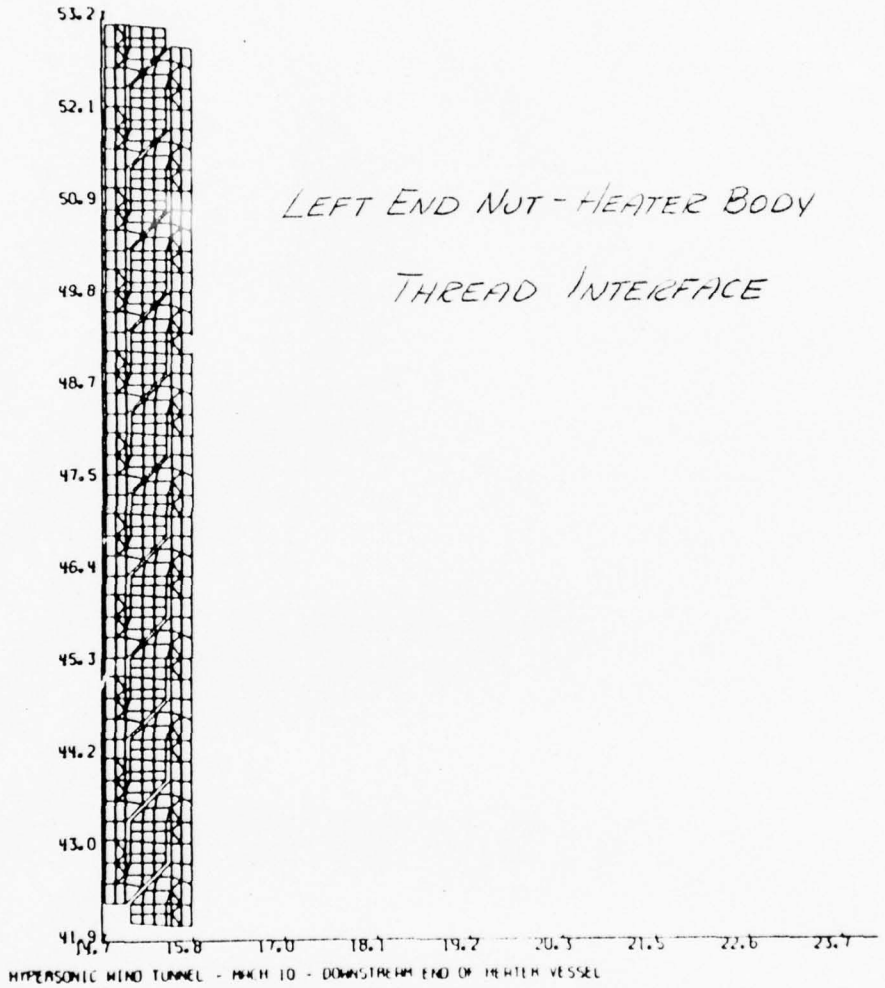

FIGURE 17 - ANSYS FINITE ELEMENT MODEL -
DOWNSTREAM END OF HEATER VESSEL

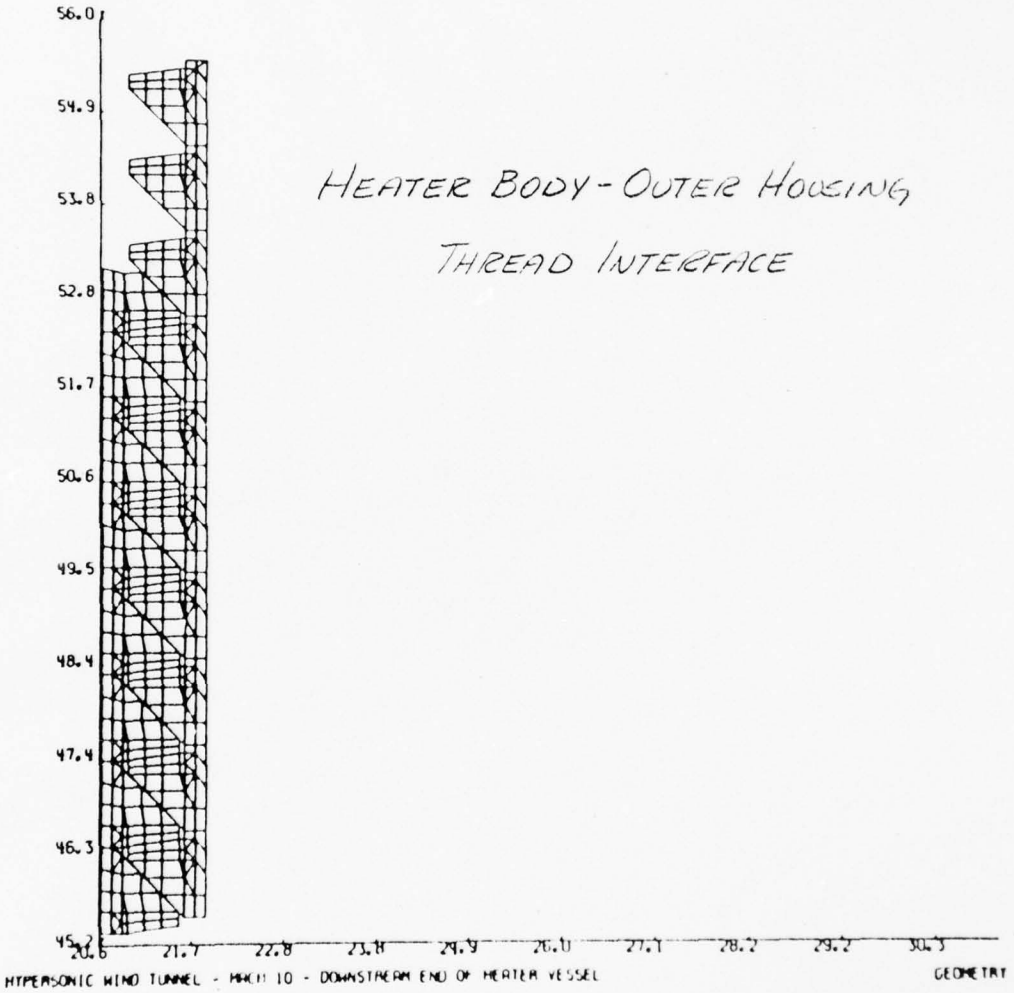

FIGURE 18 - ANSYS FINITE ELEMENT MODEL - DOWNSTREAM END OF HEATER VESSEL

5.1.5 DETAILED THREAD MODEL FOR DOWNSTREAM END OF MACH 10 HEATER VESSEL

The overall finite element model of the downstream end of the heater vessel does not have sufficient detail in the thread areas to adequately analyze a single tooth. This was accomplished by imposing the loading conditions (interface forces and boundary displacements) from the overall model onto a detailed finite element model of a single tooth. These are shown in Figures 19 and 20. The most severely loaded tooth in each interface was analyzed.

The total interface force was converted to an equivalent pressure applied to the area of contact between the two teeth. The corresponding boundary displacements were linearly interpolated when necessary to obtain nodal displacements for the detailed model.

5.1.6 OVERALL MODEL OF THE THREADED CLOSURE FOR THE MACH 10 PISTON BLOCK/NOZZLE BLOCK

The configuration of the M10 Piston Block/Nozzle Block threaded closure is shown below, along with the imposed loading obtained from the overall model.

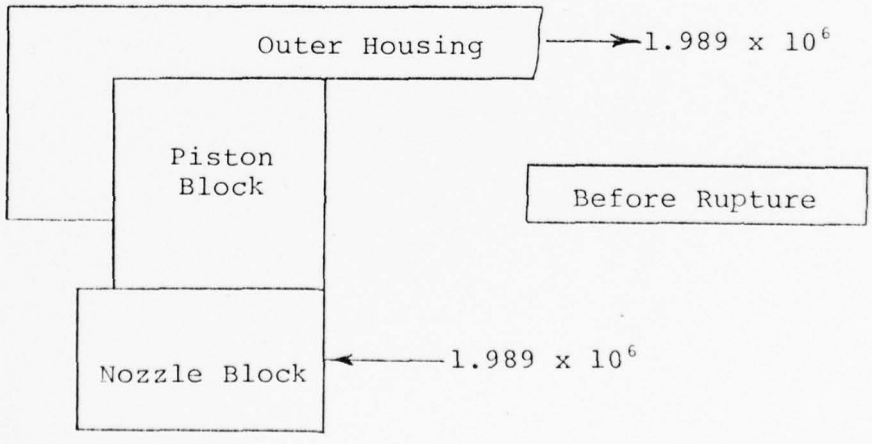

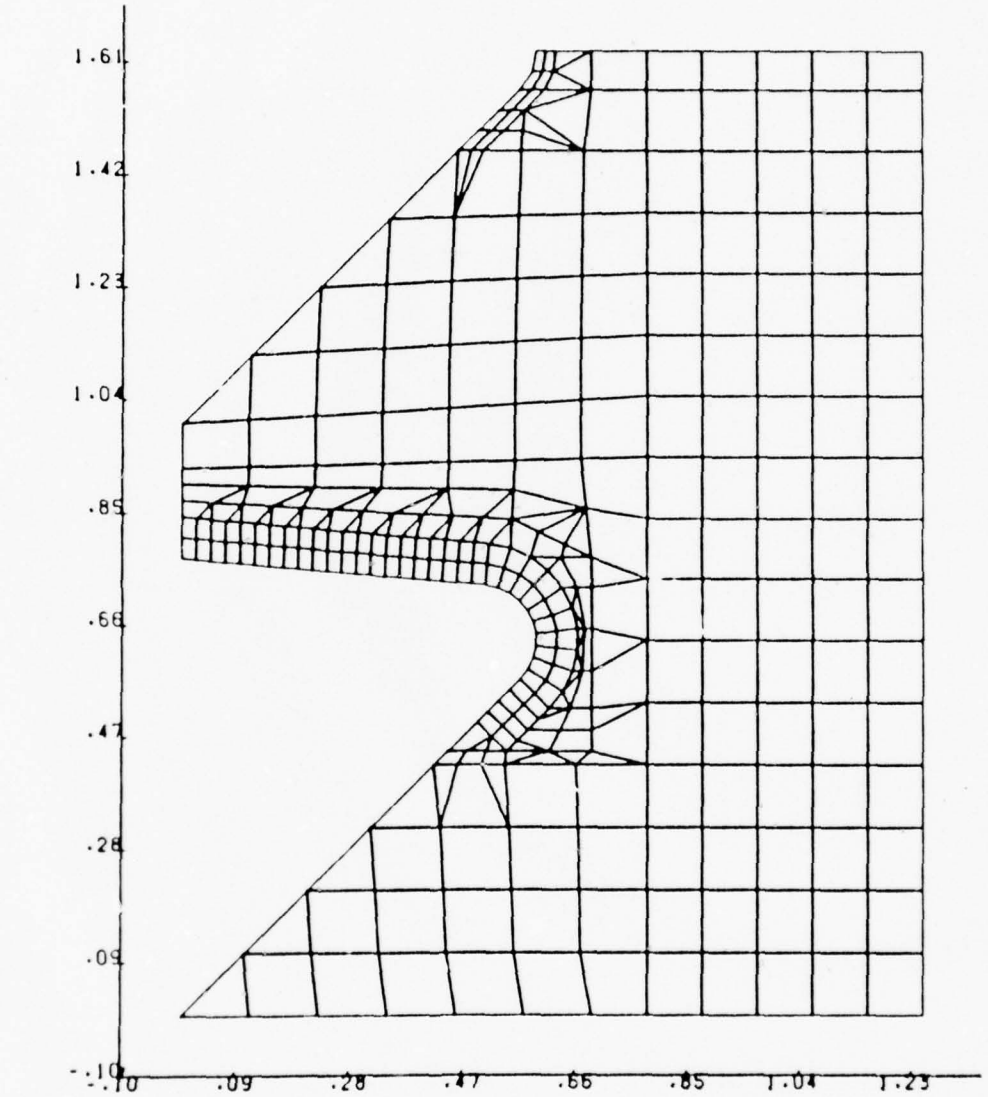

FIGURE 19 - DETAILED BUTTRESS TOOTH FINITE ELEMENT MODEL

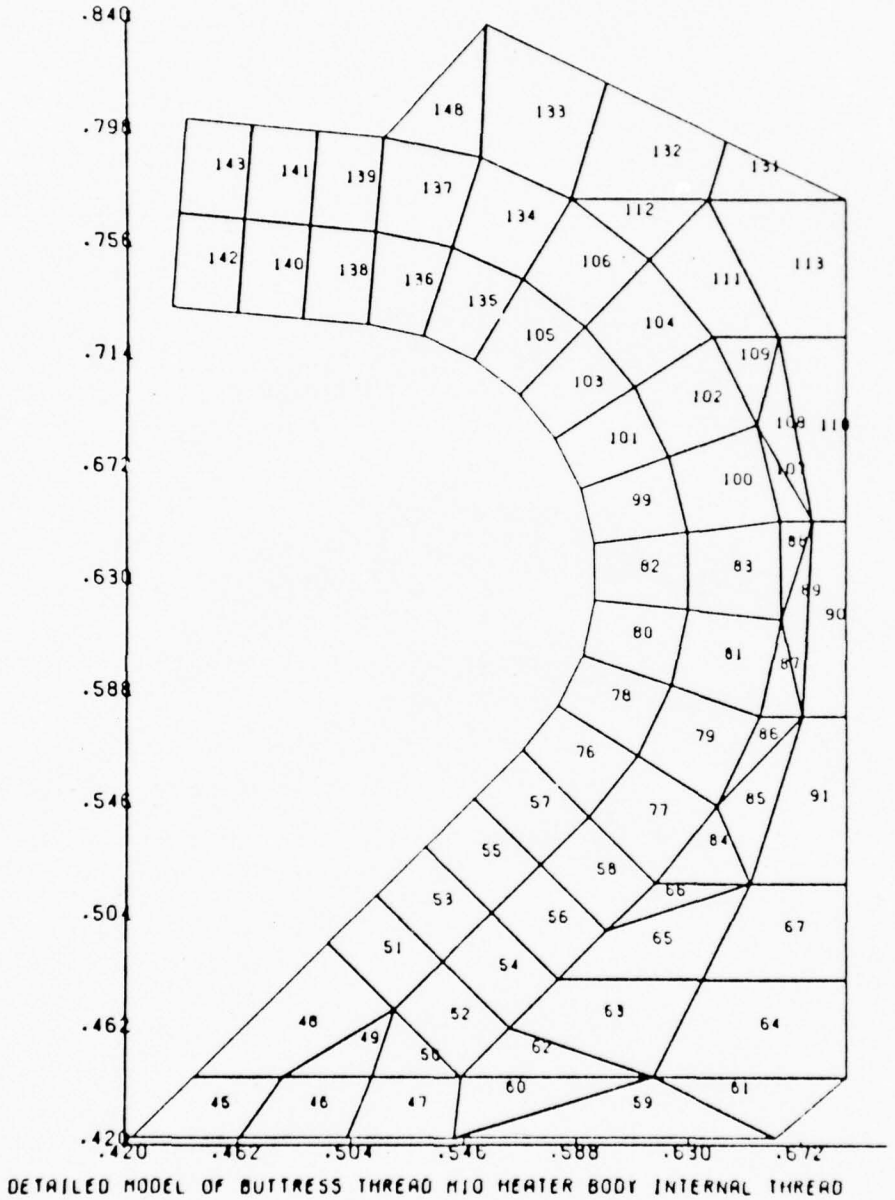

DETAILED MODEL OF BUTTRESS THREAD MID HEATER BODY INTERNAL THREAD

FIGURE 20 - DETAILED BUTTRESS TOOTH MODEL - ELEMENT NUMBERS IN HIGH STRESS REGION

The ANSYS finite element model of this area is shown in Figures 21 through 25. The model consists of 1027 Isoparametric (STIF42) elements. The method of handling the threaded closure is the same as for the downstream MACH 10 heater model, Section 5.1.4. The Nozzle block contains 8 - 2" diameter holes on a 17-1/2" diameter bolt circle. To account for the increased flexibility of nozzle block due to these holes, the modulus of elasticity, E, was adjusted as follows:

$$E_{MOD} = \frac{\text{Area excluding holes}}{\text{Area including holes}} \times 30 \times 10^6 \text{ psi}$$

$$E_{MOD} = (0.7715)(30 \times 10^6) = 23.14 \times 10^6 \text{ psi}$$

This modified E was used for those elements of the nozzle block which are within the annulus formed by the holes. To account for the resistance to rotation imposed upon the nozzle block by the nozzle thread insert carrier, all nodes along the inboard surface of the nozzle block were required to have the same radial displacement.

5.1.7 DETAILED THREAD MODEL OF A SINGLE TOOTH FOR THE MACH 10 HEATER VESSEL NOZZLE AREA

Following the same procedure outlined in Section 5.1.5, a detailed model was developed of a single buttress tooth. The maximum loaded tooth was evaluated using this model, shown in Figure 26.

5.2 MACH 14/18 HEATER VESSEL MODELS OF ORIGINAL DESIGN

The finite element models used to analyze the original MACH 14/18 Heater Vessel design are described in the following subsections.

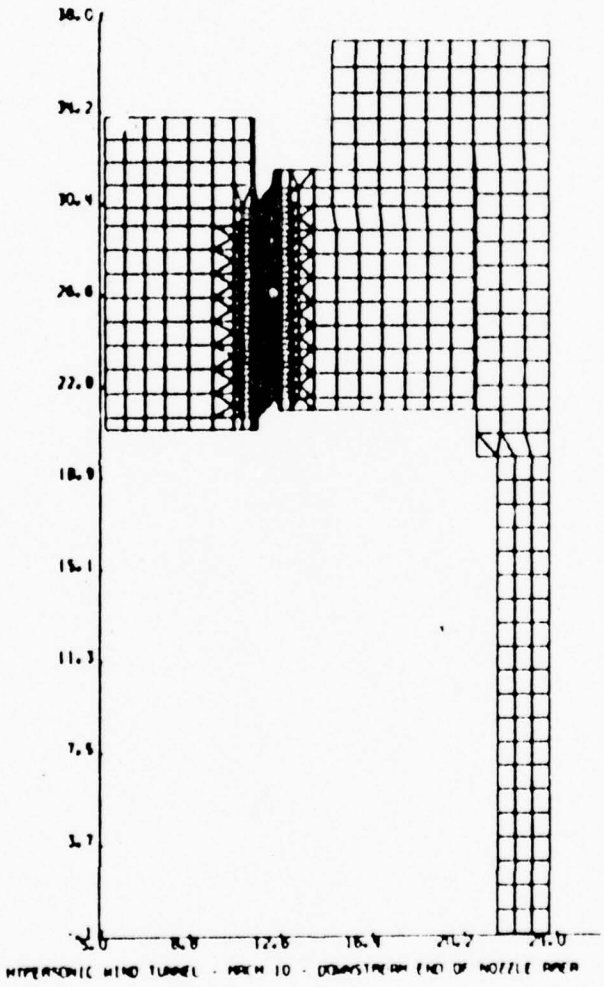

FIGURE 21 - ANSYS FINITE ELEMENT MODEL -
NOZZLE BLOCK/PISTON BLOCK

MACH 10

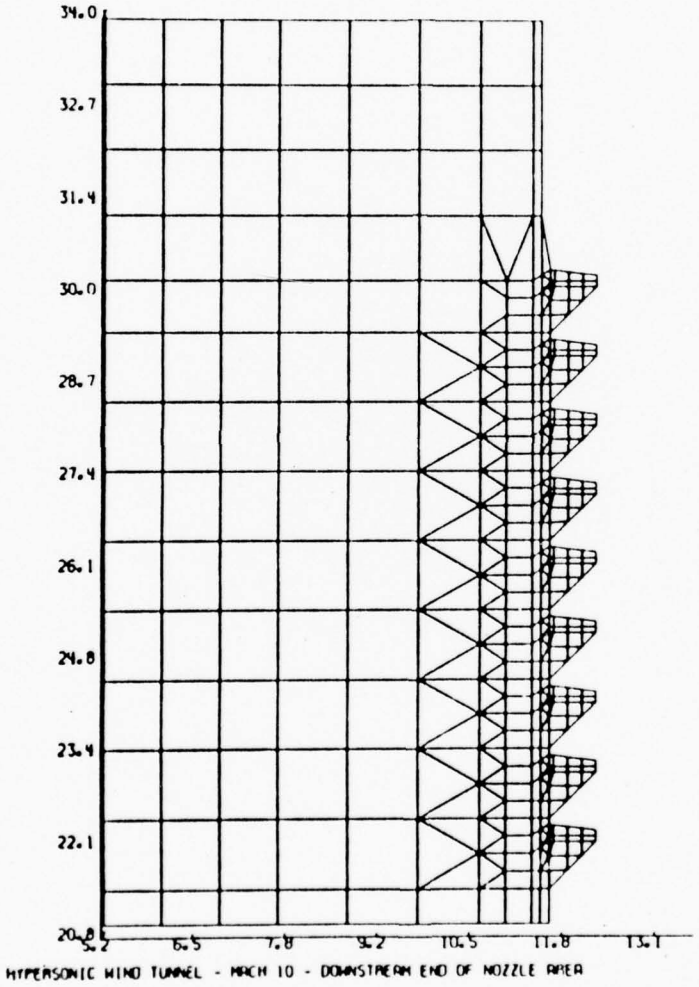

NOZZLE BLOCK
ELEMENTS 1-442

FIGURE 22 - ANSYS FINITE ELEMENT MODEL -
NOZZLE BLOCK/PISTON BLOCK
MACH 10

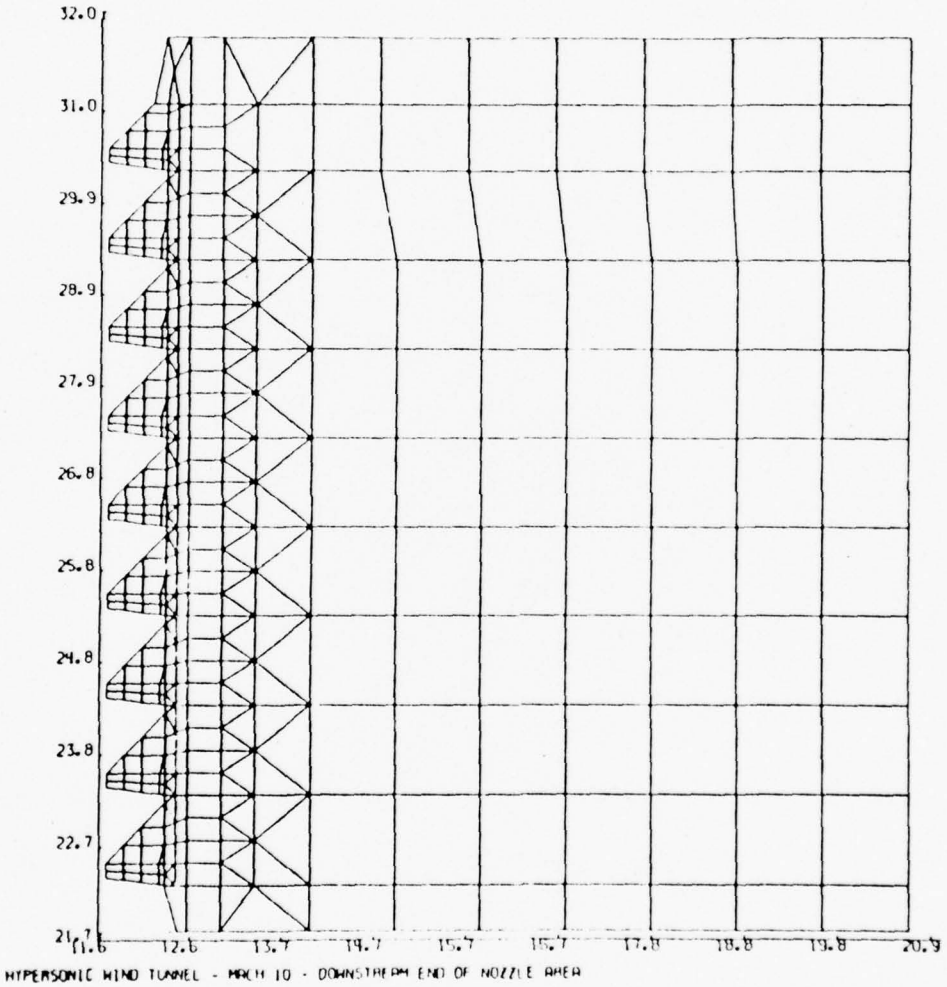

Piston Block Elements 443-884

FIGURE 23 - ANSYS FINITE ELEMENT MODEL -
NOZZLE BLOCK/PISTON BLOCK

MACH 10

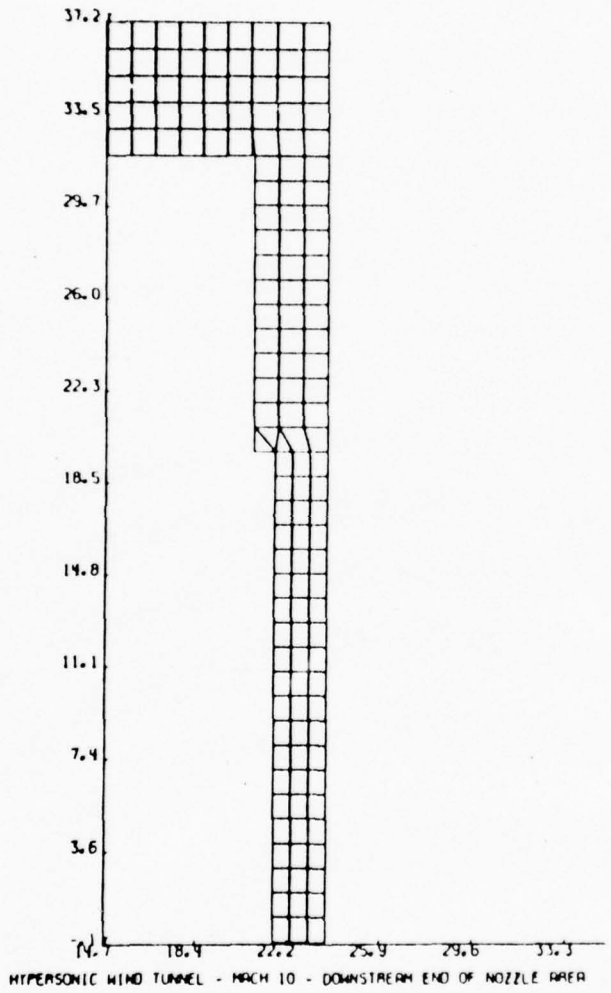

Outer Housing Elements 885-1027

FIGURE 24 - ANSYS FINITE ELEMENT MODEL - NOZZLE BLOCK/PISTON BLOCK MACH 10

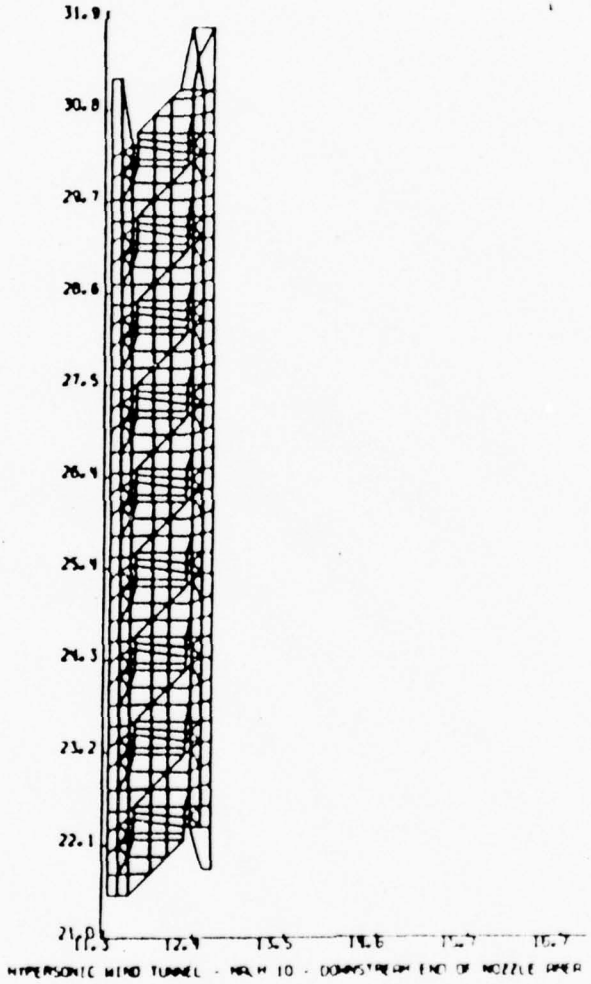

Thread Interface

FIGURE 25 - ANSYS FINITE ELEMENT MODEL -
NOZZLE BLOCK/PISTON BLOCK
MACH 10

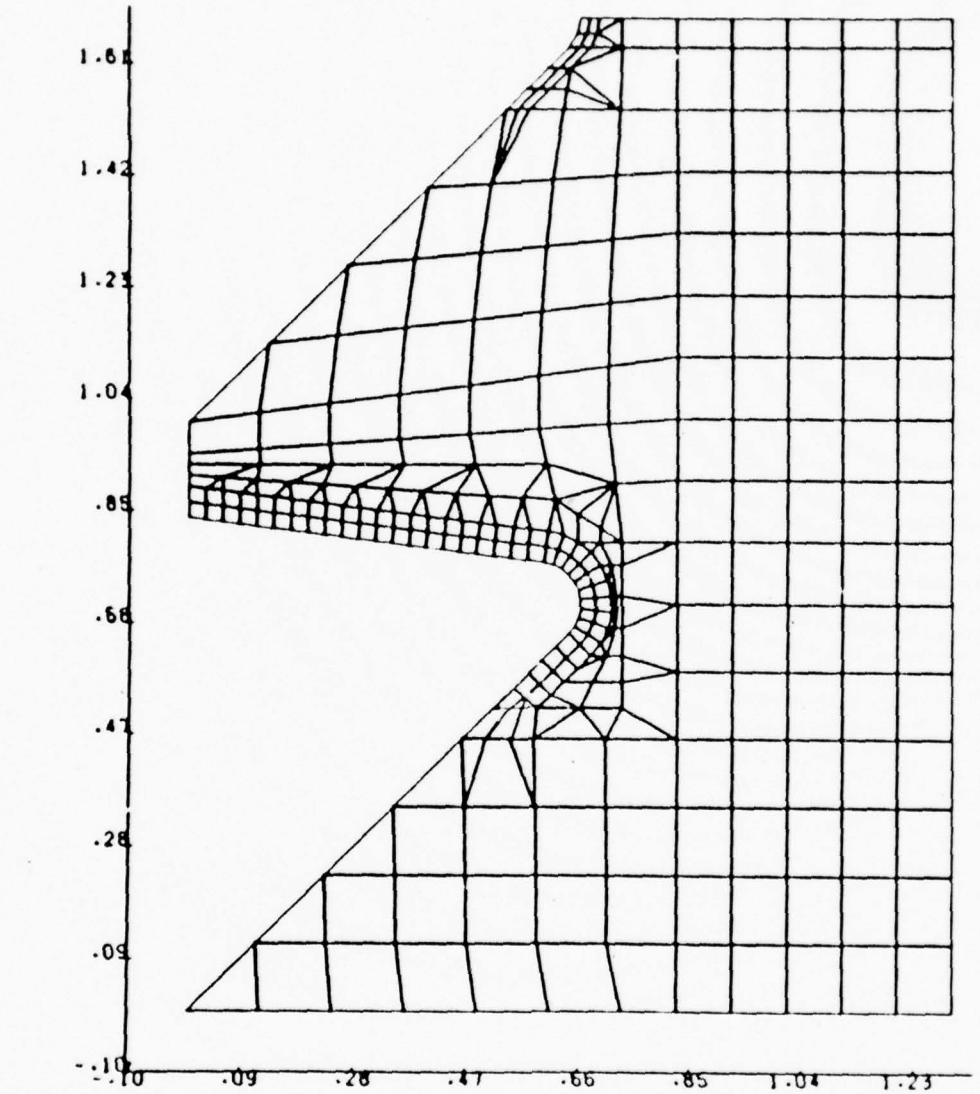

FIGURE 26 - DETAILED BUTTRESS TOOTH FINITE ELEMENT MODEL

5.2.1 OVERALL MODEL FOR BOTTOM END OF MACH 14/18 HEATER VESSEL

A finite element model of the bottom end closure on the MACH 14/18 Heater Vessel was prepared and used in conjunction with the ANSYS computer program, Reference 5, to calculate the maximum loads and stresses in this closure due to the internal design pressure loading. A computer-drawn scale plot of this overall model is shown in Figure 27. The model consists of four parts -- the liner, the main cylinder, the nut, and the cover. There is a shrink fit of 0.017" on the radius between the liner and the main cylinder. The liner and the main cylinder are shown in Figure 28. The nut is shown in Figure 29. The cover is shown in Figure 30. This model is made up of 2998 Isoparametric (STIF42) elements.

The cylinder part was modeled to a distance of approximately $\pi\lambda$ beyond the end of the taper on the cylinder, where λ is the attenuation length (see Figure 28):

$$\lambda = \frac{\sqrt{R_{mean}\, t}}{1.285}$$

where R_{mean} is the mean radius of the cylinder, and t is the thickness.

As shown in the Figures, the nut and cylinder threads were modeled individually. The nut threads alone are shown in Figure 29. A detail of one cylinder thread is shown in Figure 31, and a detail of one nut thread is shown in Figure 32. The thread meshing is similar to that shown in Figure 7. The mating pairs of nodes between the nut and cylinder threads are specified to have the same displacements in the direction perpendicular to the tooth surface. This transmits the load from one thread tooth to the other without any friction between mating threads.

An internal pressure of 46,000 psi was applied to the inside surfaces of the overall model. The load on each of the individual threads was then obtained from the computer results. The resulting maximum thread load was then converted into an equivalent uniform load and applied to the tooth surface on the

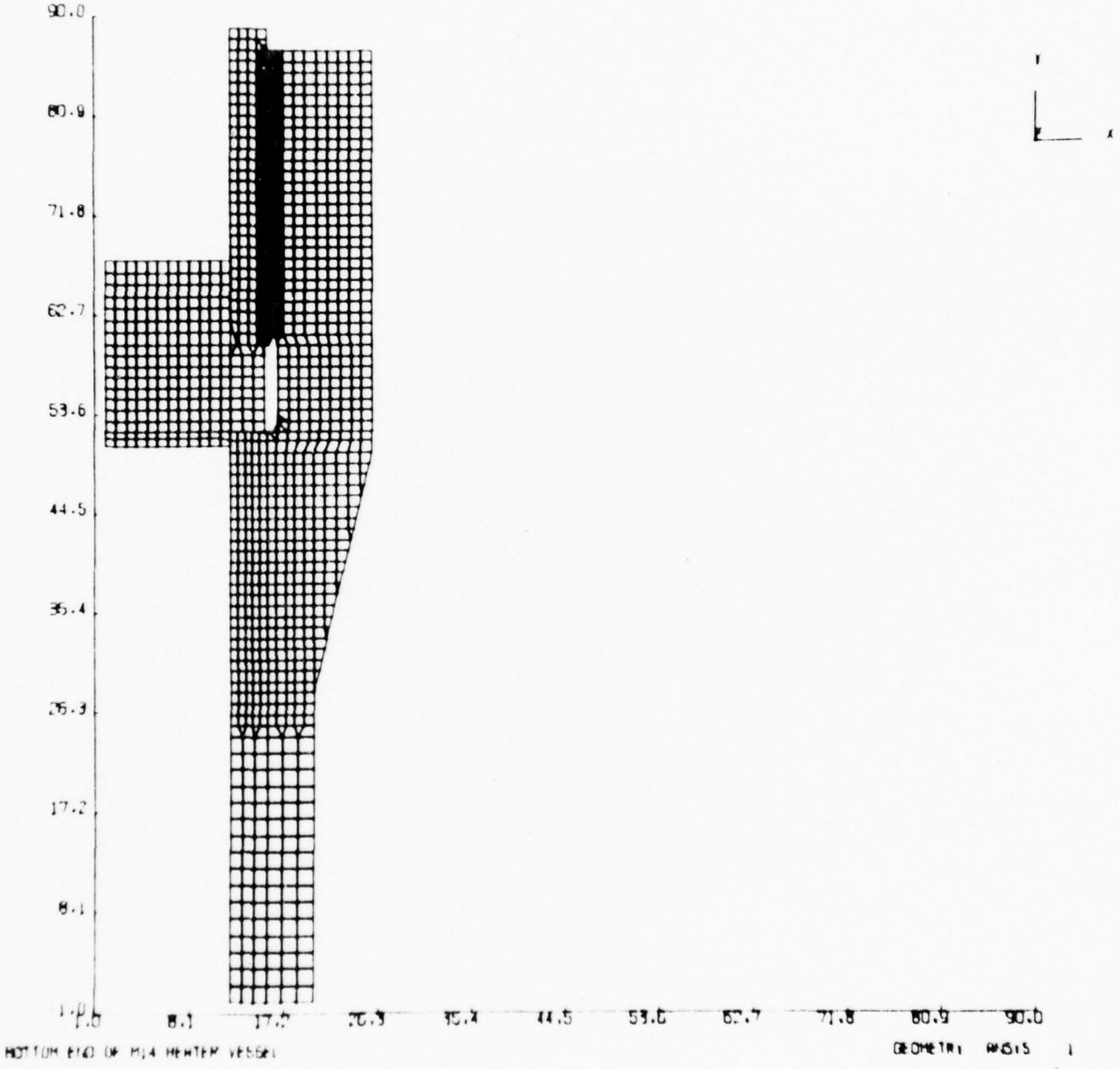

FIGURE 27 - OVERALL MODEL - BOTTOM END OF MACH 14/18 HEATER VESSEL

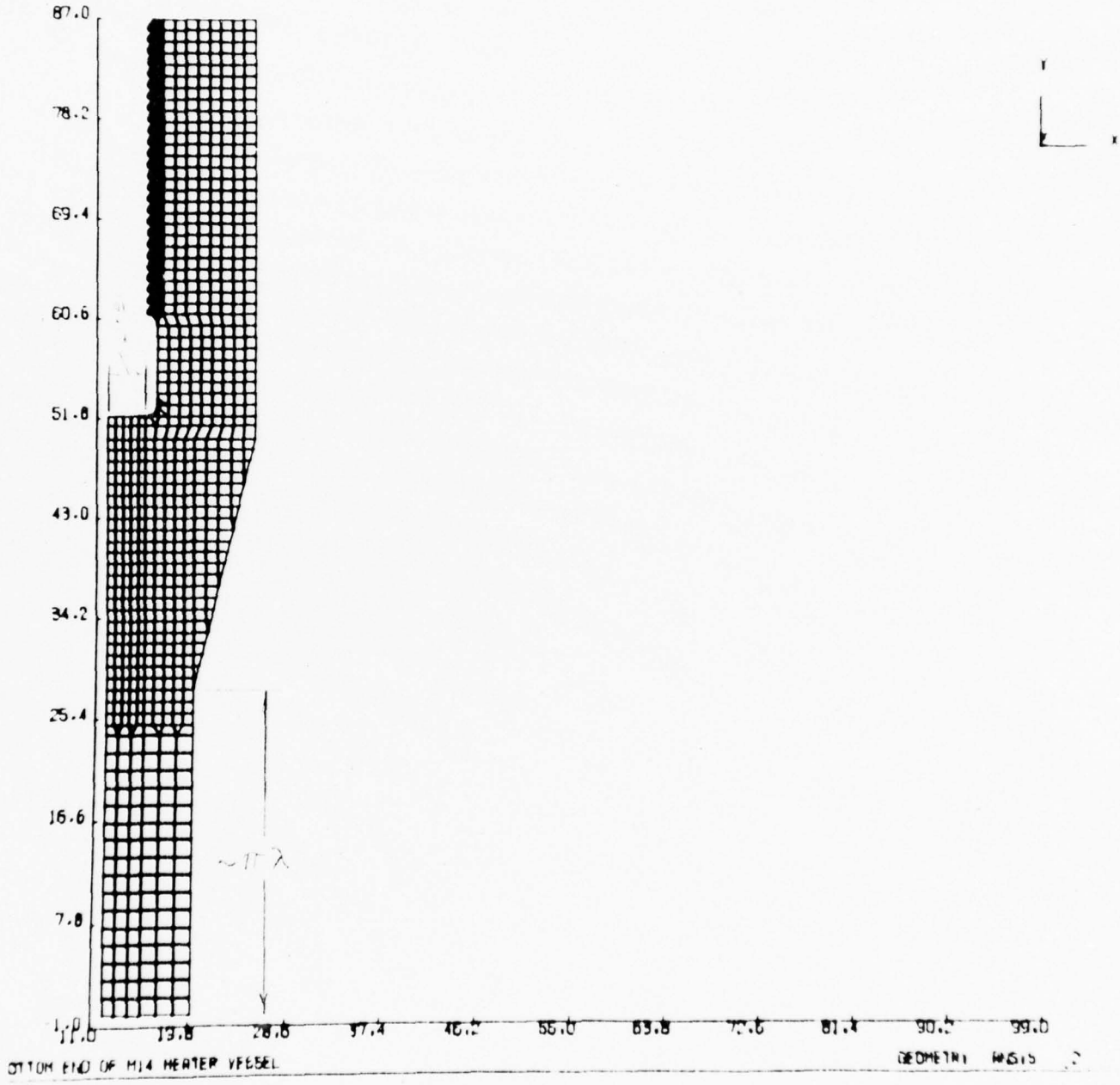

FIGURE 28 - LINER AND MAIN CYLINDER ON OVERALL MODEL - BOTTOM END OF MACH 14/18 HEATER VESSEL

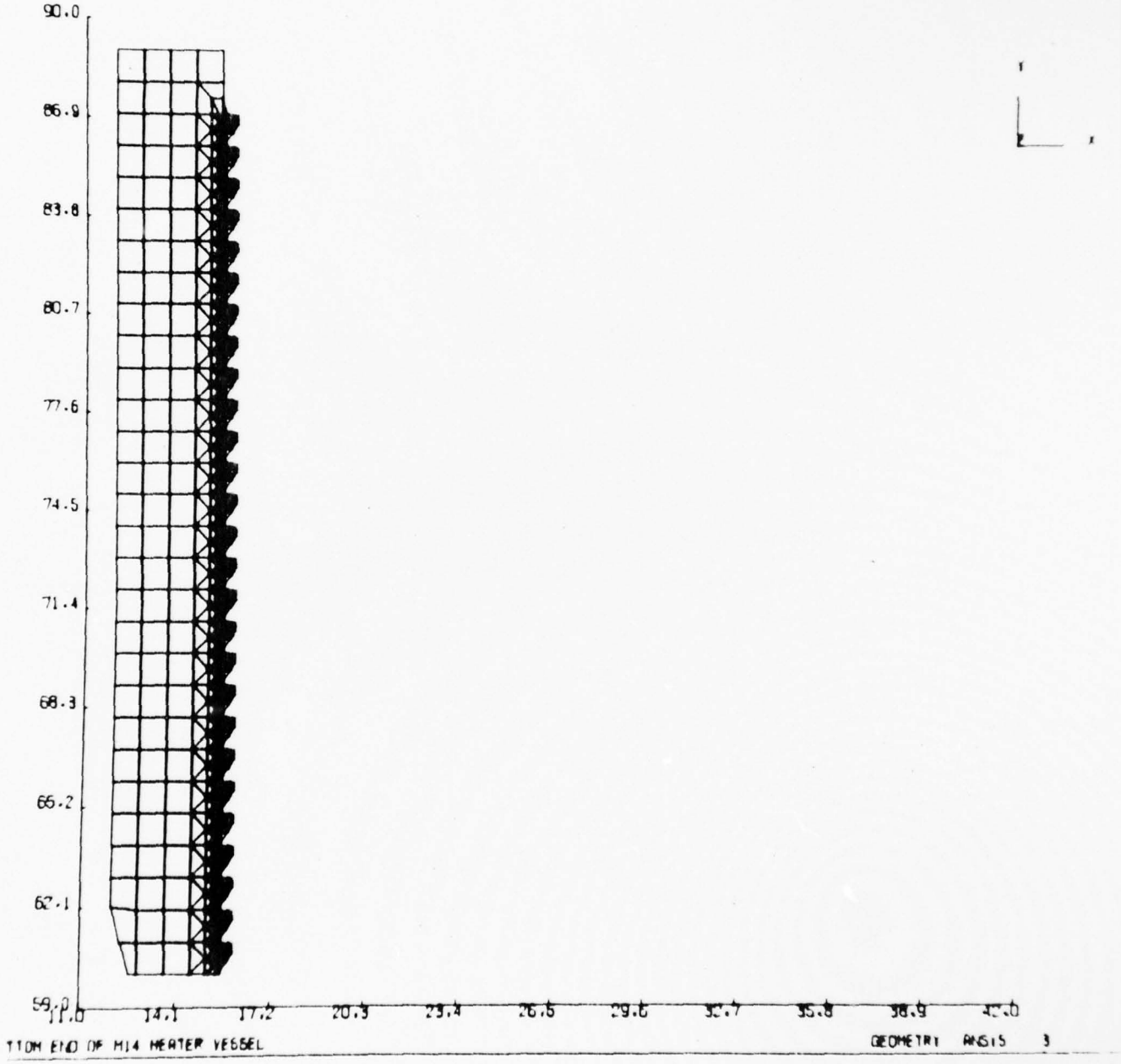

FIGURE 29 - NUT ON OVERALL MODEL -
BOTTOM END OF MACH 14/18 HEATER VESSEL

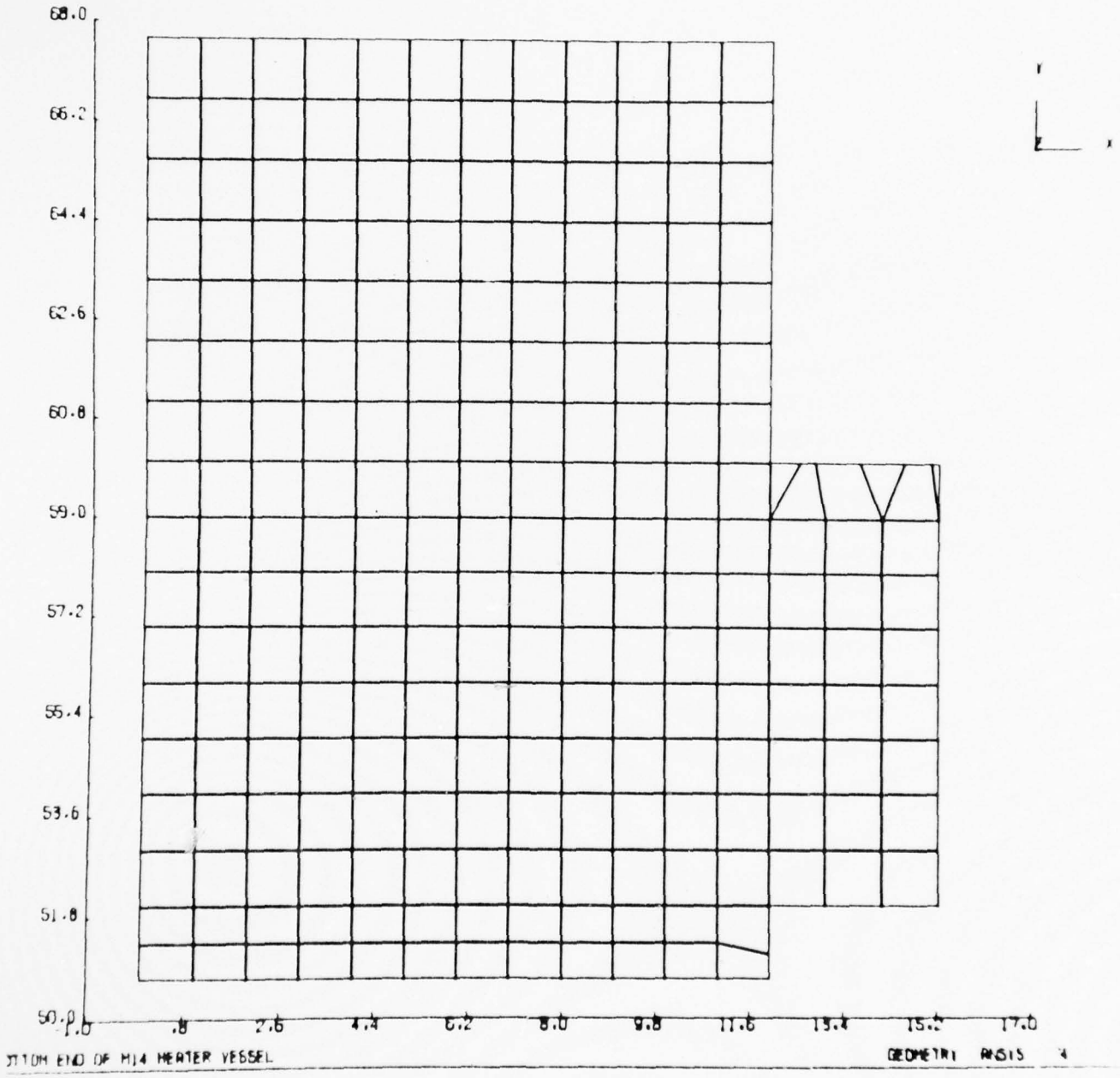

FIGURE 30 - COVER ON OVERALL MODEL -
BOTTOM END OF MACH 14/18 HEATER VESSEL

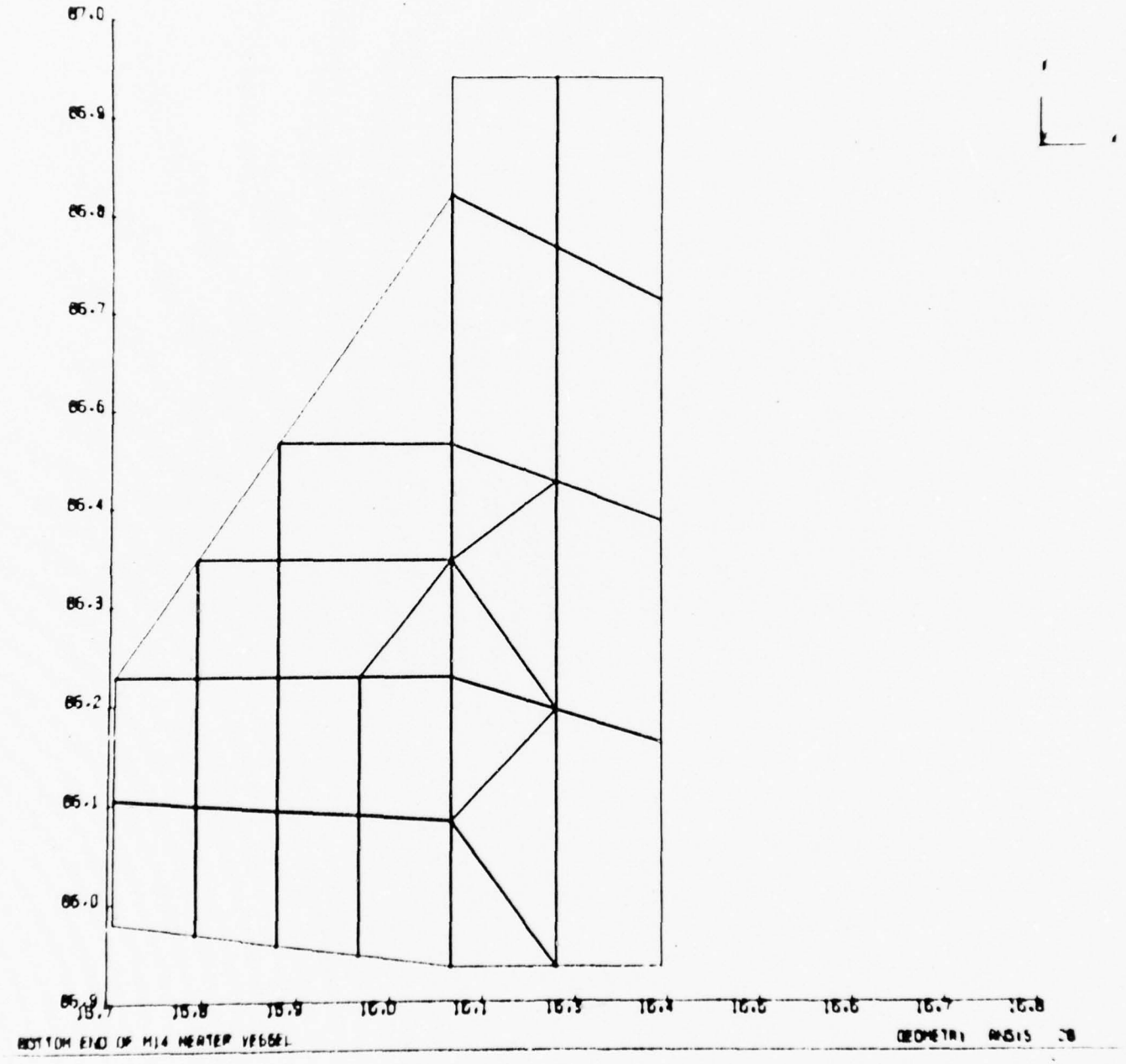

FIGURE 31 - DETAIL OF ONE CYLINDER THREAD ON OVERALL MODEL - BOTTOM END OF MACH 14/18 HEATER VESSEL

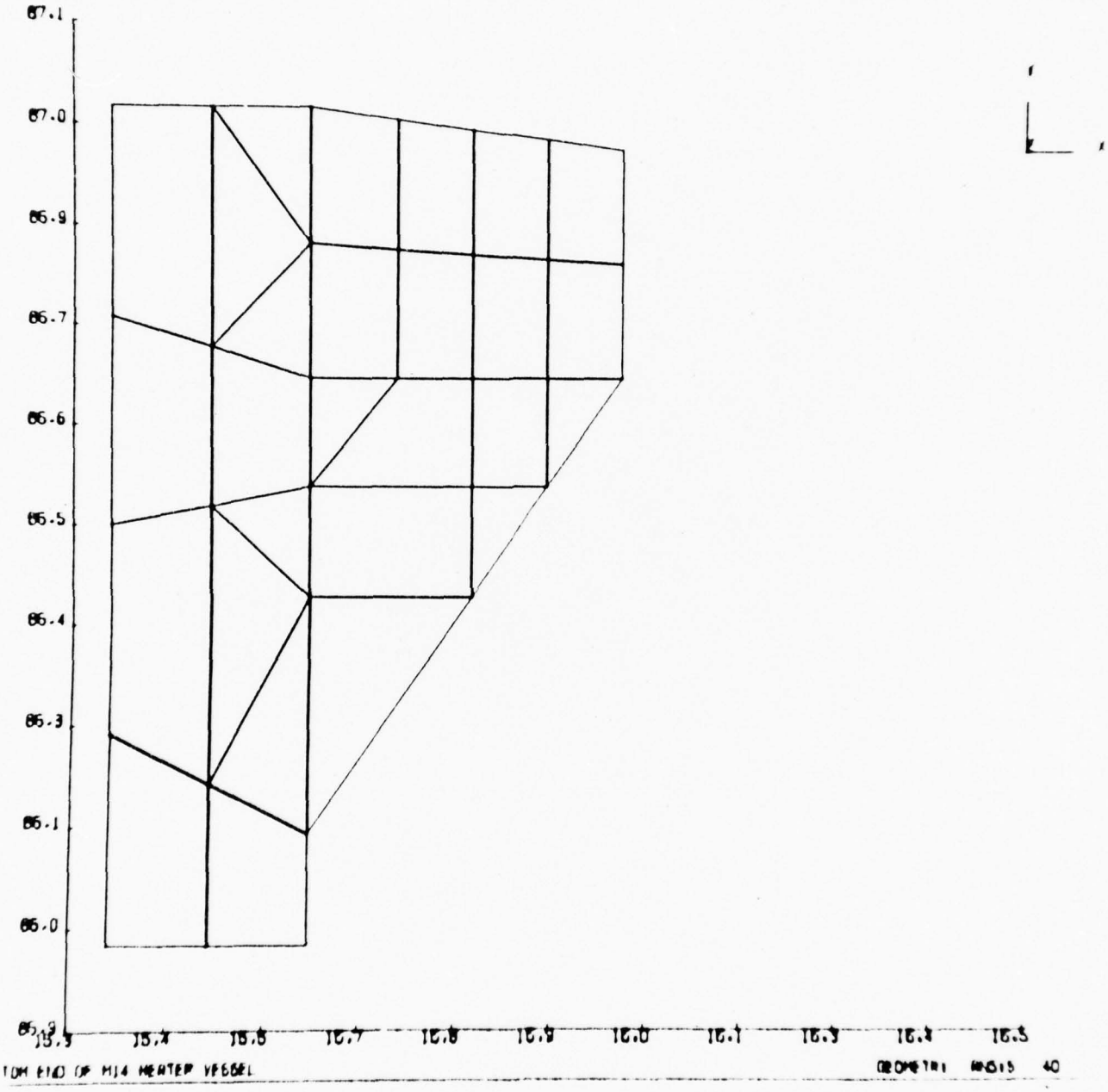

FIGURE 32 - DETAIL OF ONE NUT THREAD ON OVERALL MODEL - BOTTOM END OF MACH 14/18 HEATER VESSEL

detailed thread model. In addition, displacements from the overall model in the vicinity of the thread where the maximum thread load occurs were applied as boundary conditions on the edges of the detailed model.

5.2.2 DETAILED THREAD MODEL OF FIRST THREAD ON BOTTOM END OF MACH 14/18 HEATER VESSEL

A computer-drawn scale plot of the detailed thread model for the first thread with an elliptical undercut for the bottom end of the MACH 14/18 Heater Vessel is shown in Figure 33. This model is made up of many two-dimensional Isoparametric (STIF42) elements. The thread load on the first thread from the overall model was converted into an equivalent pressure load and applied to the tooth surface on the detailed model (see Appendix 6A). The displacements from the overall model in the area around the first thread were applied as boundary conditions on the edges of this detailed model. This detailed model was used to calculate the maximum stresses in the elliptical undercut region of the first thread on the MACH 14/18 Heater Vessel Bottom End Closure.

5.2.3 DETAILED THREAD MODEL OF A TYPICAL THREAD ON BOTTOM END OF MACH 14/18 HEATER VESSEL

A computer-drawn scale plot of the detailed thread model for the MACH 14/18 Heater Vessel is shown in Figure 34. This model is made up of many two-dimensional Isoparametric (STIF42) elements. The maximum thread load on the overall model was converted into an equivalent pressure load and applied to the tooth surface on the detailed model (see Appendix 4B). The displacements from the overall model in the vicinity of the thread where the maximum thread load occurs were applied as boundary conditions on the edges of this detailed model.

This detailed model was used to calculate the maximum stresses in the thread root for the bottom end closures.

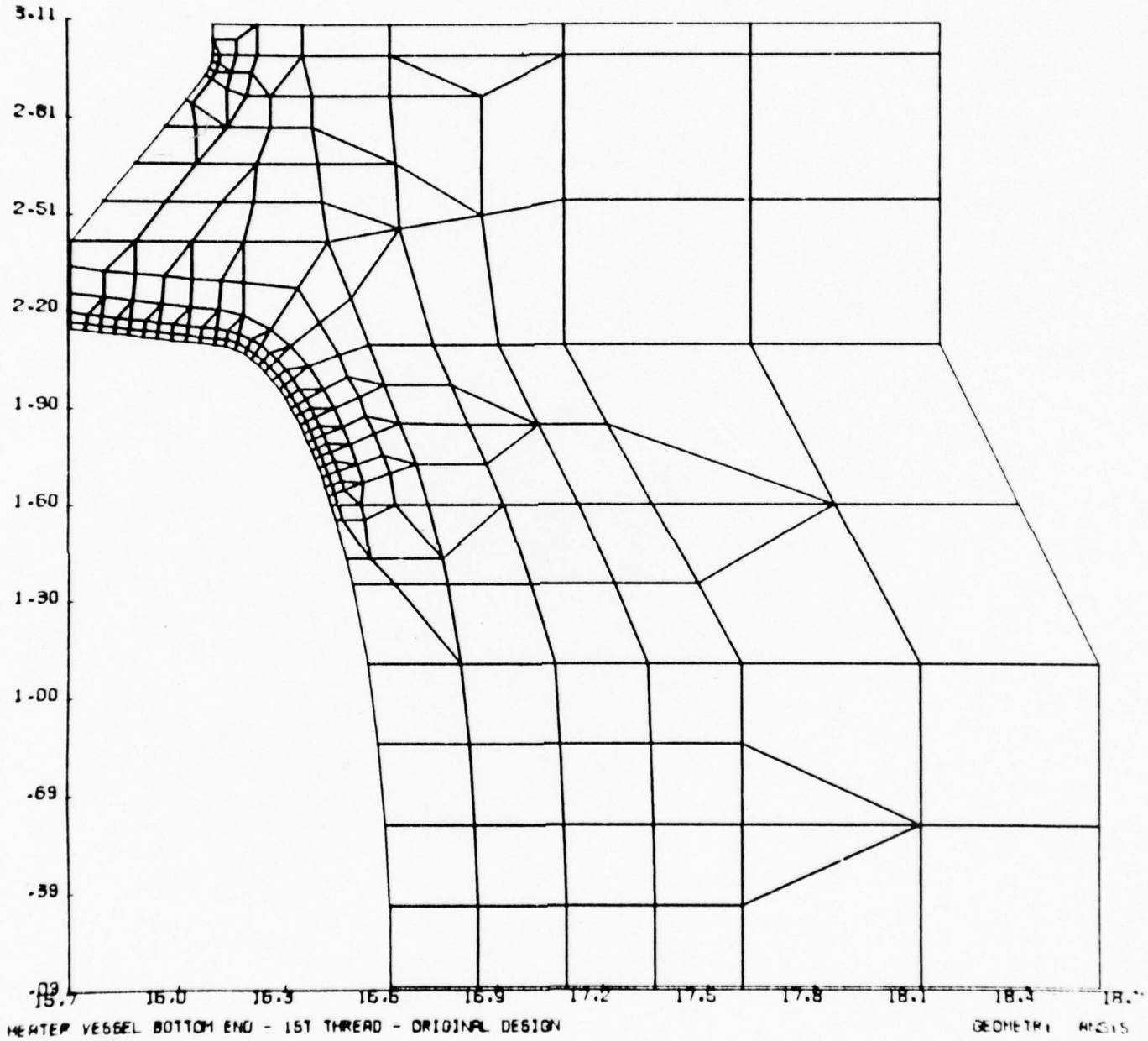

Figure 33- Detailed Thread Model of First Thread With Elliptical Undercut For Mach 14/18 Heater Vessel

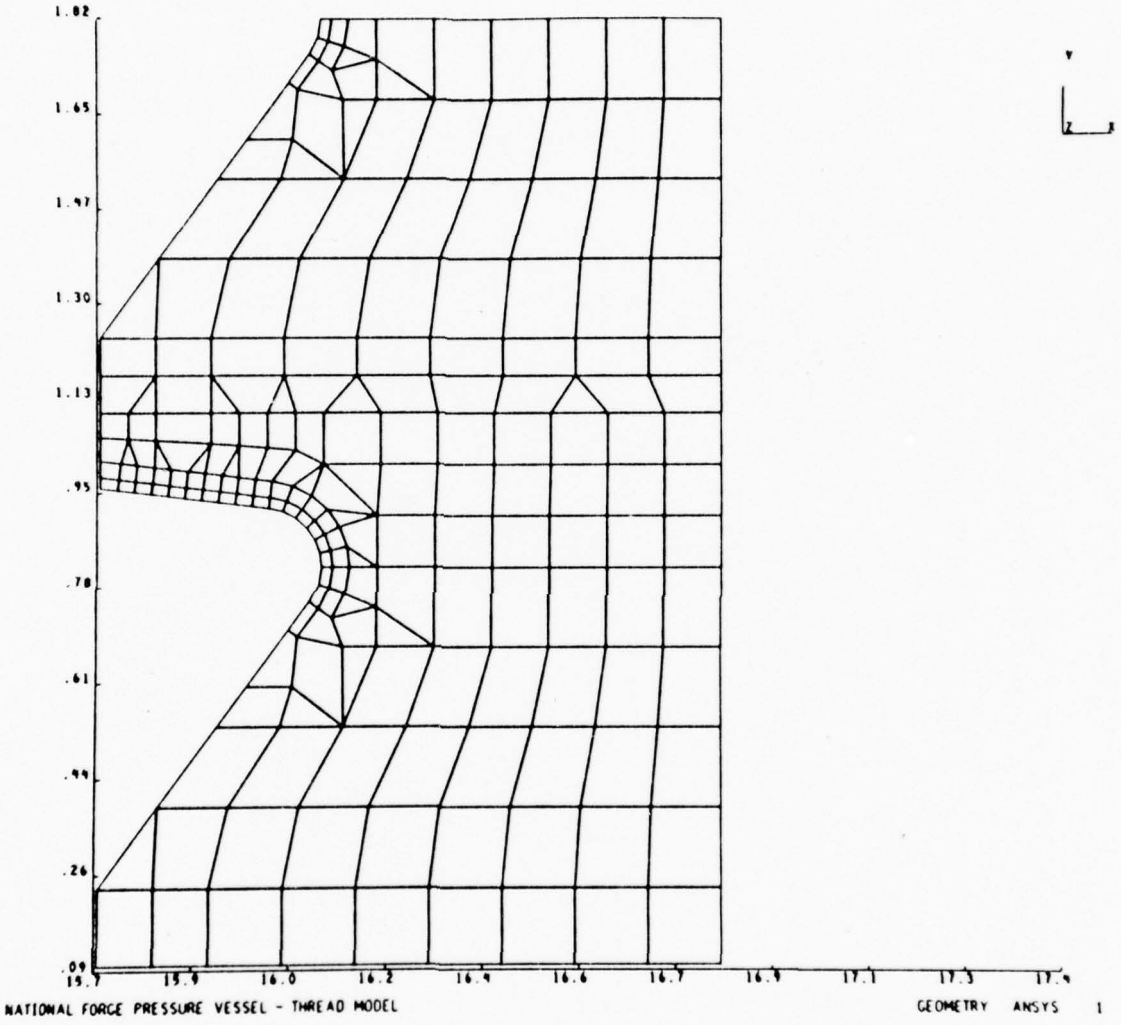

FIGURE 34 - DETAILED THREAD MODEL FOR
MACH 14/18 HEATER VESSEL
(32" - 1N FEMALE THREAD ON BODY)

5.2.4 OVERALL MODEL FOR TOP END OF MACH 14/18 HEATER VESSEL

A finite element model of the outlet end of the MACH 14/18 Heater Vessel was used to evaluate the maximum loads and stresses existing in the closure due to design pressure loading. The overall model is shown in Figure 35 and is shown broken down into various sections in Figures 36, 37, 38, and 39. The model consists of four parts--the liner, the main cylinder, the top nut, and the lower portion of the elbow assembly. The total model consists of 3914 isoparametric (STIF 42) elements.

The straight section of the cylinder was modeled to a distance of 2.5λ beyond the end of the taper.

As shown in the figures of the overall model, the threads were modeled individually. Figures 40 and 41 show a typical male and female tooth. The interface between teeth was required to have the same normal displacements, while being allowed to slide tangentially. No friction was assumed between the mating surfaces.

The other boundary conditions imposed upon the model were an internal design pressure of 46,000 psi, no rotation at symmetry lines at the end of the cylinder, and at the end of the elbow section. An end load was applied to the end of the elbow section to account for the vertical pressure force not included in the model. This force was computed as an equivalent negative pressure as follows:

A_M = Area of end of elbow section = $\pi(12.068^2 - 5.0^2)$

$$A_M = 378.991 \text{ in}^2$$

A_A = Area not included in model = $\pi(5^2) = 78.540 \text{ in}^2$

F_E = End load on elbow section = $\frac{(46{,}000)(78.540)}{(378.991)}$

$$F_E = 9532.76 \text{ psi}$$

The shrink fit between the liner and the vessel was handled in the same method as for the bottom closure.

OVERALL MODEL OF OUTLET END OF
MACH 14/18 HEATER VESSEL

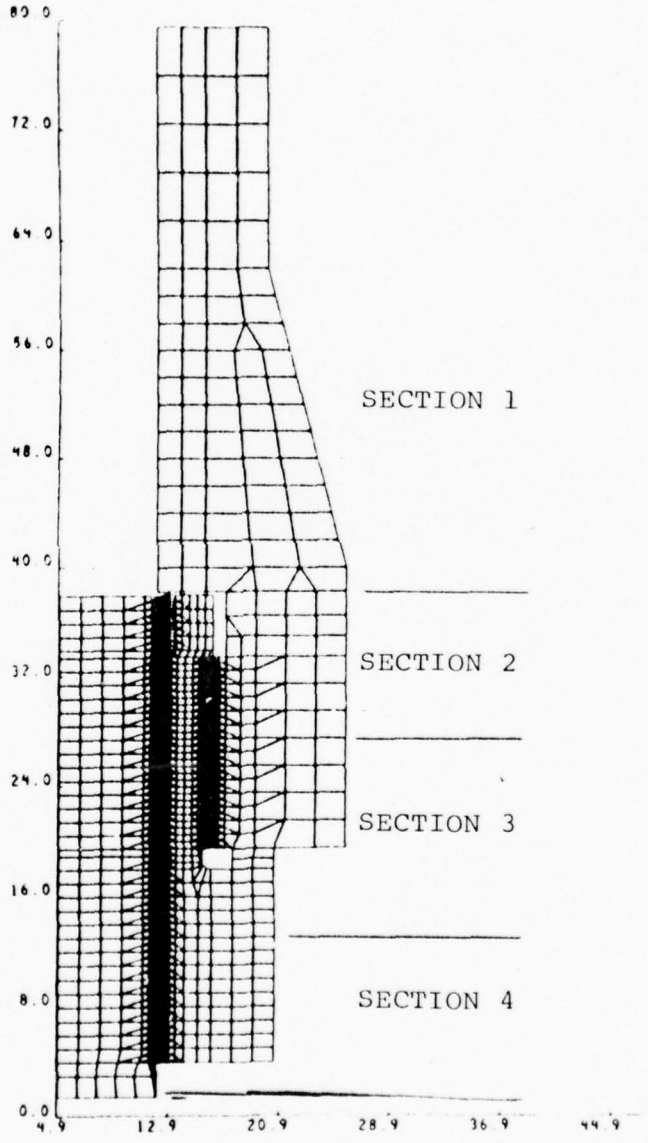

Figure 35

SECTION 1 OF MACH 14/18 HEATER VESSEL
OUTLET END

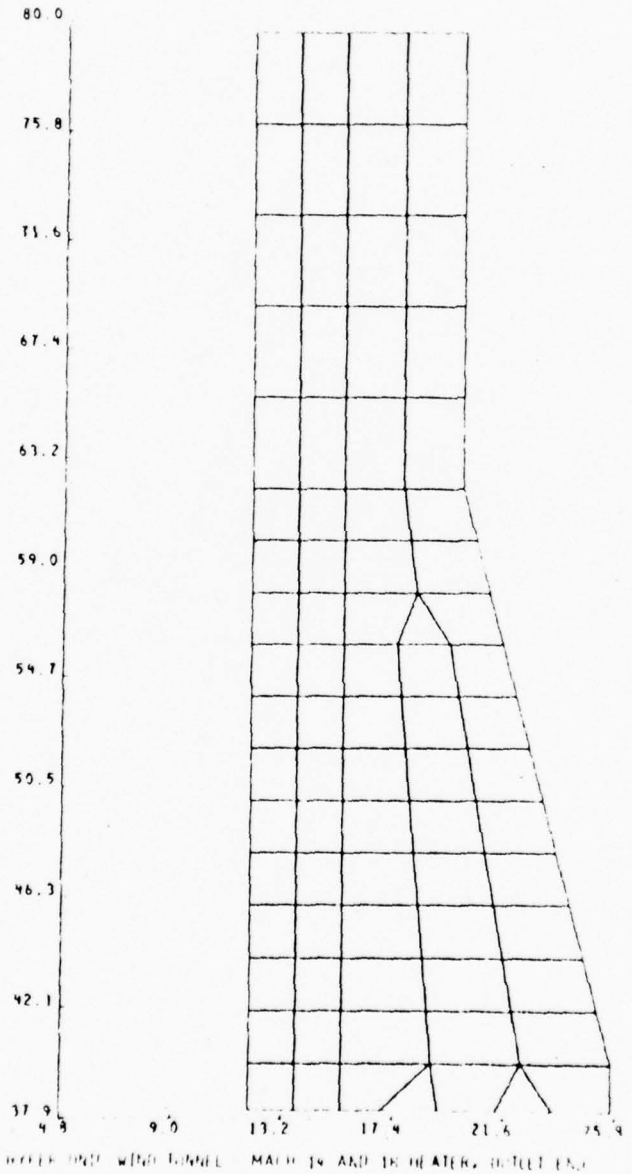

Figure 36

SECTION 2 OF MACH 14/18 HEATER VESSEL
OUTLET END

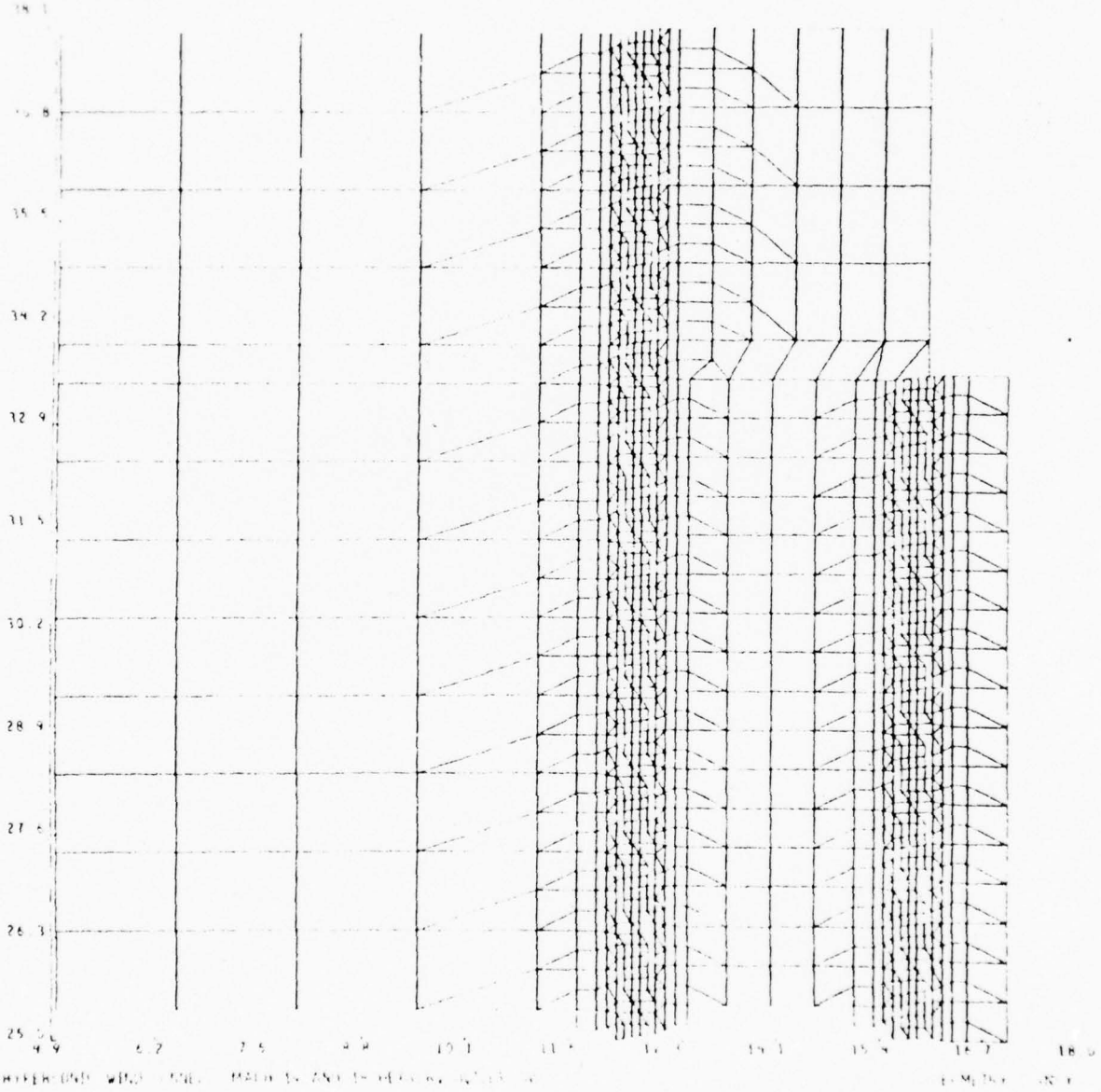

Figure 37

SECTION 3 OF MACH 14/18 HEATER VESSEL
OUTLET END

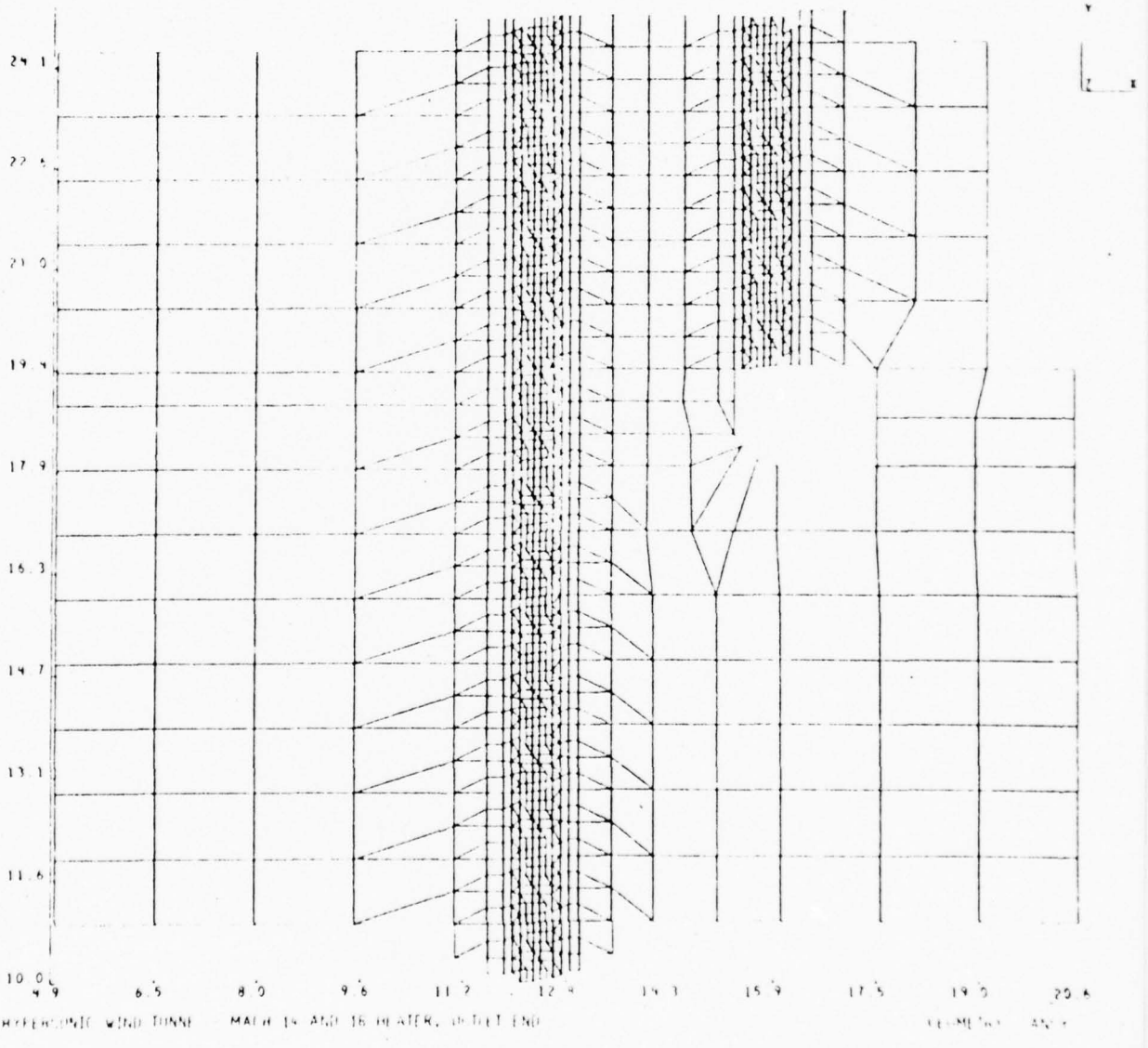

Figure 38

SECTION 4 OF MACH 14/18 HEATER VESSEL
OUTLET END

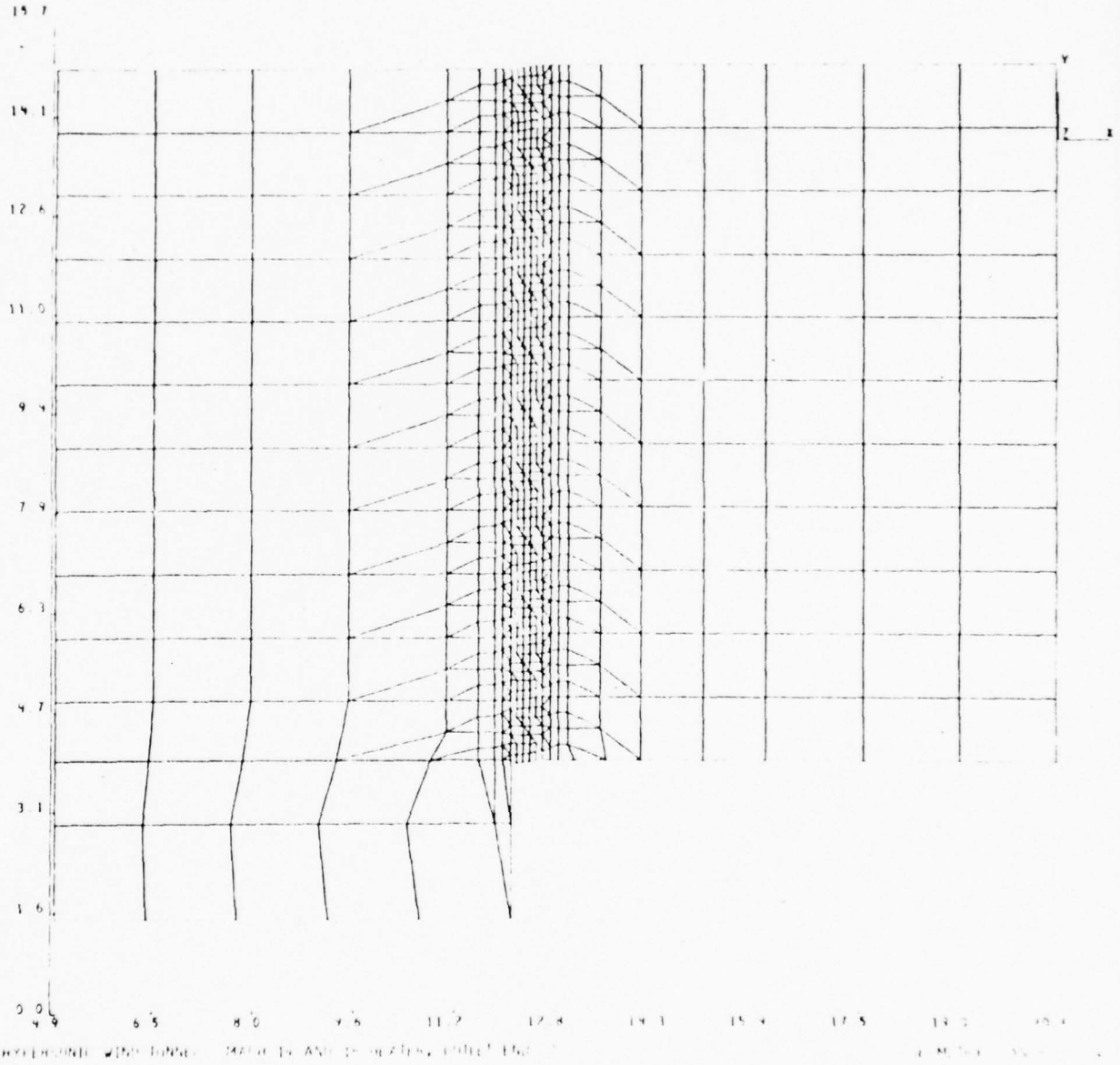

Figure 39

TYPICAL COARSE MODEL OF FEMALE TOOTH

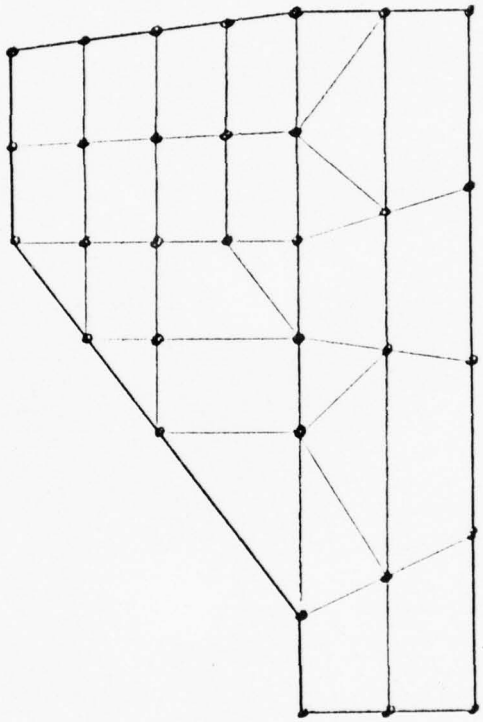

Figure 40

TYPICAL COARSE MODEL OF MALE TOOTH

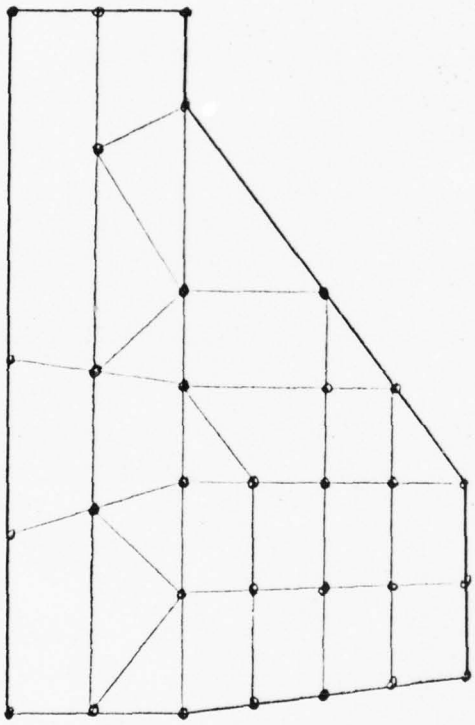

Figure 41

5.2.5 DETAILED THREAD MODEL FOR TOP END OF MACH 14/18 HEATER VESSEL

A detailed model of an individual tooth was used to determine the detailed stress state existing in the most severely loaded teeth. This model is shown in Figure 42. The imposed loadings and boundary displacements were handled in the same manner as described in Section 5.2.3.

5.3 DRIVER VESSEL MODELS FOR ORIGINAL DESIGN

The finite element models used to analyze the original driver vessel design are described in the following subsections.

5.3.1 OVERALL MODEL FOR INLET END OF DRIVER VESSEL

A finite element model of the inlet end closure on the driver vessel was prepared and used in conjunction with the ANSYS computer program, Reference 5, to calculate the maximum loads and stresses in this closure due to the internal operating pressure loading. A computer-drawn scale plot of this overall model is shown in Figure 43. This model is made up of many two-dimensional isoparametric (STIF 42) elements. The model consists of five parts--the liner, the main cylinder, the outer ring, the nut, and the cover. There is a shrink fit of 0.021" on the radius between the liner and the main cylinder. There is a shrink fit of 0.010" on the radius between the outer ring and the main cylinder. The liner, main cylinder, and outer ring are shown in Figure 44. The nut is shown in Figure 45. The cover is shown in Figure 46.

The cylinder part was modeled to a distance of approxiately $\pi\lambda$ beyond the end of the taper on the cylinder, where λ is the attenuation length (see Figure 44):

$$\lambda = \frac{\sqrt{R_{mean}\, t}}{1.285}$$

where R_{mean} is the mean radius of the cylinder, and t is the thickness.

DETAILED MODEL OF BUTTRESS TOOTH

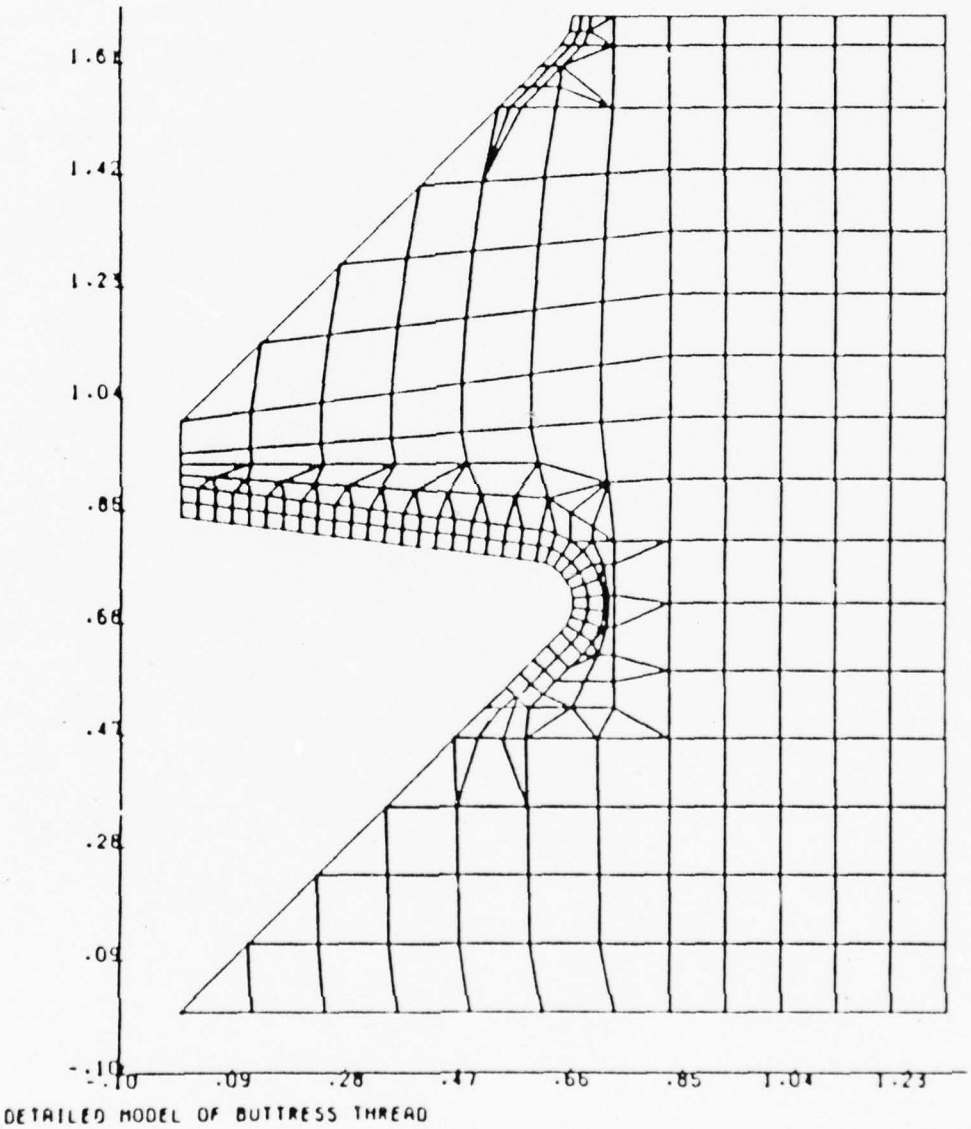

Figure 42

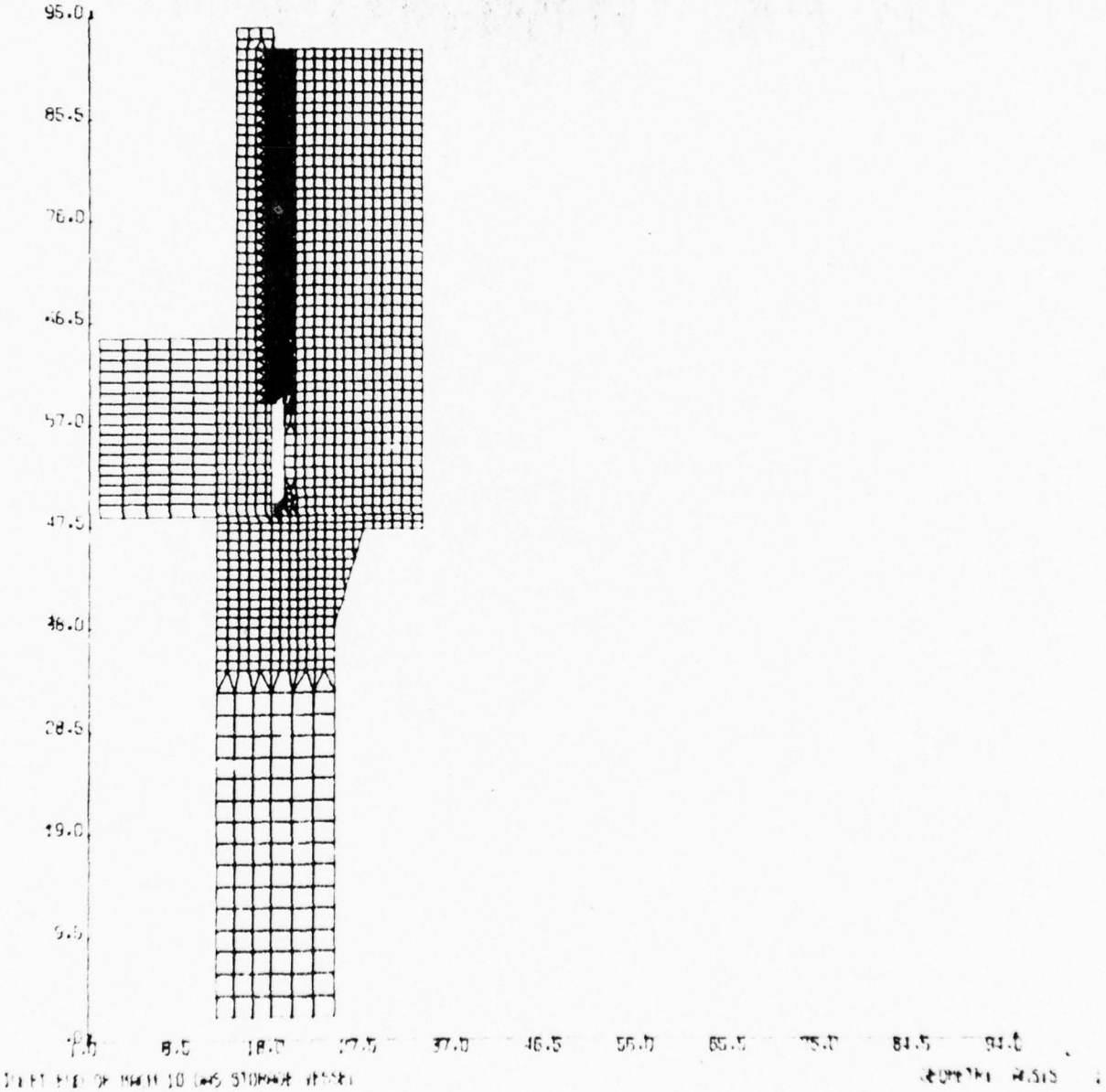

FIGURE 43 - OVERALL MODEL - INLET END OF DRIVER VESSEL

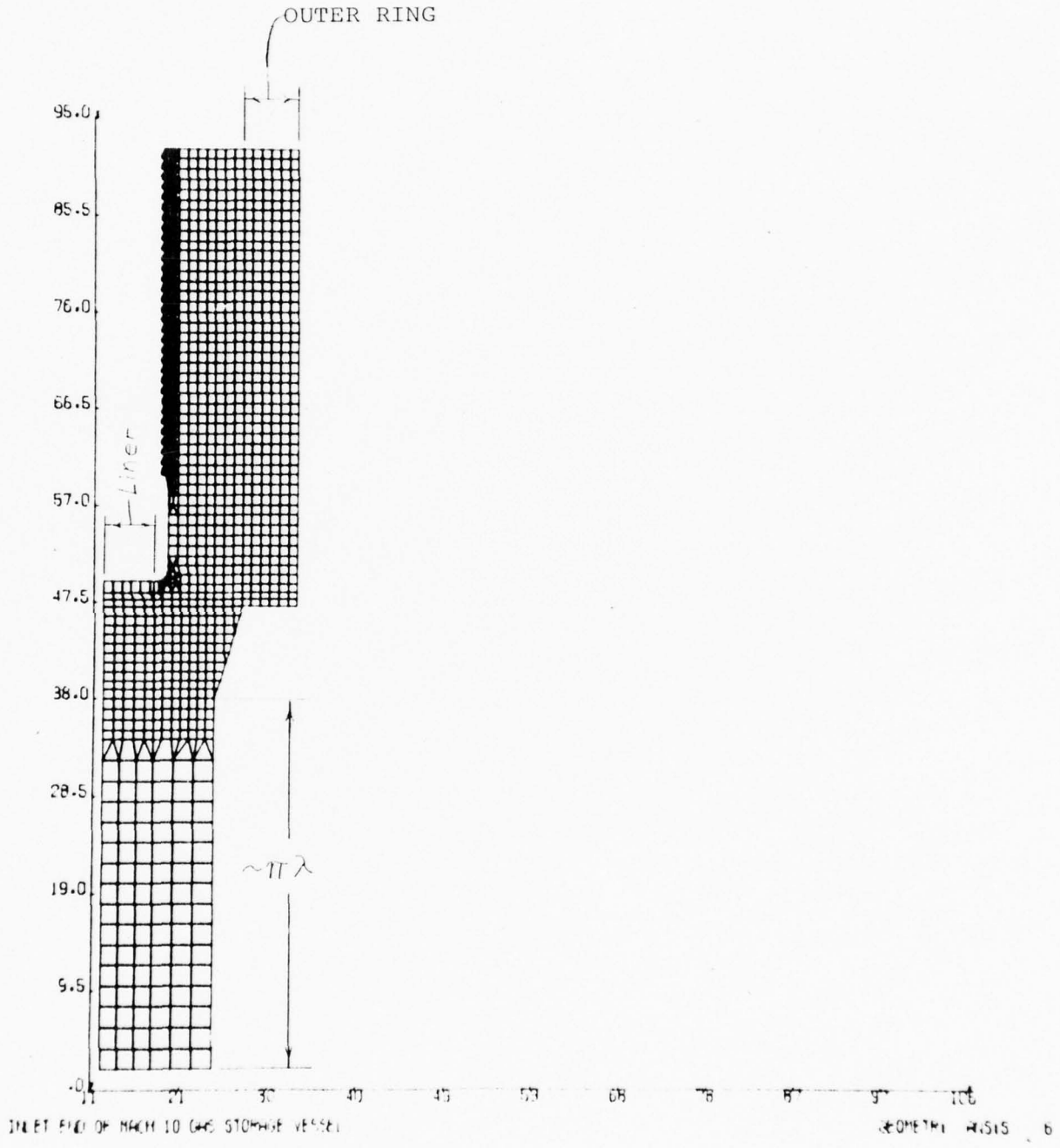

FIGURE 44 - LINER, MAIN CYLINDER, AND OUTER RING ON OVERALL - INLET END OF DRIVER VESSEL

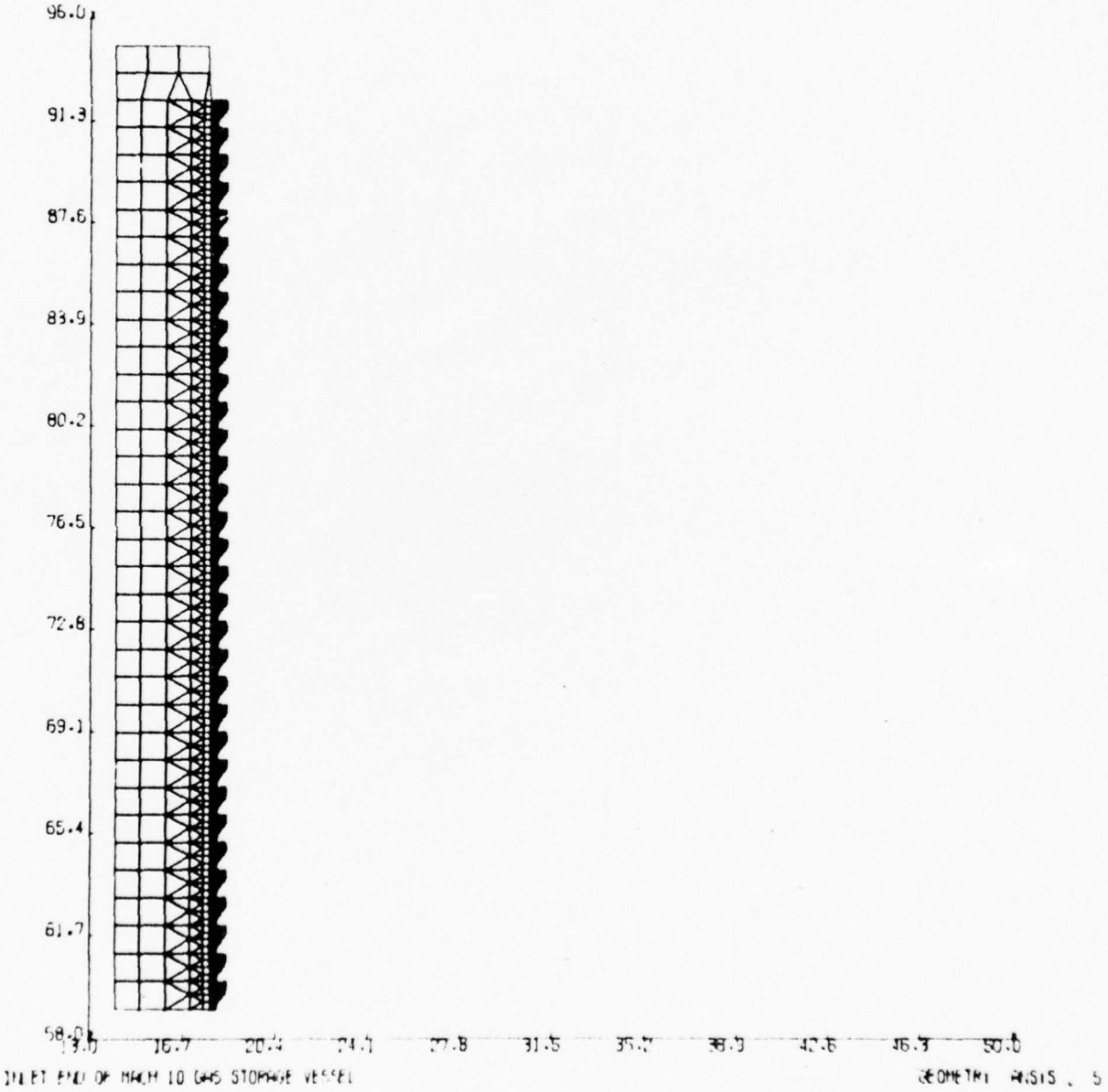

FIGURE 45 - NUT ON OVERALL MODEL - INLET END OF DRIVER VESSEL

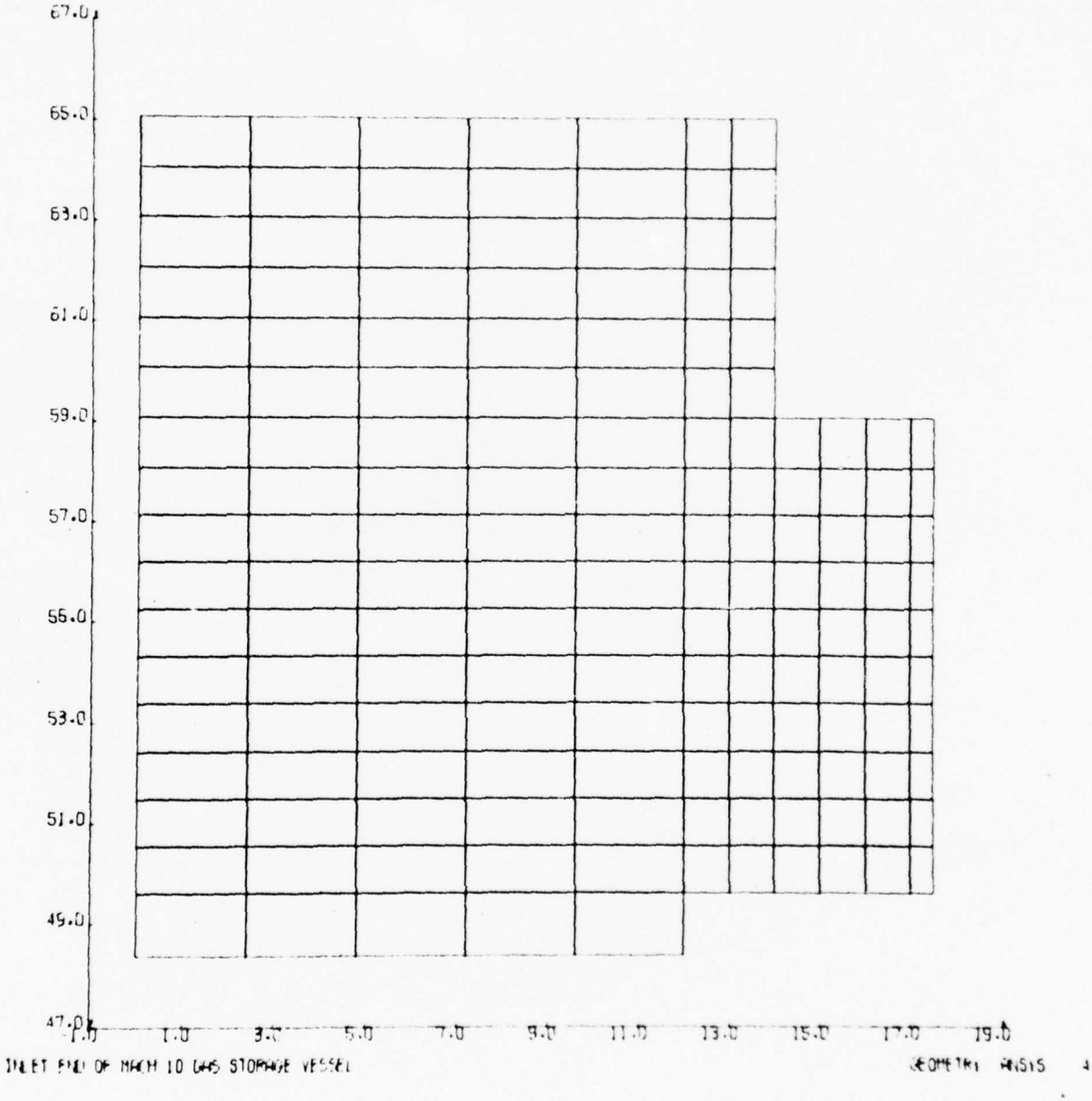

FIGURE 46 - COVER ON OVERALL MODEL - INLET END OF DRIVER VESSEL

As shown in the Figures, the nut and cylinder threads have been modeled individually. The nut threads alone are shown in Figure 45, and the cylinder threads are shown in Figure 44. Typical nut and cylinder threads are shown in Figures 47 and 48, respectively. A detail of one cylinder thread is shown in Figure 49, and a detail of one nut thread is shown in Figure 50. The meshing of the first nut and cylinder thread is shown in Figure 51. The meshing of the threads shown in Figure 51 is typical for all of the threads.

The mating pairs of nodes at the nut to cylinder thread intersection are specified to have the same displacements in the direction perpendicular to the thread tooth surface. This transmits the load from one thread tooth to the other with no sliding friction between mating threads.

An internal pressure of 60,000 psi was applied to the inside surfaces of the overall model. The load on each of the individual threads was then obtained from the computer results. The resulting maximum thread load was then used to calculate the maximum stress in the threads of the inlet end closure by ratioing the stress results obtained from the detailed thread model for the maximum load on the outlet end closure threads.

5.3.2 DETAILED THREAD MODEL OF FIRST THREAD ON INLET END OF DRIVER VESSEL

A computer-drawn scale plot of the detailed thread model for the first thread with an elliptical undercut for the driver vessel is shown in Figure 52. This model is made up of many two-dimensional isoparametric (STIF 42) elements. The thread load on the first thread from the overall model was converted into an equivalent pressure load and applied to the tooth surface on the detailed model (see Appendix 7A). The displacements from the overall model in the vicinity of the first thread were applied as boundary conditions on the edges of this detailed model. This detailed model was used to calculate the maximum stresses in the

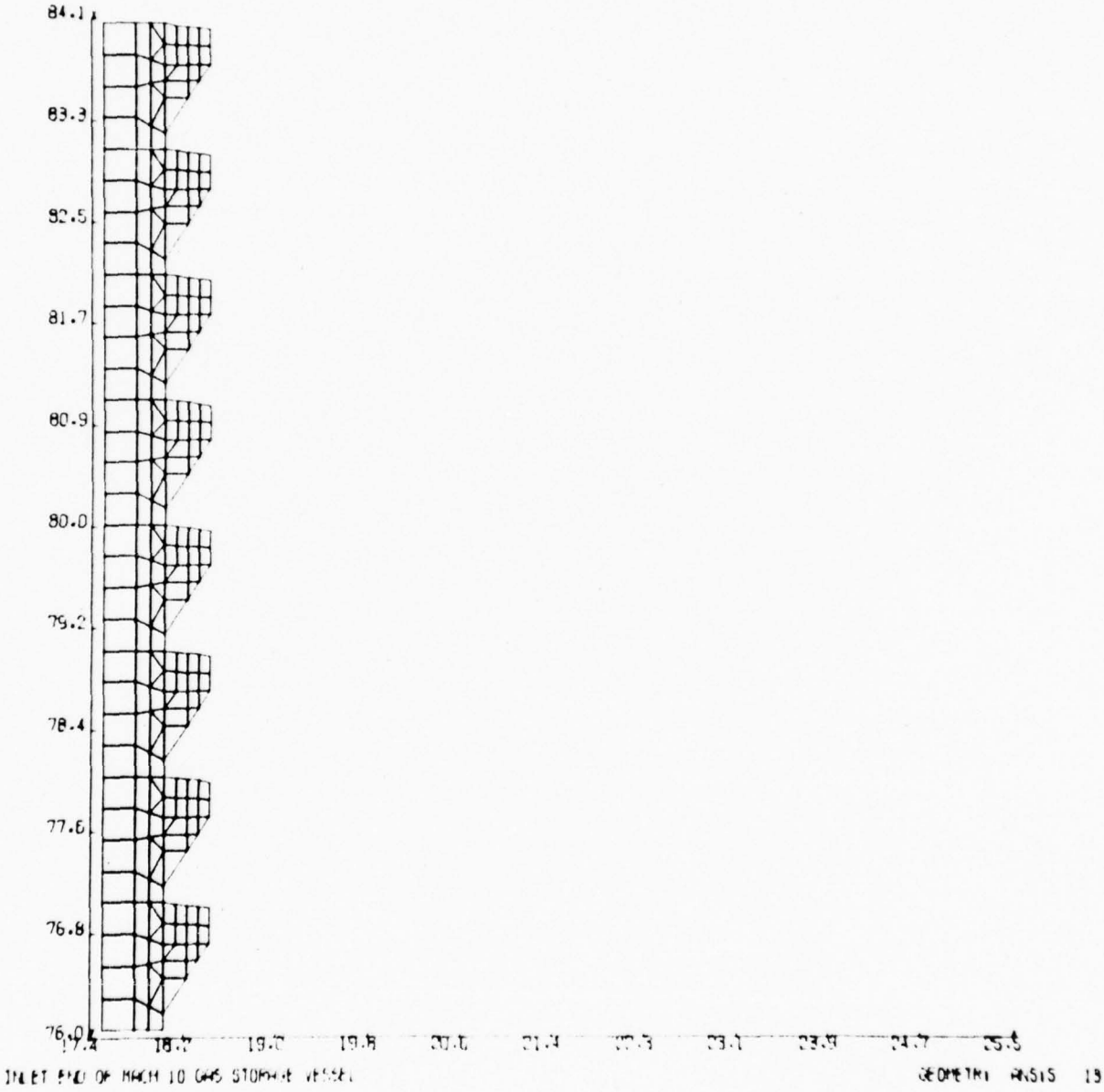

FIGURE 47 - TYPICAL THREADS ON NUT OF OVERALL MODEL - INLET END OF DRIVER VESSEL

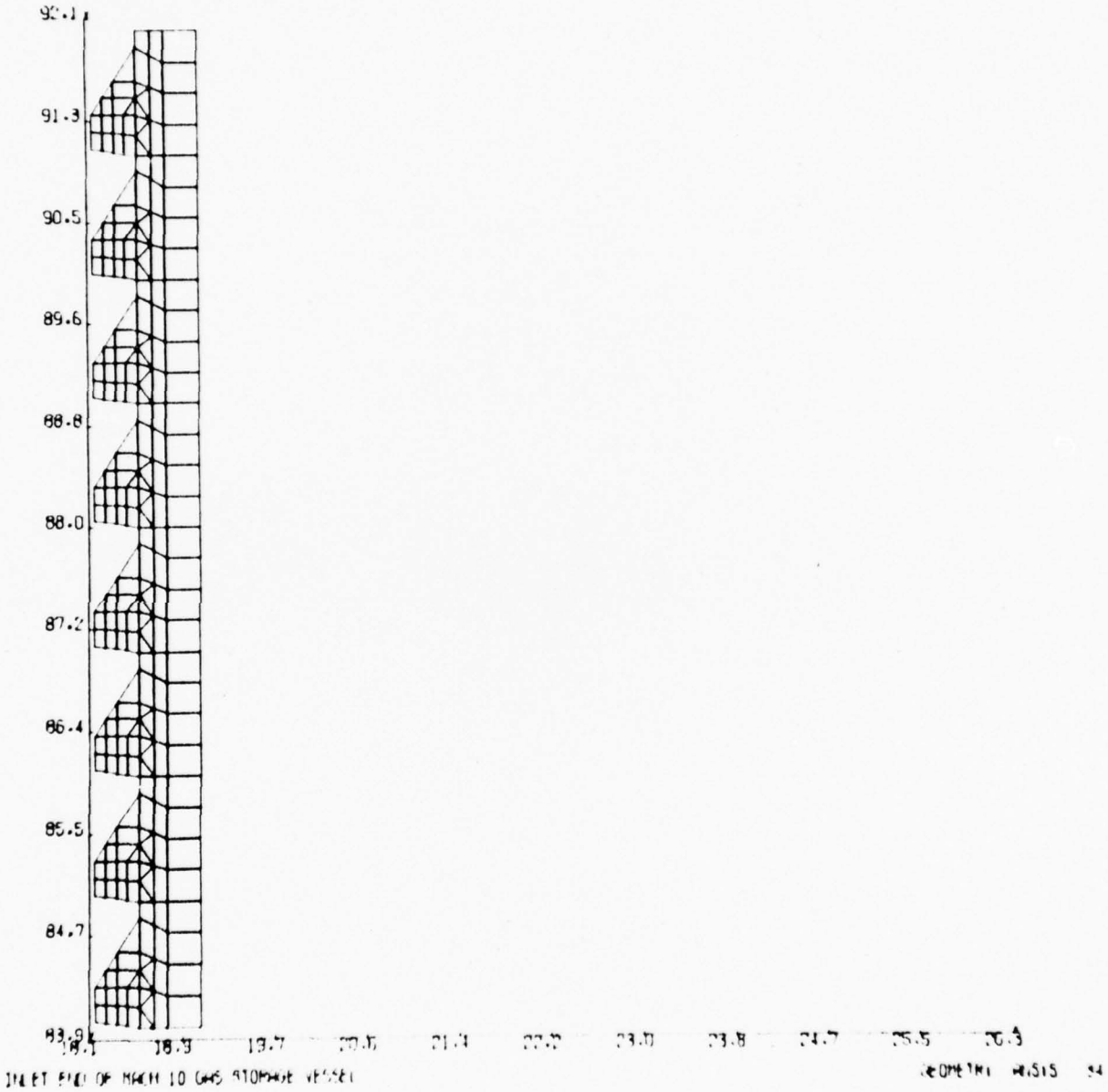

FIGURE 48 - TYPICAL THREADS ON CYLINDER OF OVERALL MODEL - INLET END OF DRIVER VESSEL

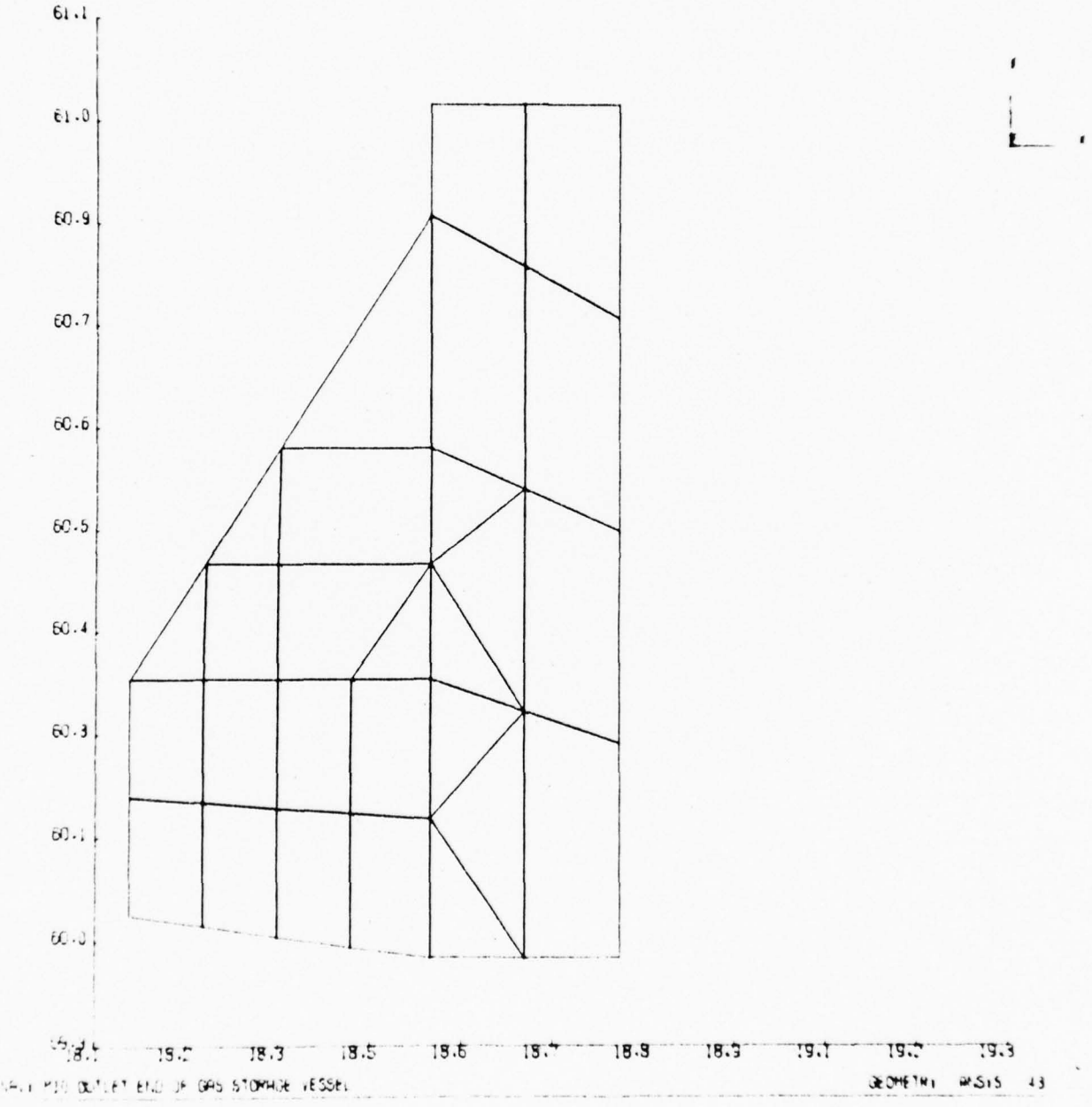

FIGURE 49 - DETAIL OF ONE CYLINDER THREAD ON OVERALL MODEL - OUTLET END OF DRIVER VESSEL

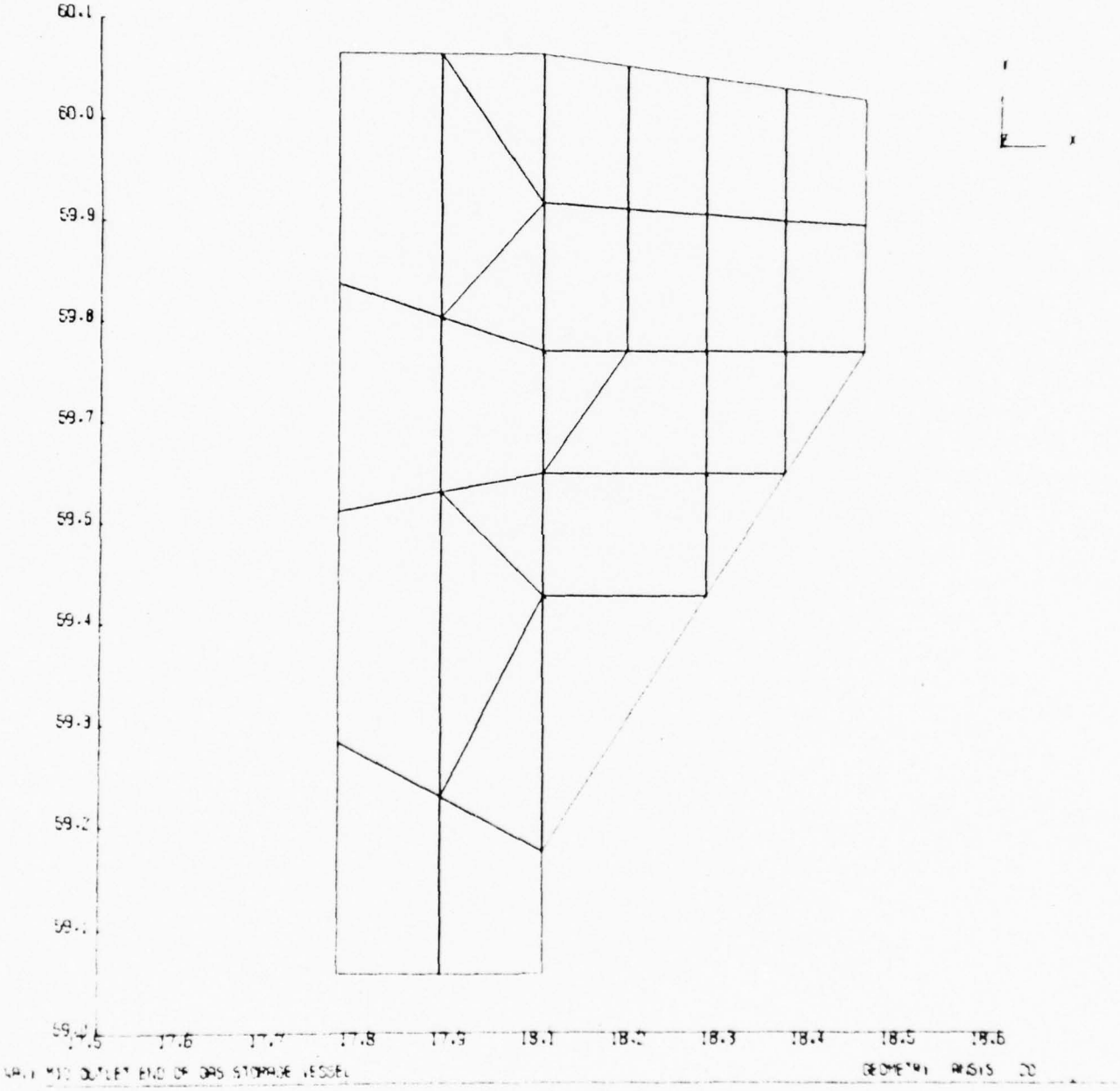

FIGURE 50- DETAIL OF ONE NUT THREAD ON OVERALL MODEL - OUTLET END OF DRIVER VESSEL

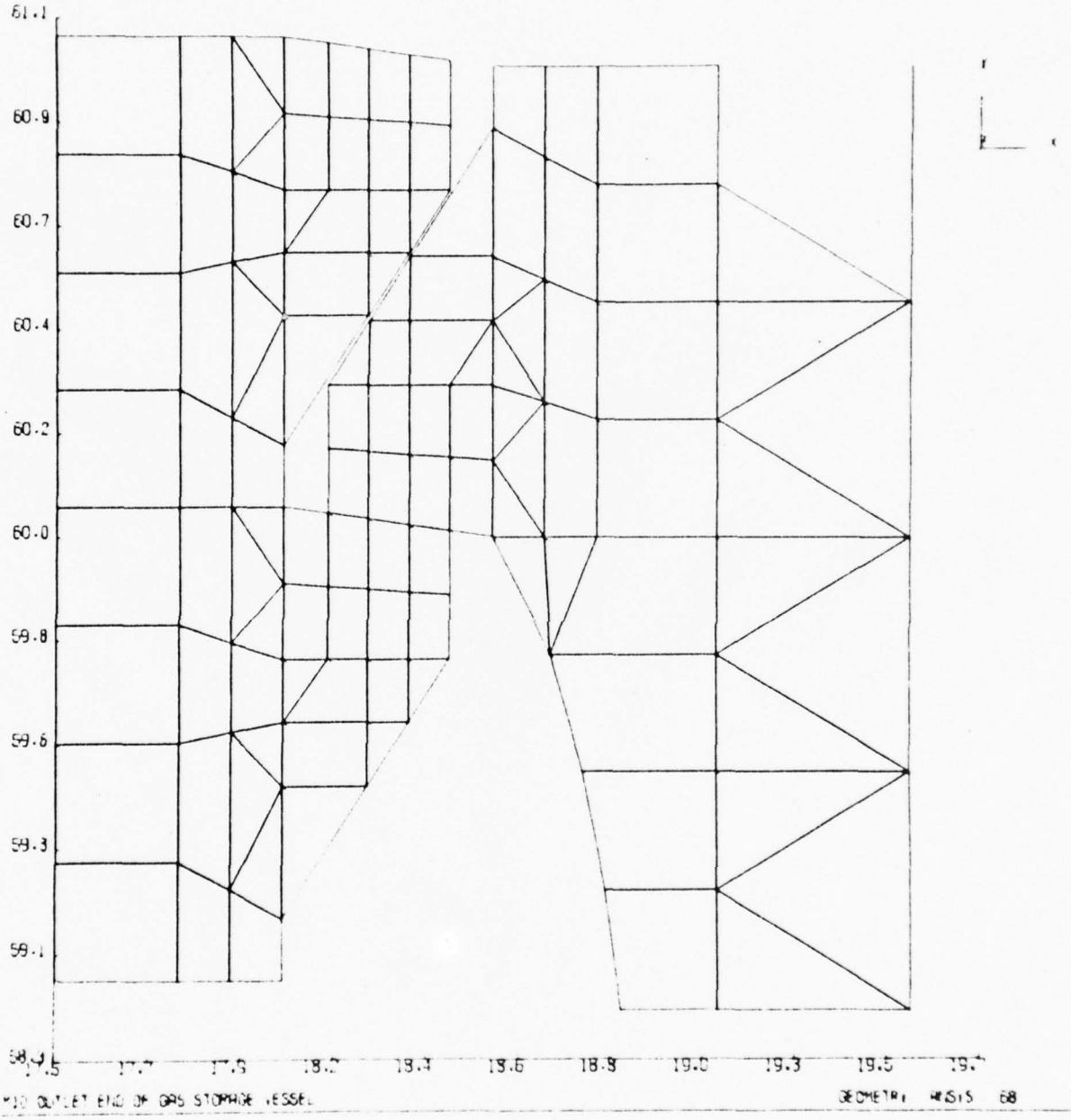

FIGURE 51 - INTERSECTION OF FIRST NUT AND CYLINDER THREAD ON OVERALL MODEL - OUTLET END OF DRIVER VESSEL

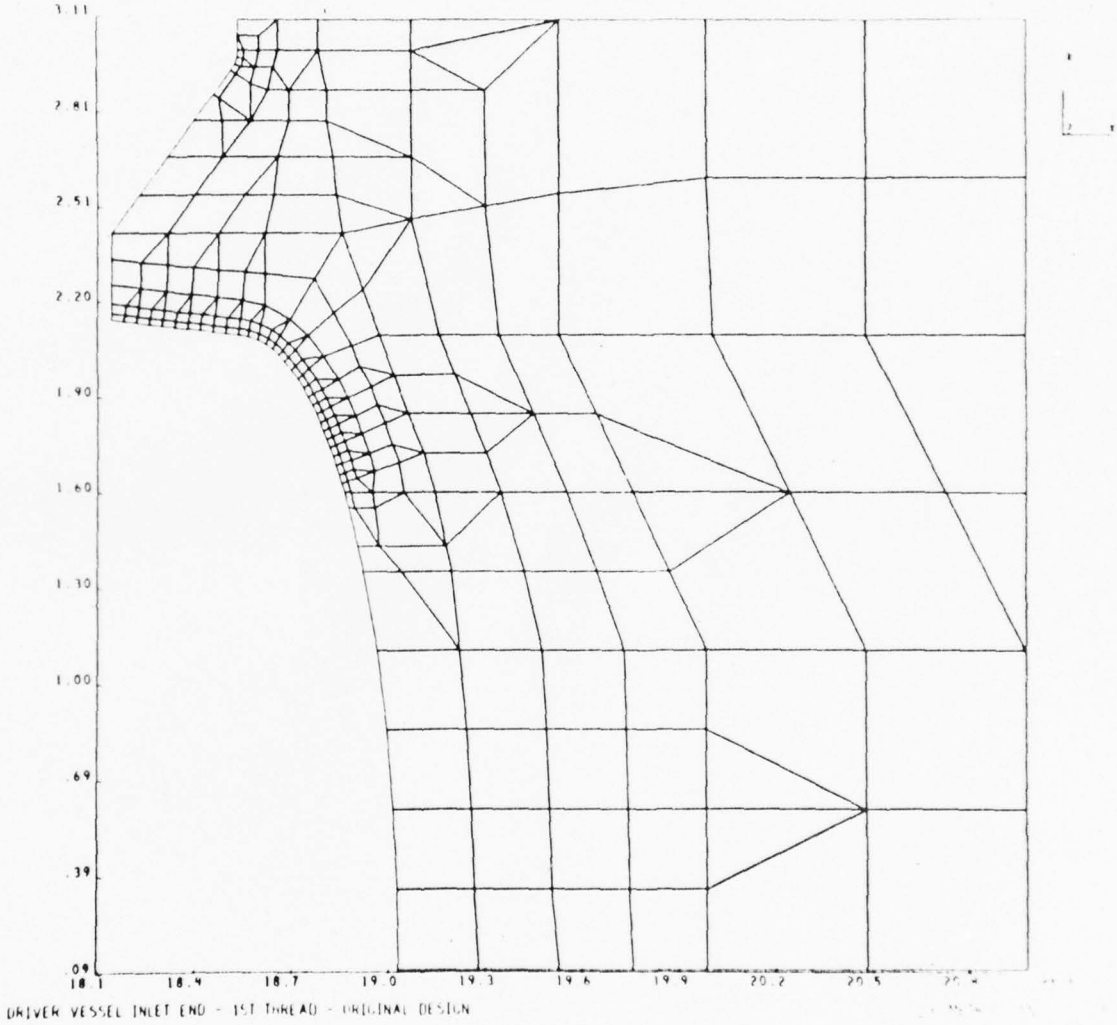

Figure 52 - Detailed Thread Model of First Thread With Elliptical Undercut For Driver Vessel

elliptical undercut region of the first thread on the Driver Vessel Inlet End Closure.

5.3.3 DETAILED THREAD MODEL OF A TYPICAL THREAD FOR DRIVER VESSEL

This detailed model was used to calculate the maximum stresses in the thread root for both the outlet and inlet end closures. The maximum thread load on the outlet end closure was applied to this model, and the resulting maximum stress at the thread root on the outlet end was calaculated using the ANSYS computer program. The maximum stress in the thread root for the inlet end was obtained by ratioing the stress results obtained for the outlet end using the maximum thread load obtained from the overall model of the inlet end closure.

A computer-drawn scale plot of the detailed thread model for the gas storage vessel is shown in Figure 53. This model is made up of many two-dimensional isoparametric (STIF 42) elements. The maximum thread load on the overall model was converted into an equivalent pressure load and applied to the tooth surface on the detailed model (see Appendix 5B). The displacements from the overall model in the vicinity of the thread where the maximum thread load occurs were applied as boundary conditions on the edges of this detailed model.

5.3.4 OVERALL MODEL FOR OUTLET END OF DRIVER VESSEL

A finite element model of the outlet end closure on the driver vessel was prepared and used in conjunction with the ANSYS computer program, Reference 5, to calculate the maximum loads and stresses in this closure due to the internal operating pressure loading. A computer-drawn scale plot of this overall model is shown in Figure 54. The model consists of five parts--the liner, the main cylinder, the outer ring, the nut, and the cover. There is a shrink fit of 0.021" on the radius between the liner and the main cylinder. There is a shrink fit of 0.010" on the radius

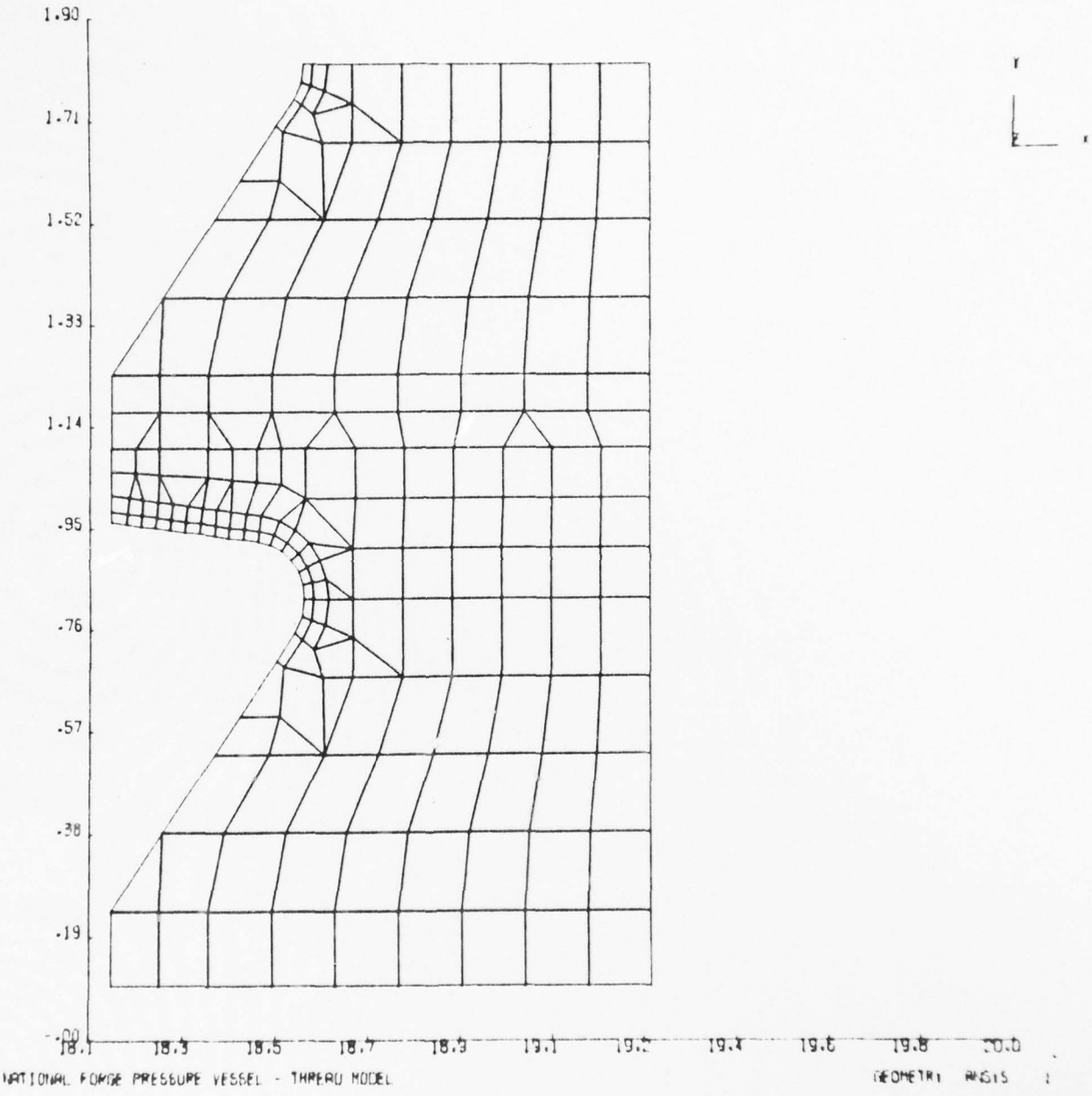

FIGURE 53- DETAILED THREAD MODEL FOR DRIVER VESSEL

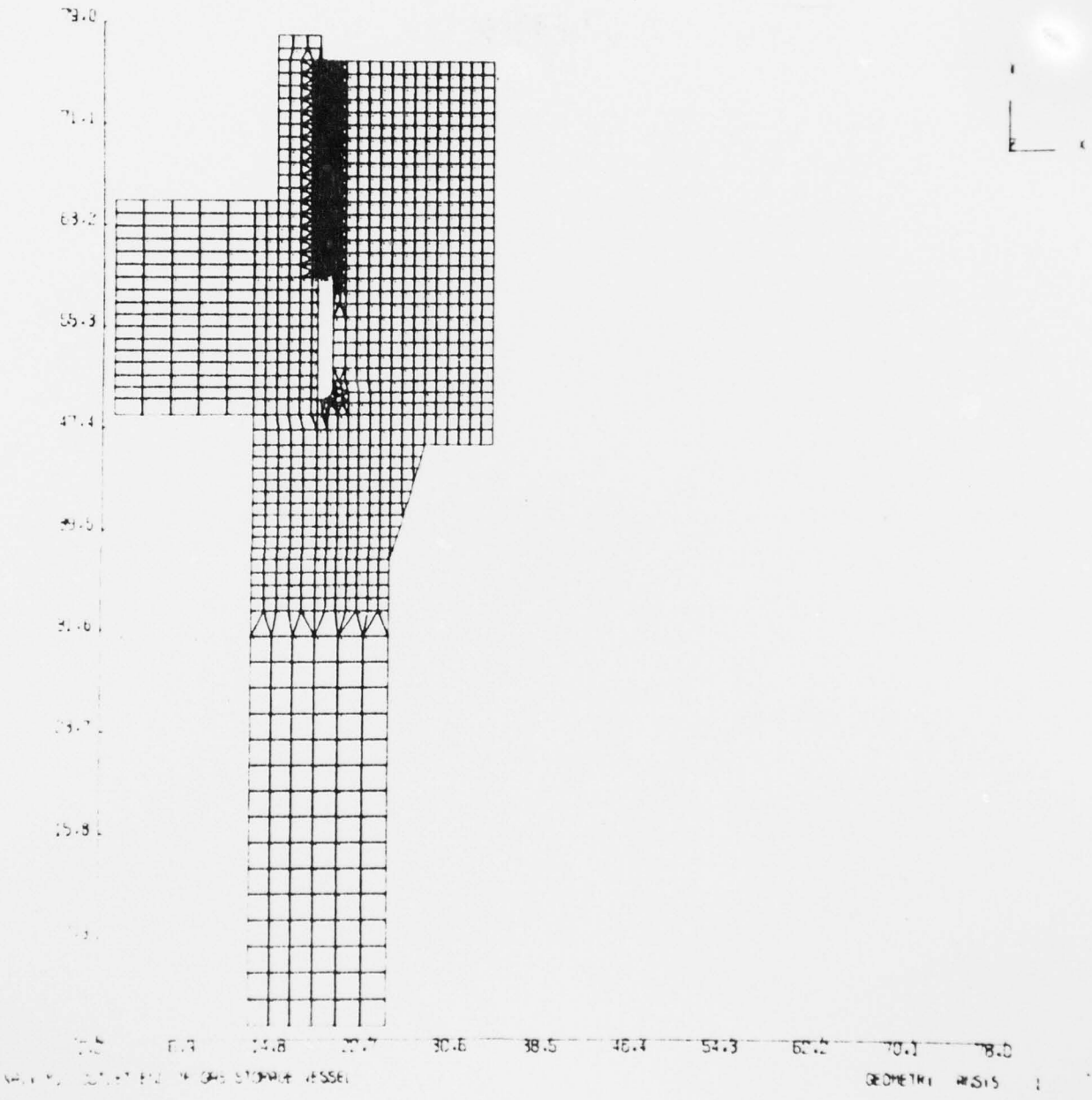

FIGURE 54- OVERALL MODEL - OUTLET END
OF DRIVER VESSEL

between the outer ring and the main cylinder. The liner, main cylinder, and outer ring are shown in Figure 55. The nut is shown in Figure 56. The cover is shown in Figure 57. This model consists of many isoparametric (STIF 42) elements.

The cylinder part was modeled to a distance of approximately $\pi\lambda$ beyond the end of the taper on the cylinder, where λ is the attenuation length (see Figure 55):

$$\lambda = \frac{\sqrt{R_{mean} t}}{1.285}$$

where R_{mean} is the mean radius of the cylinder, and t is the thickness.

As shown in the Figures, the nut and cylinder threads have been modeled individually. The nut threads alone are shown in Figure 56, and the cylinder threads are shown in Figure 58. A detail of one cylinder thread is shown in Figure 49, and a detail of one nut thread is shown in Figure 50. The meshing of the first nut and cylinder thread is shown in Figure 51. The thread meshing shown in Figure 51 is typical. The mating pairs of nodes between the nut and cylinder threads are specified to have the same displacements in the direction perpendicular to the tooth surface. This transmits the load from one thread tooth to the other without any friction between mating threads.

An internal pressure of 60,000 psi was applied to the inside surfaces of the overall model. The load on each of the individual threads was then obtained from the computer results. The resulting maximum thread load was then converted into an equivalent uniform load and applied to the tooth surface on the detailed thread model. In addition, displacements from the overall model in the vicinity of the thread where the maximum thread load occurs were applied as boundary conditions on the edges of the detailed model.

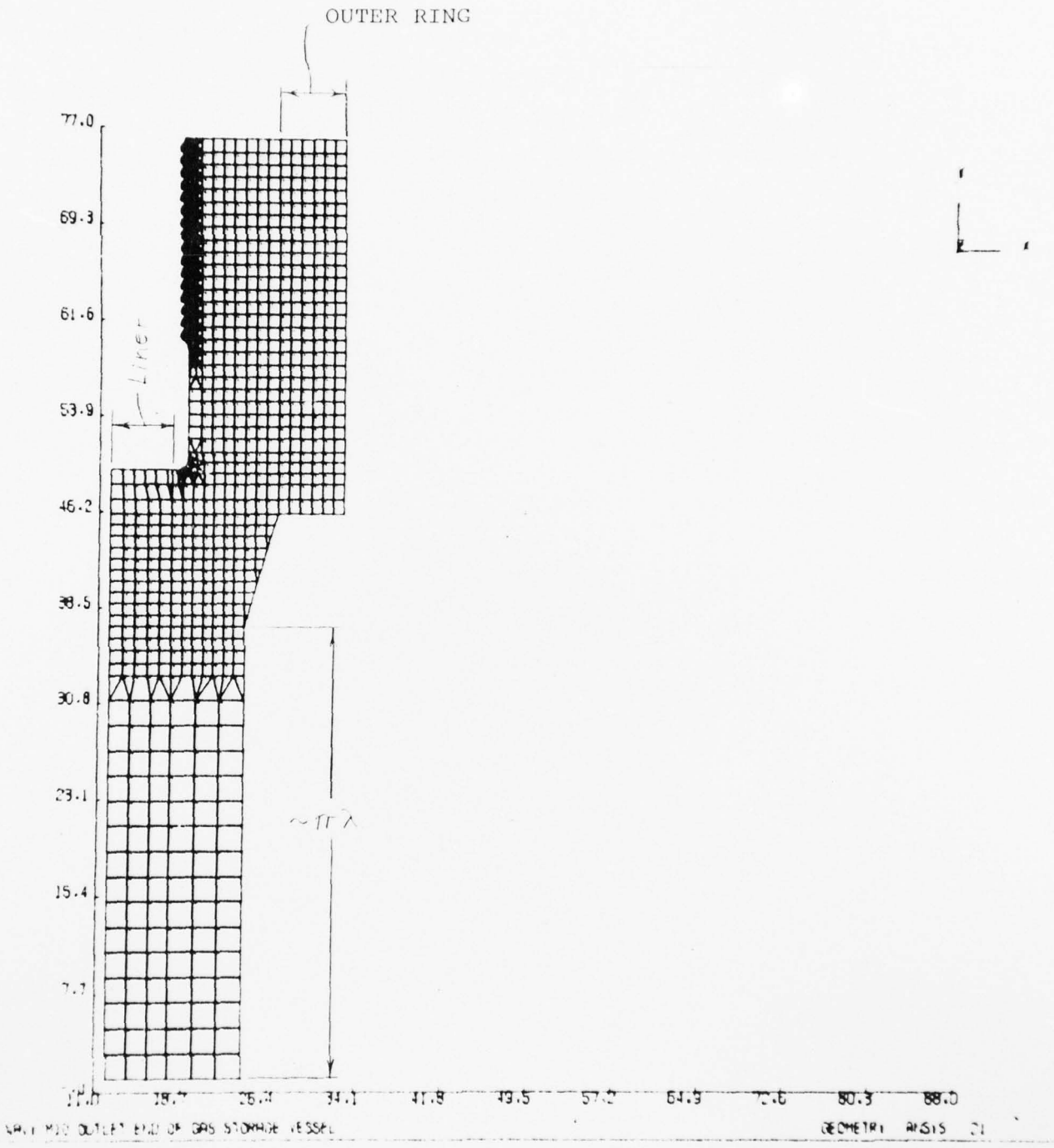

FIGURE 55- LINER, MAIN CYLINDER, AND OUTER RING ON OVERALL MODEL - OUTLET END OF DRIVER VESSEL

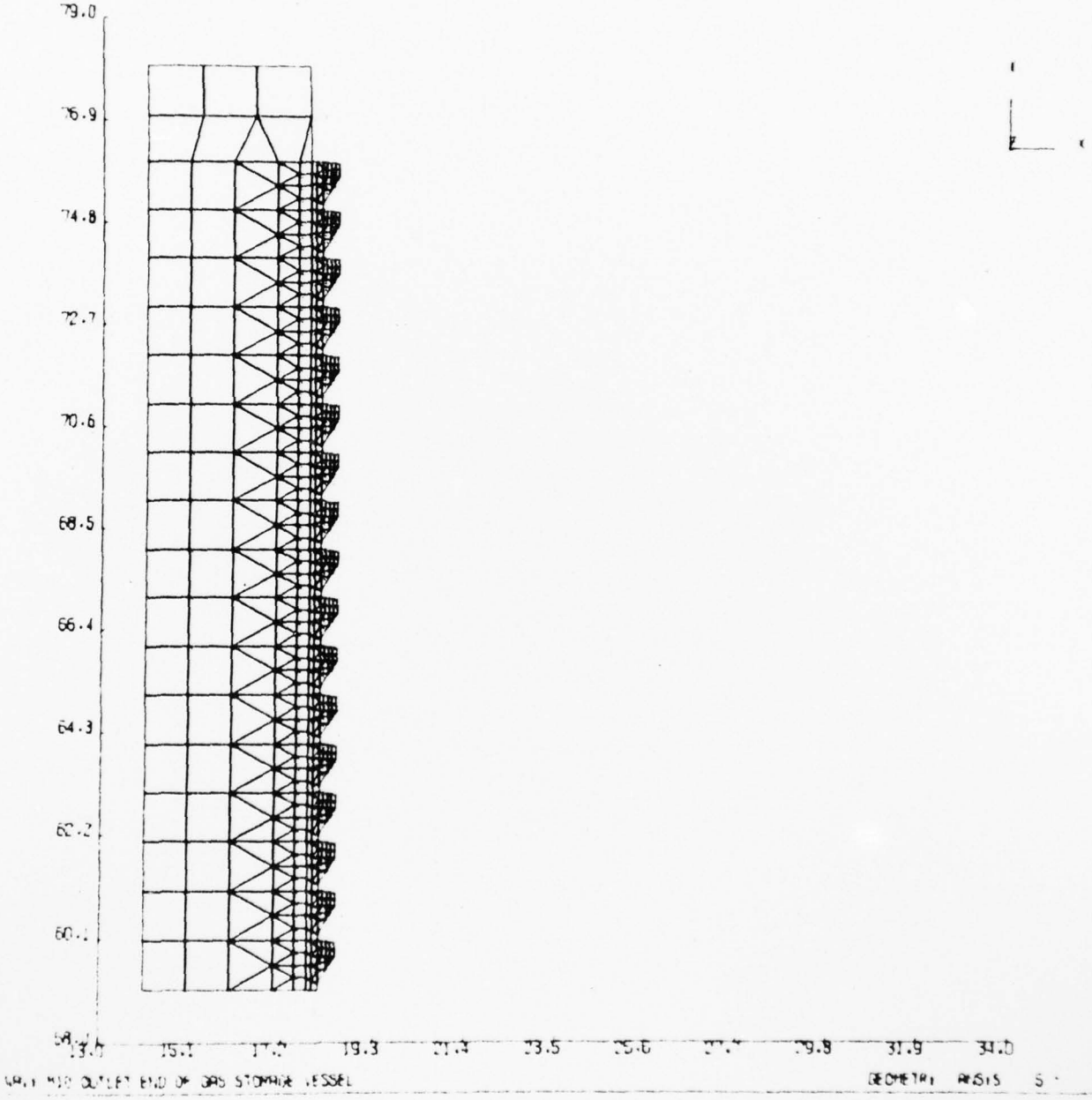

FIGURE 56- NUT ON OVERALL MODEL - OUTLET END OF DRIVER VESSEL

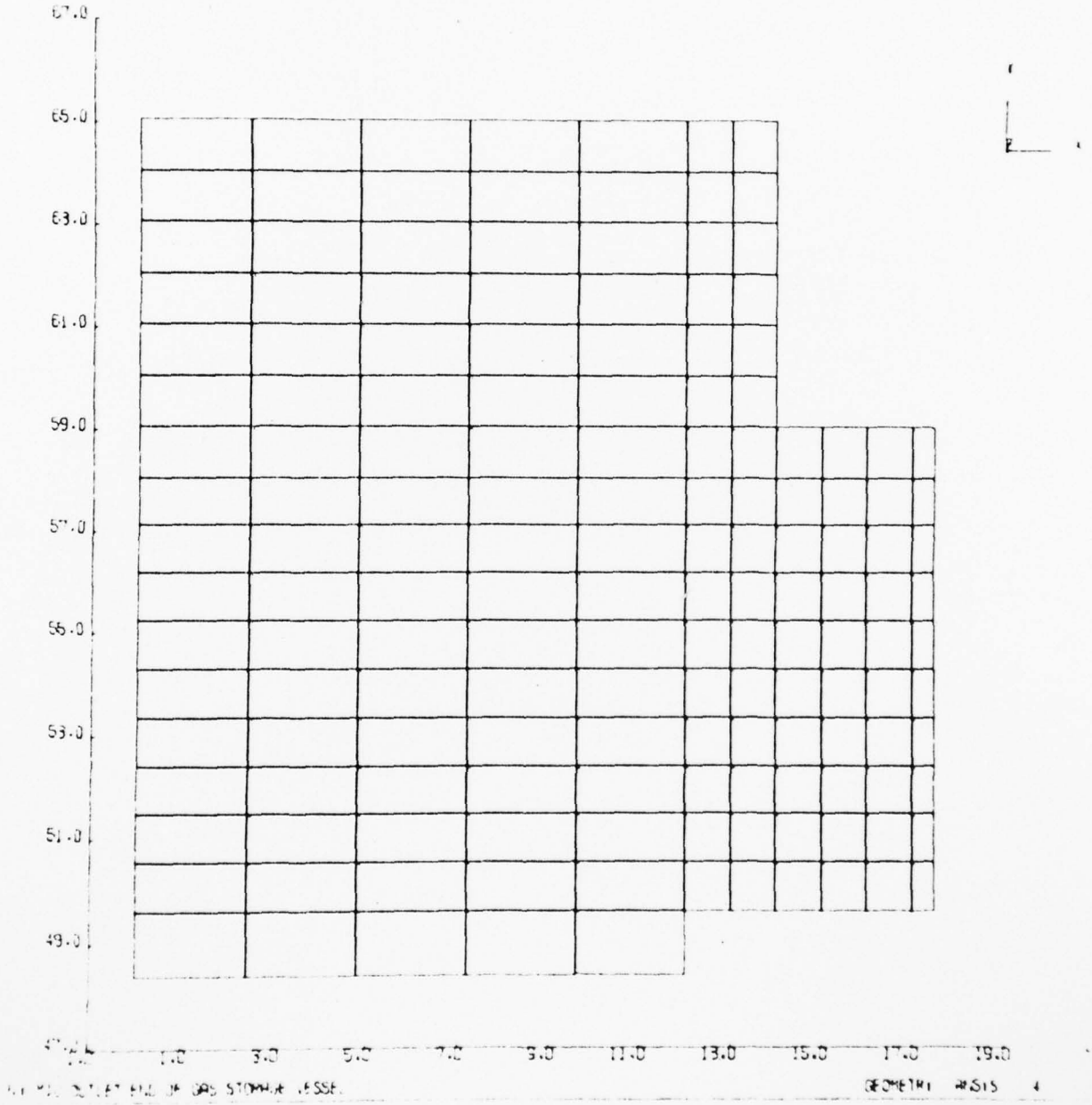

FIGURE 57- COVER ON OVERALL MODEL -
OUTLET END OF DRIVER VESSEL

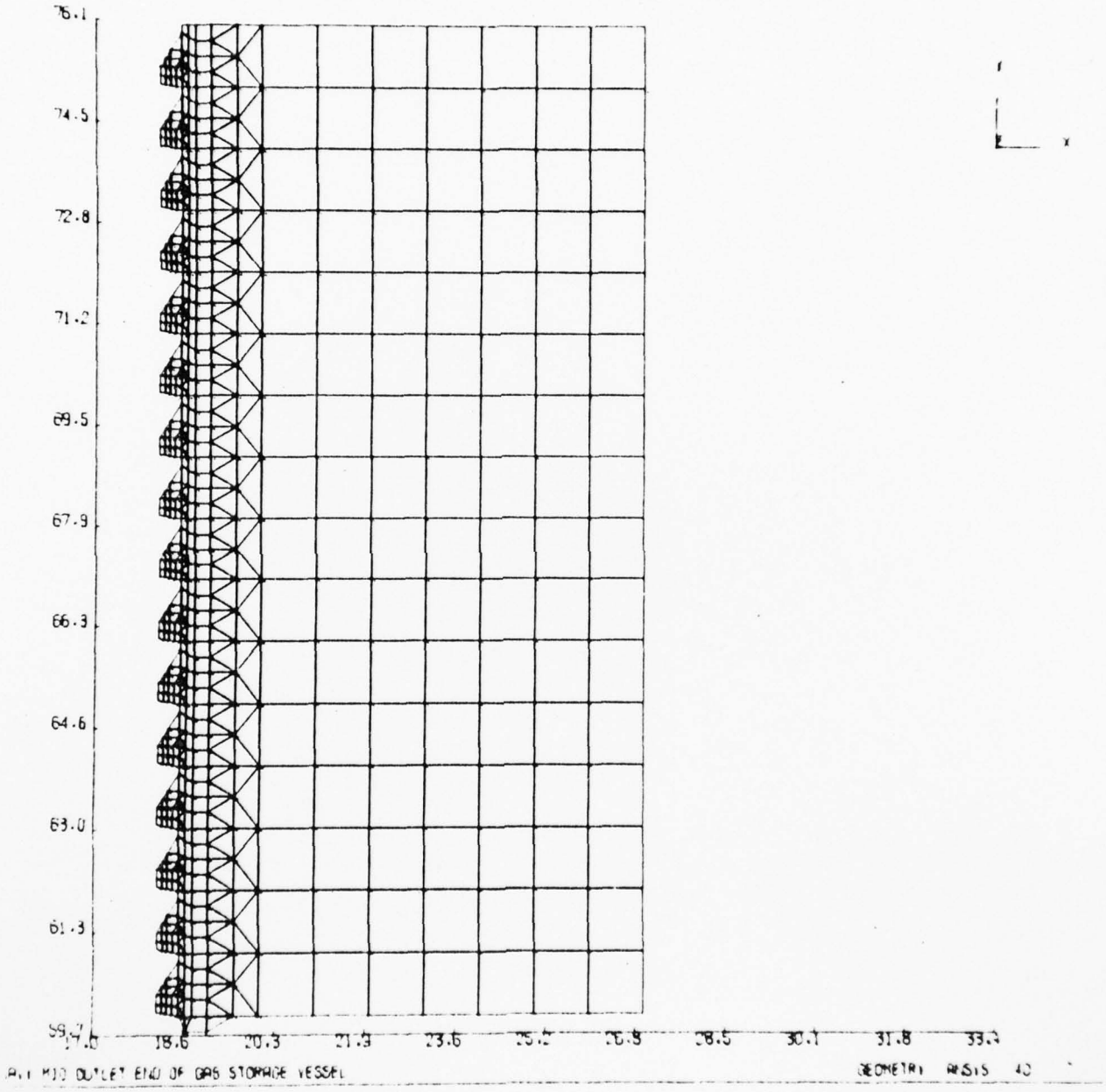

FIGURE 58- THREADED PORTION OF MAIN CYLINDER ON OVERALL MODEL - OUTLET END OF DRIVER VESSEL

5.4 MACH 14/18 HEATER VESSEL MODELS FOR DESIGN MODIFICATIONS

The finite elements models used to analyze two different design modifications that were made to increase the design life of the bottom end closure on the MACH 14/18 Heater Vessel are described in the following subsections.

5.4.1 DESCRIPTION OF DESIGN MODIFICATIONS

Two different bottom end design modifications, which utilize various undercut configurations on the inside end of the main nut on the bottom end of the MACH 14/18 Heater Vessel, were evaluated. The Rev. 1 design modification is shown in Figure 59. The Rev. 2 design modification is shown in Figure 60.

5.4.2 OVERALL MODELS OF BOTTOM END DESIGN MODIFICATIONS FOR MACH 14/18 HEATER VESSEL

The overall finite element model used in the original analysis (see Section 5.2.1) was modified in accordance with the revised designs. Figures 61 through 65 show the revised model for the Rev. 1 design modification. Figures 66 through 71 show the revised model for the Rev. 2 design modification. All other components of the overall model were unchanged from the original analysis.

5.4.3 DETAILED THREAD MODELS

The same detailed thread models as described in Sections 5.2.2 and 5.2.3 were used to calculate the maximum stresses in the threads for the design modifications on the MACH 14/18 Heater Vessel bottom end closure.

5.5 DRIVER VESSEL MODELS FOR DESIGN MODIFICATIONS

The finite element models used to analyze four different inlet end design modifications that were made to increase the design life of the driver vessel inlet end closure are described in the following subsections.

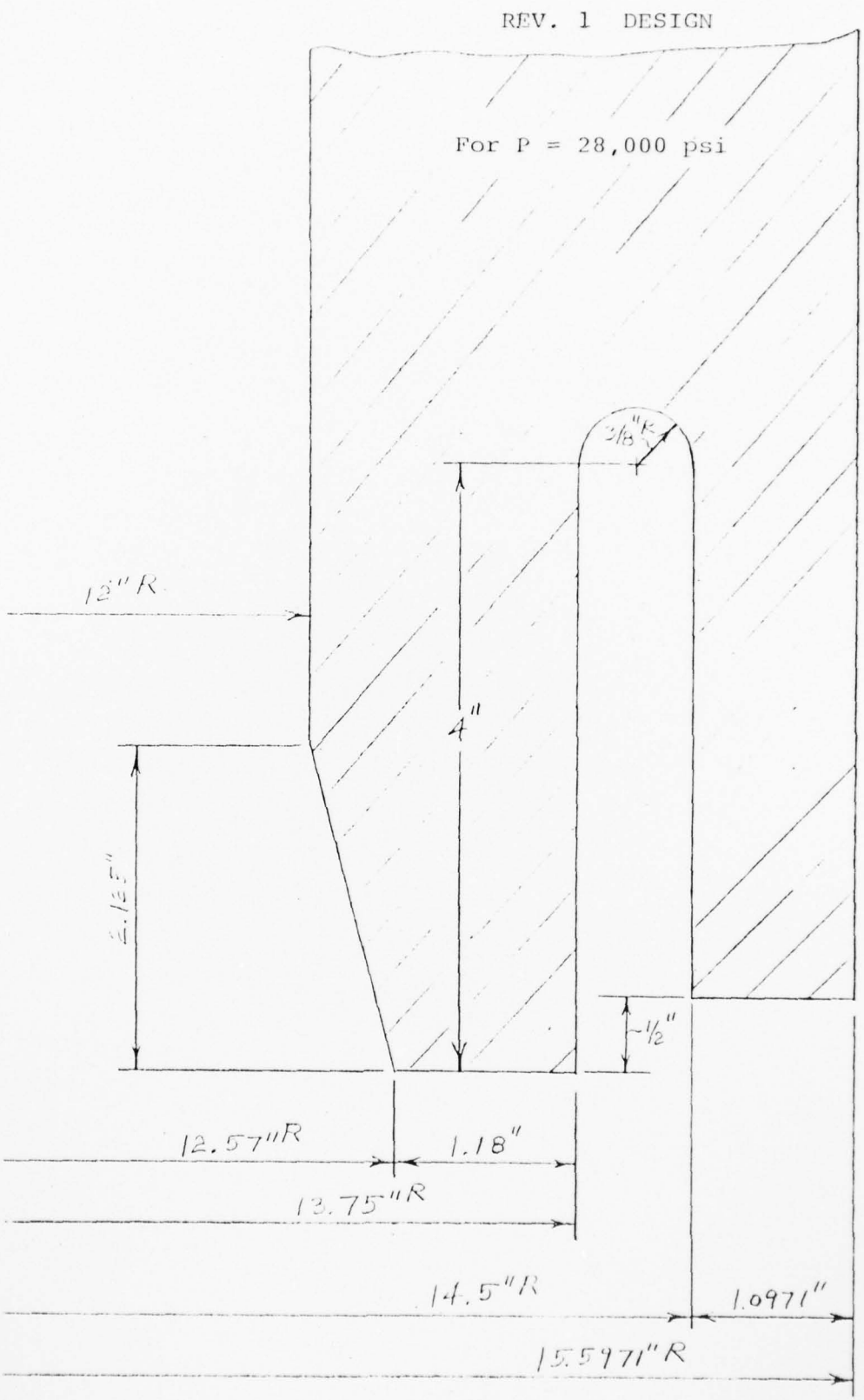

Figure 59
MACH 14/18 HEATER VESSEL REV. 1 DESIGN MODIFICATION

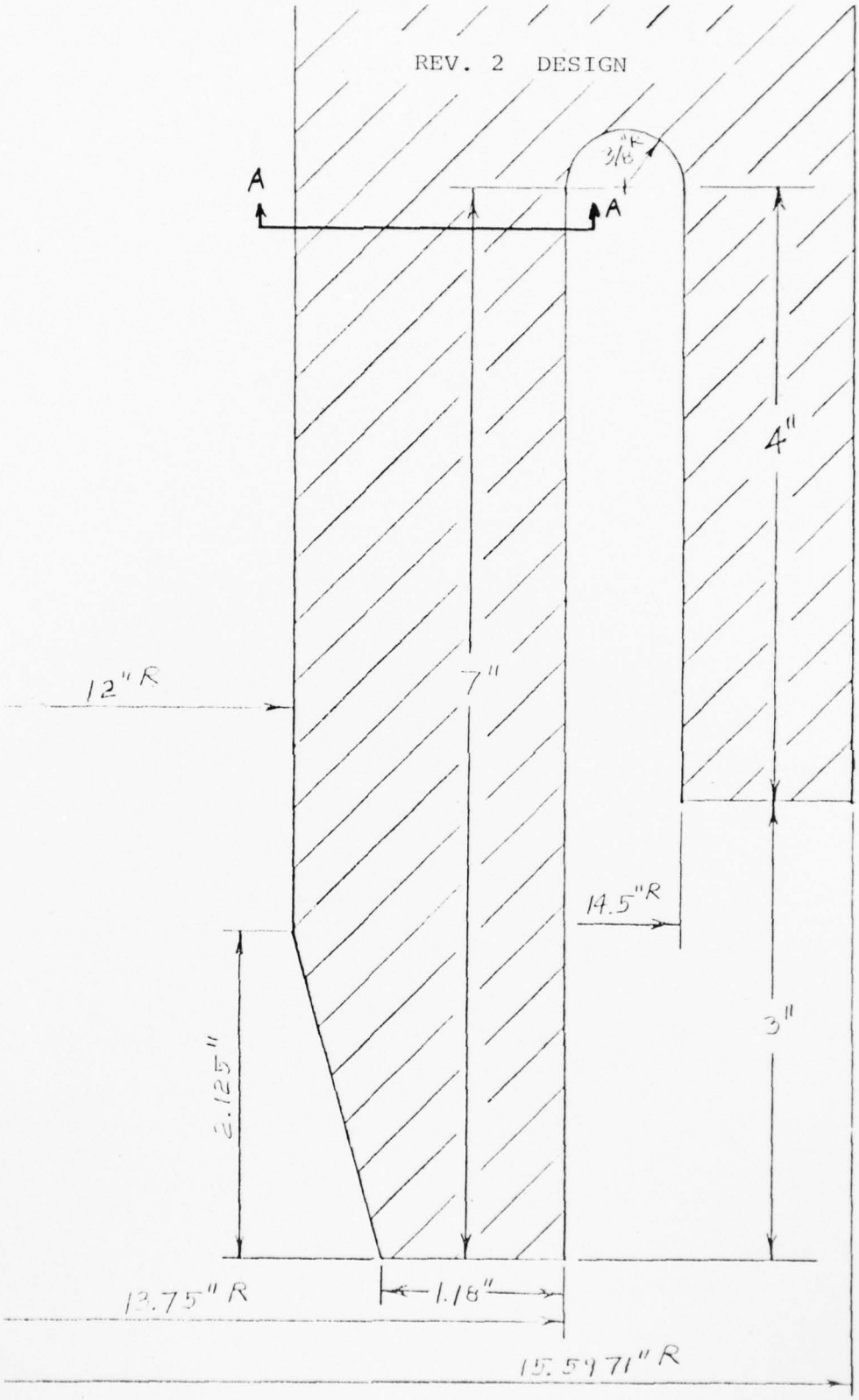

Figure 60
MACH 14/18 HEATER VESSEL REV. 2 DESIGN MODIFICATION

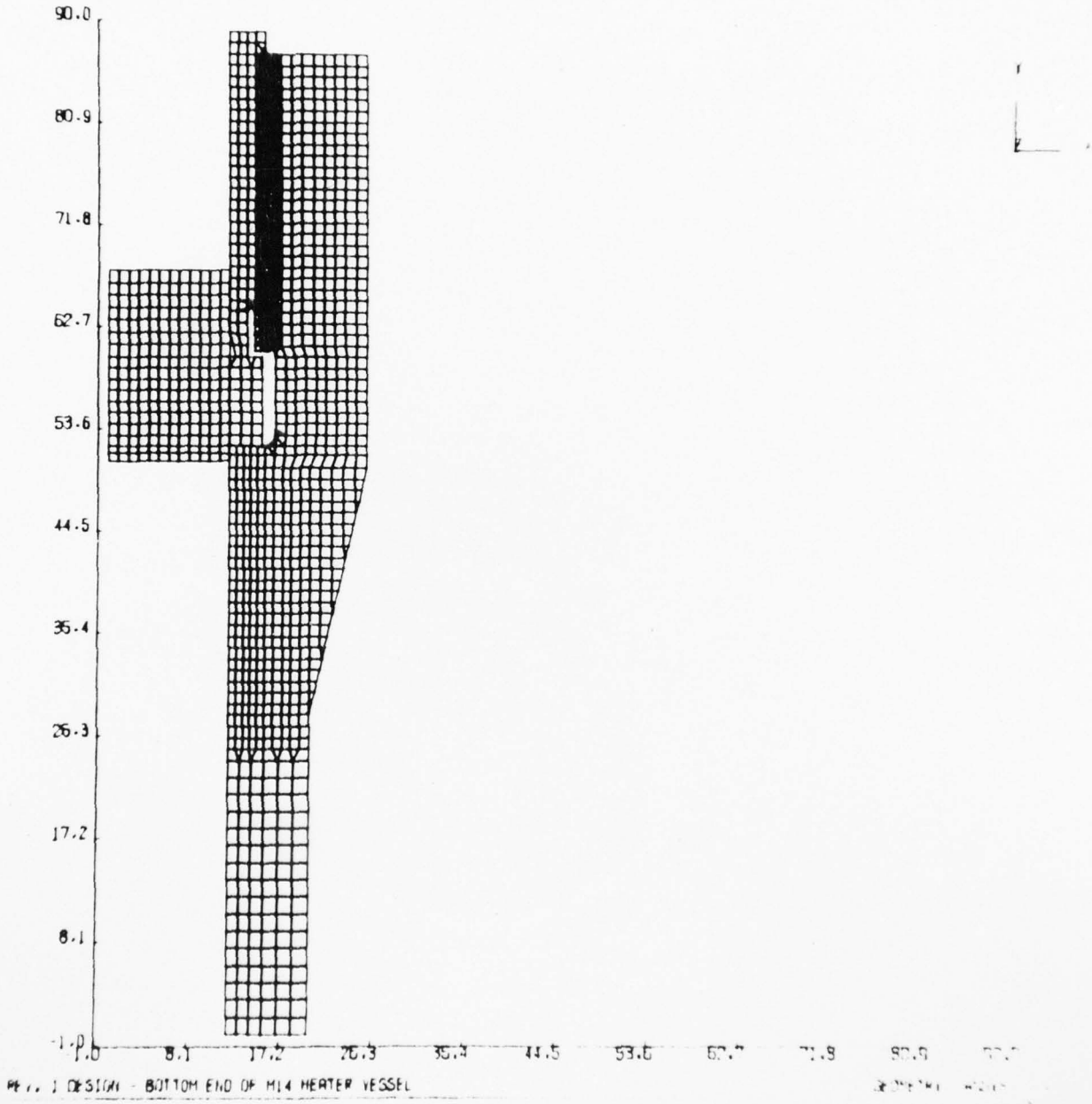
90.0
80.9
71.8
62.7
53.6
44.5
35.4
26.3
17.2
8.1
-1.0
1.0
8.1
17.2
26.3
35.4
44.5
53.6
62.7
71.8
80.9
90.0
DESIGN - BOTTOM END OF MLA HEATER VESSEL

Figure 61

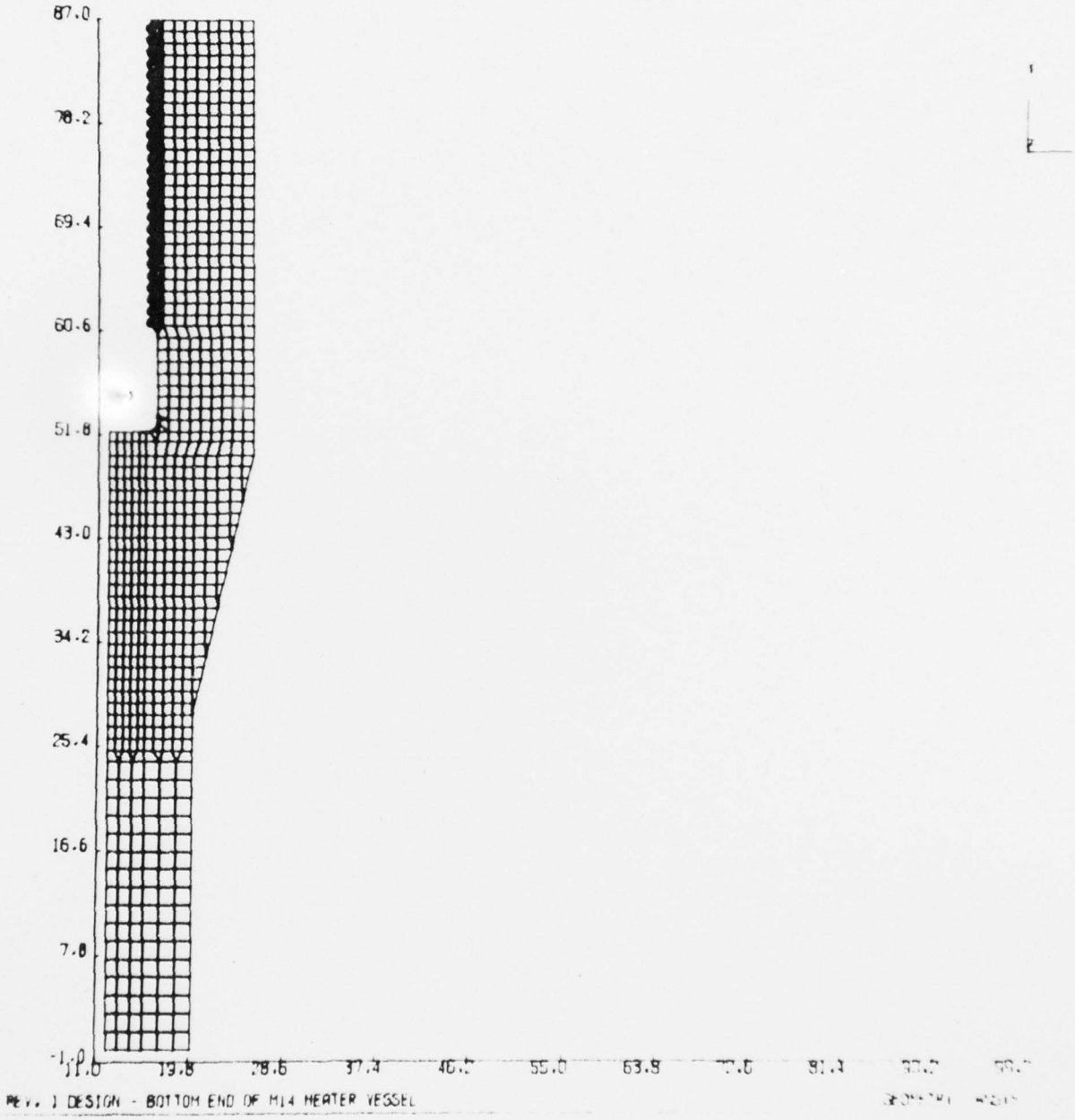
87.0
78.2
69.4
60.6
51.8
43.0
34.2
25.4
16.6
7.8
19.8
28.6
37.4
55.0
63.8
91.4
REV. 1 DESIGN - BOTTOM END OF M14 HEATER VESSEL

Figure 62

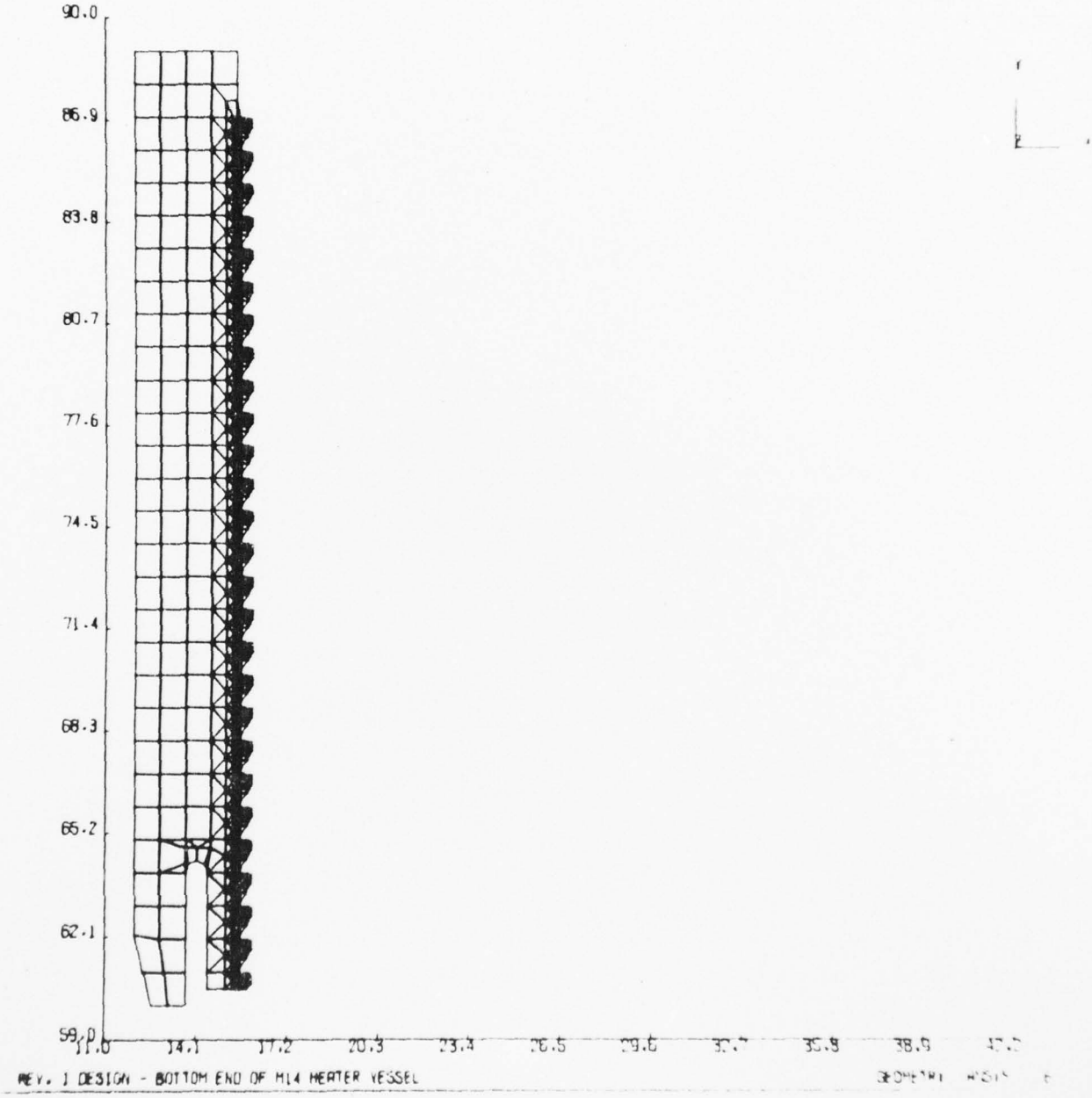
90.0
86.9
83.8
80.7
77.6
74.5
71.4
68.3
65.2
62.1
59.0
11.0
14.1
17.2
20.3
23.4
26.5
29.6
32.7
35.8
38.9
REV. 1 DESIGN - BOTTOM END OF M14 HEATER VESSEL

Figure 63

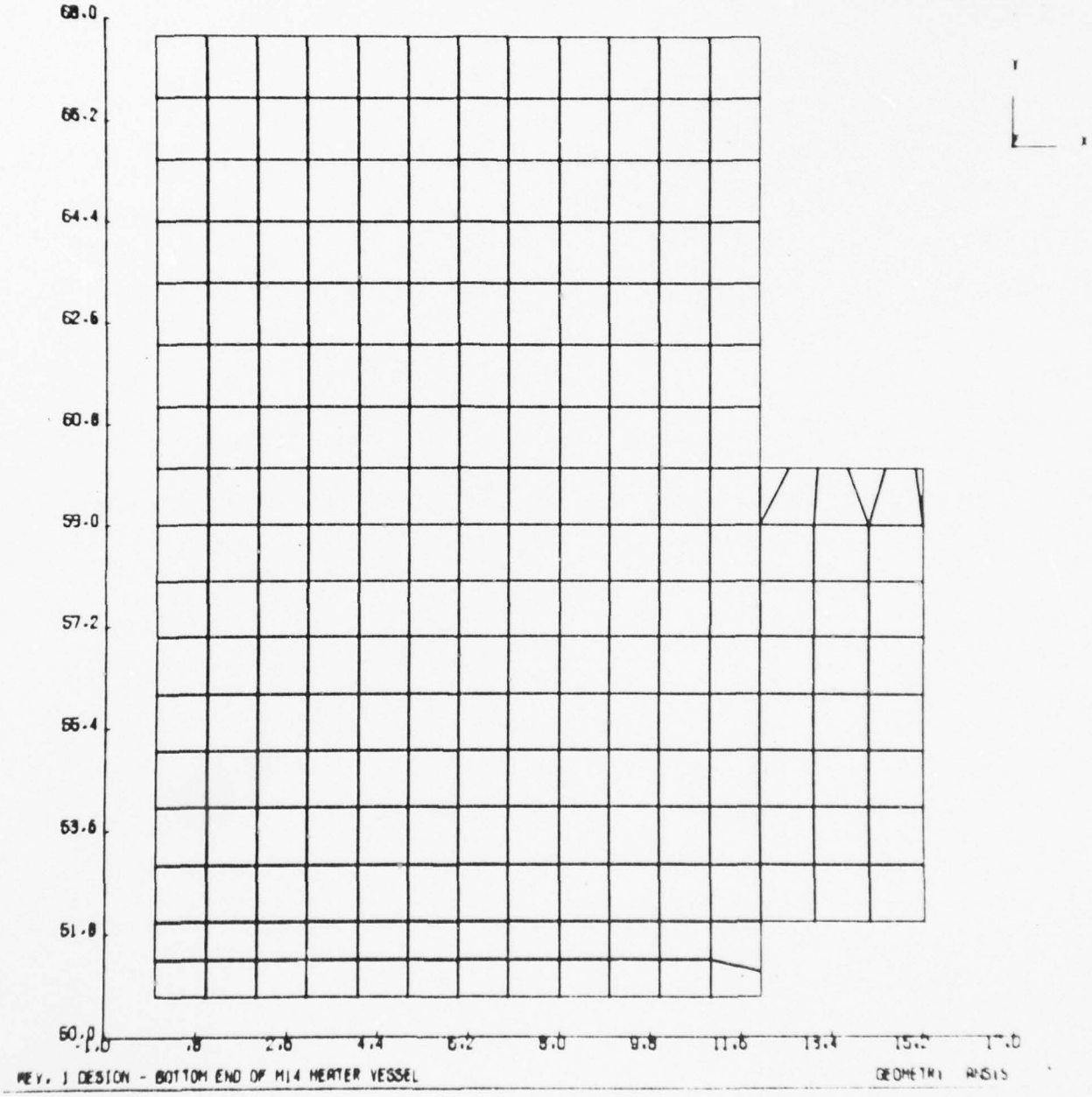
68.0
66.2
64.4
62.6
60.8
59.0
57.2
55.4
53.6
51.8
50.0
.8
2.6
4.4
6.2
8.0
9.8
11.6
13.4
15.2
17.0
Y
Z
X
REV. 1 DESIGN - BOTTOM END OF M14 HEATER VESSEL
GEOMETRY ANSYS

Figure 64

AD-A071 029 O'DONNELL AND ASSOCIATES INC PITTSBURGH PA F/G 13/7
HYPERVELOCITY WIND TUNNEL COMPONENTS STRUCTURAL EVALUATION. VOL--ETC(U)
MAY 79 D PETERSON, E WESTERMANN N60921-78-C-0013
UNCLASSIFIED ODAI-1270-8-79-VOL-1 NL

2 OF 2
AD A071029

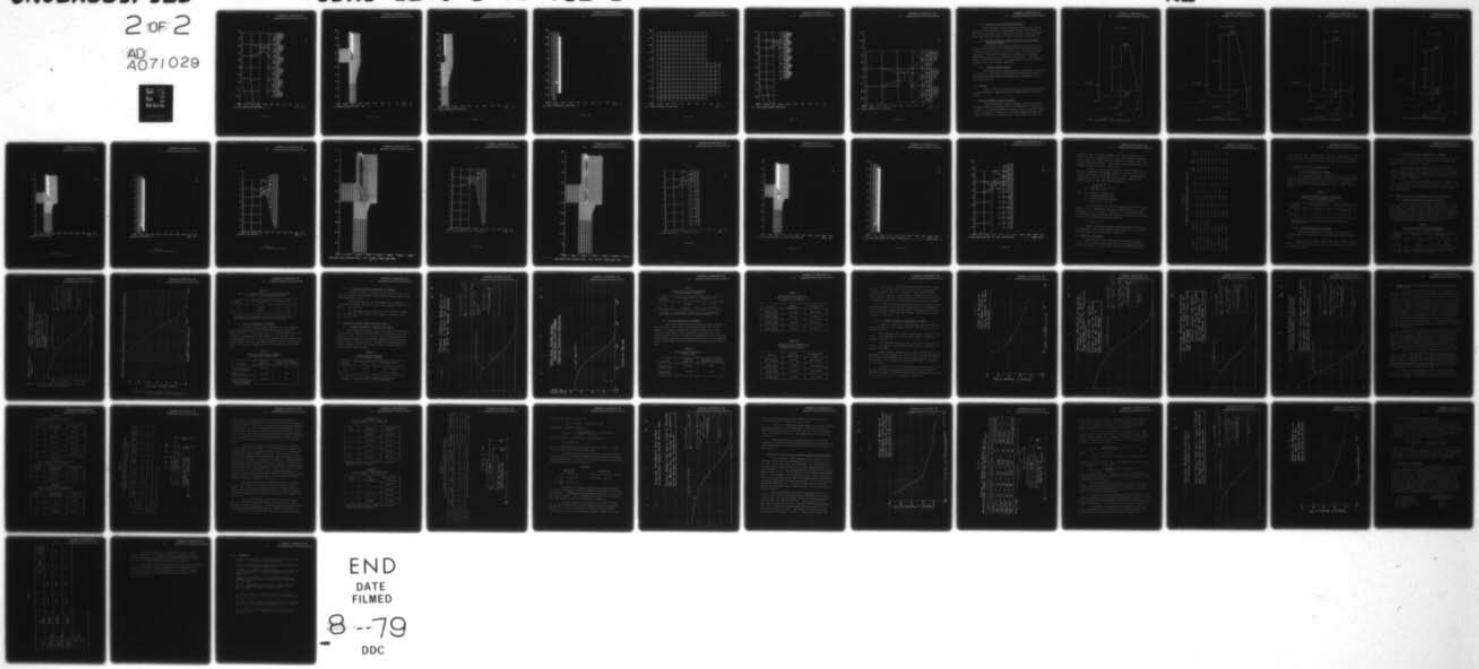

END
DATE FILMED
8-79
DDC

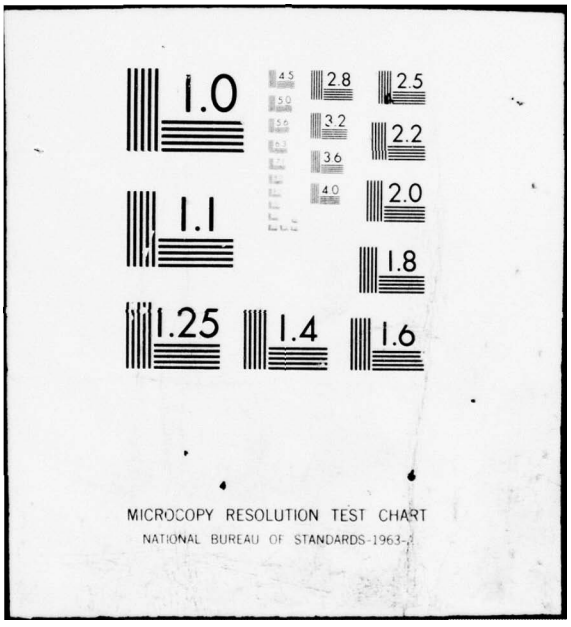
1.0
1.1
1.25
1.4
1.6
1.8
2.0
2.2
2.5
2.8
3.2
3.6
4.0
4.5
5.0
5.6
6.3
7.1
MICROCOPY RESOLUTION TEST CHART
NATIONAL BUREAU OF STANDARDS-1963-A

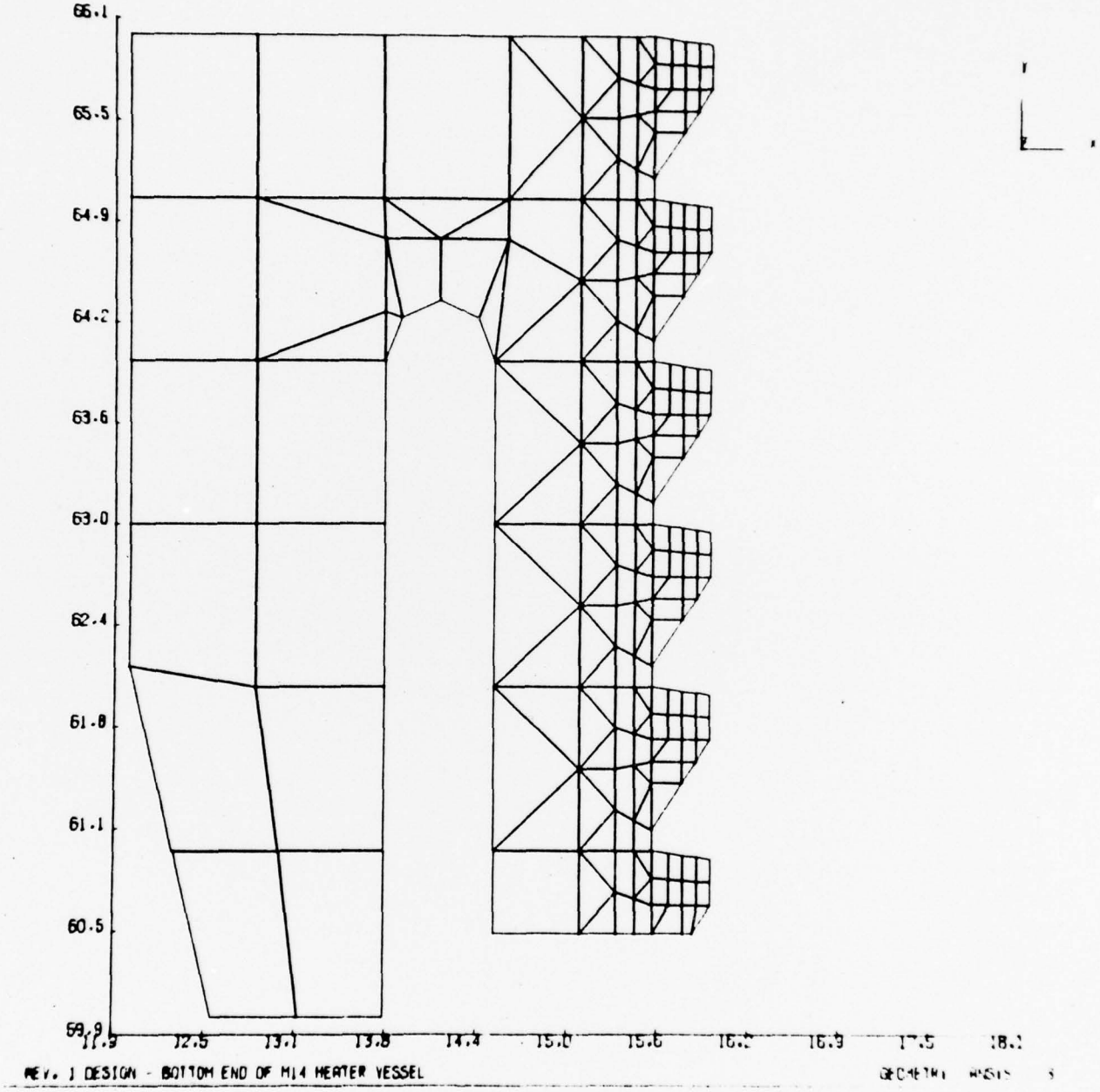
66.1
65.5
64.9
64.2
63.6
63.0
62.4
61.8
61.1
60.5
59.9
12.5
13.1
13.8
14.4
15.0
15.6
16.2
16.9
17.5
18.1
REV. 1 DESIGN - BOTTOM END OF M14 HEATER VESSEL

Figure 65

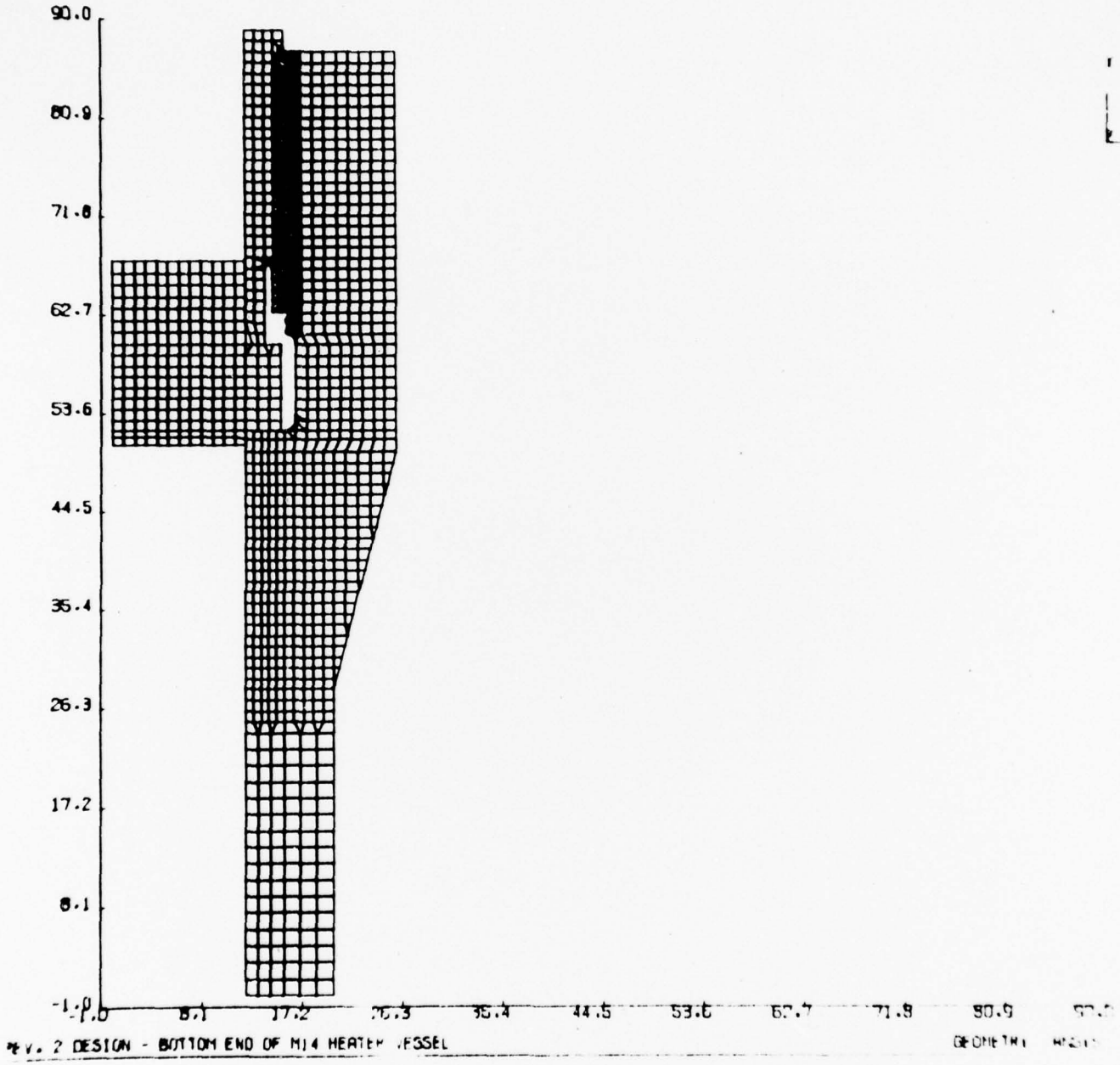
90.0
80.9
71.8
62.7
53.6
44.5
35.4
26.3
17.2
8.1
-1.0
8.1
17.2
26.3
35.4
44.5
53.6
62.7
71.8
80.9
V. 2 DESIGN - BOTTOM END OF M14 HEATER VESSEL

Figure 66

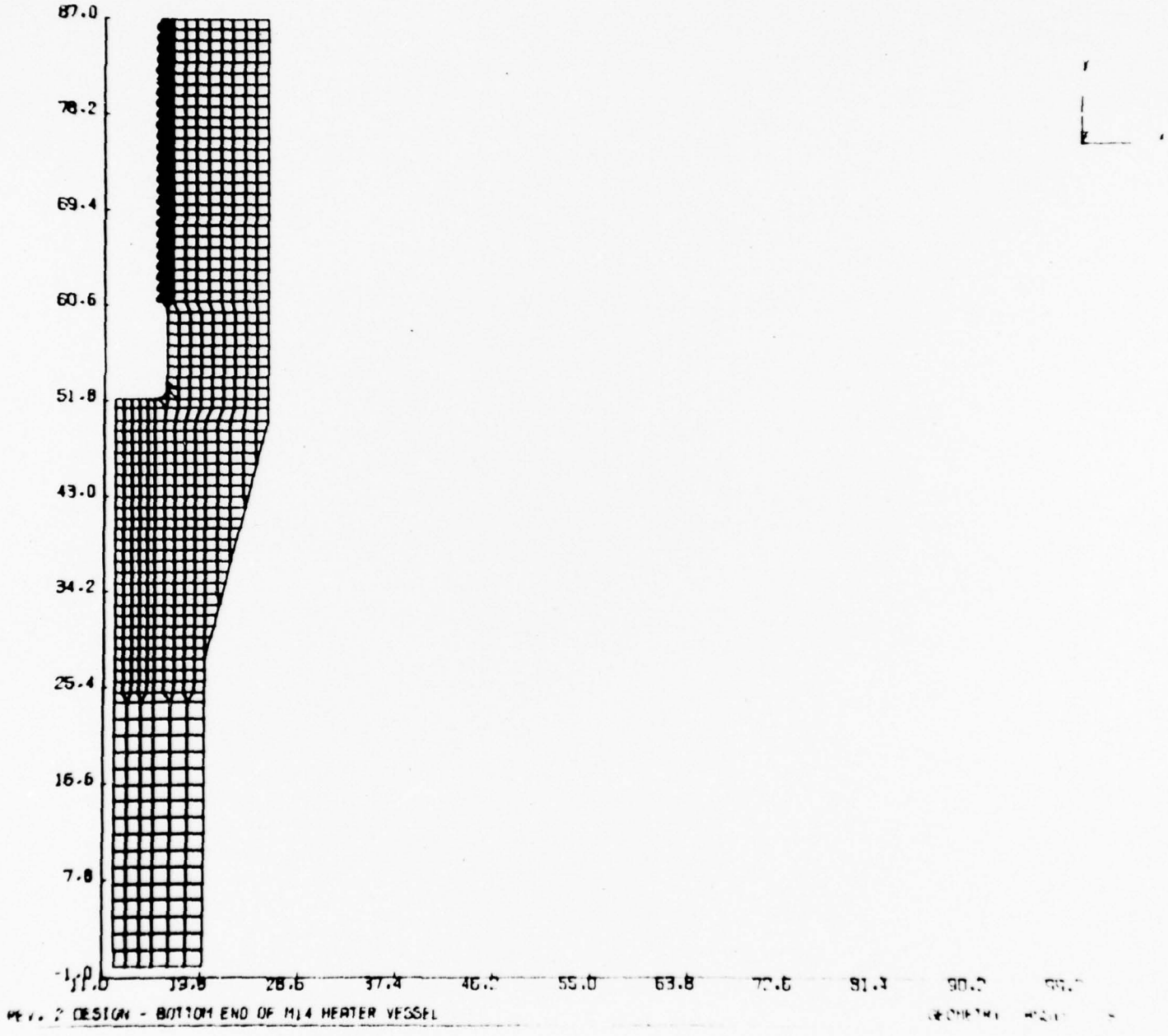
87.0
78.2
69.4
60.6
51.8
43.0
34.2
25.4
16.6
7.8
-1.0
10.0
19.8
28.6
37.4
46.2
55.0
63.8
72.6
81.4
90.2
99.0
DESIGN - BOTTOM END OF M14 HEATER VESSEL

Figure 67

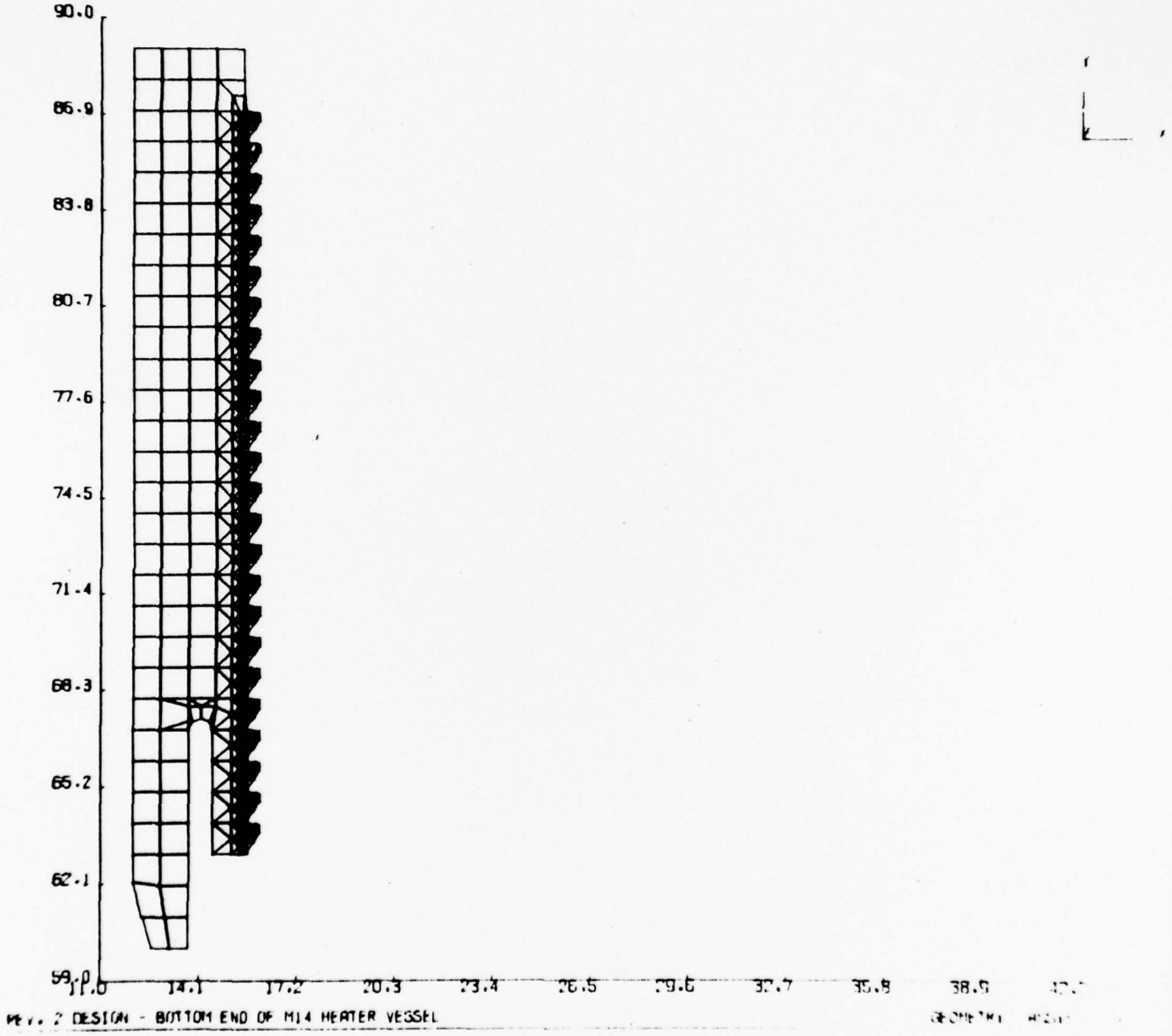
90.0
86.9
83.8
80.7
77.6
74.5
71.4
68.3
65.2
62.1
59.0
11.0
14.1
17.2
20.3
23.4
26.5
29.6
32.7
35.8
38.9
DESIGN - BOTTOM END OF M14 HEATER VESSEL

Figure 68

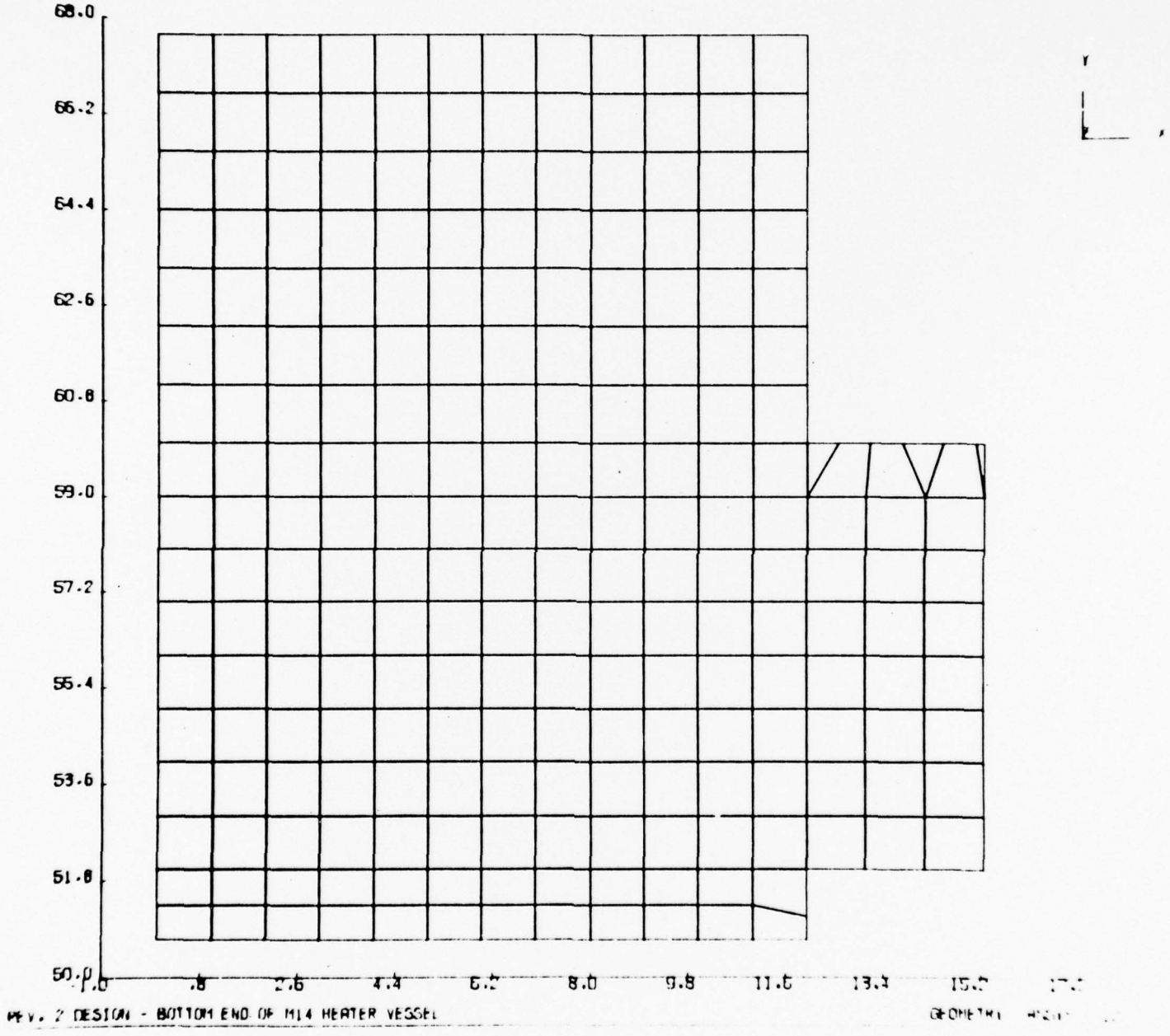
68.0
66.2
64.4
62.6
60.8
59.0
57.2
55.4
53.6
51.8
50.0
.0
.8
2.6
4.4
6.2
8.0
9.8
11.6
13.4
15.2
Y
REV. 2 DESIGN - BOTTOM END OF M14 HEATER VESSEL

Figure 69

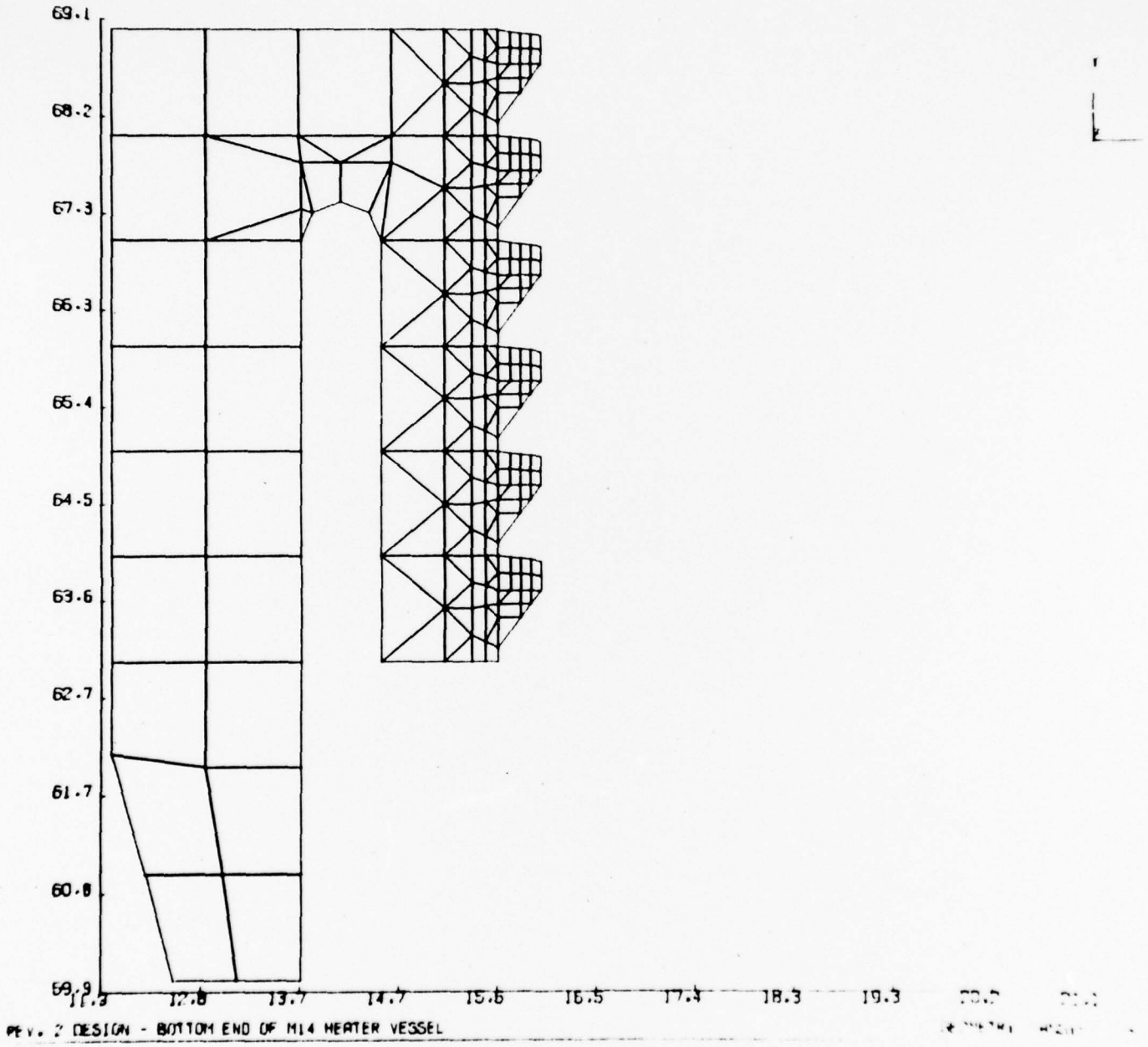
69.1
68.2
67.3
66.3
65.4
64.5
63.6
62.7
61.7
60.8
59.9
13.7
14.7
15.6
16.5
18.3
19.3
REV. 2 DESIGN - BOTTOM END OF M14 HEATER VESSEL

Figure 70

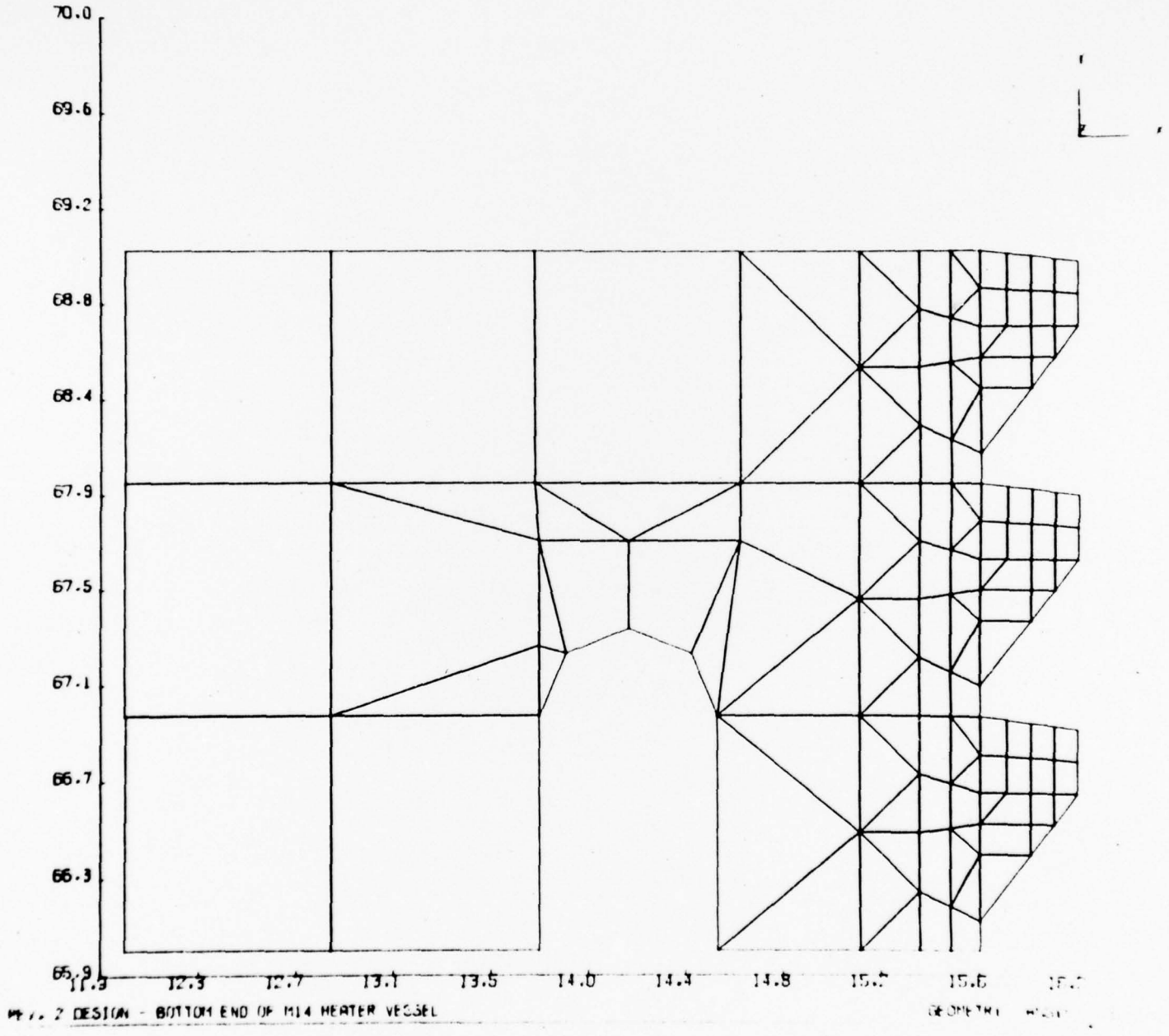
70.0
69.6
69.2
68.8
68.4
67.9
67.5
67.1
66.7
66.3
65.9
12.3
12.7
13.1
13.5
14.0
14.4
14.8
15.2
15.6
DESIGN - BOTTOM END OF M14 HEATER VESSEL

Figure 71

5.5.1 DESCRIPTION OF DESIGN MODIFICATIONS

Four different inlet end design modifications, which utilize various undercut configurations on the inside end of the main nut on the inlet end of the driver vessel, were evaluated. These design modifications are shown in Figures 72 through 75.

5.5.2 OVERALL MODELS OF INLET END DESIGN MODIFICATIONS FOR DRIVER VESSEL

The overall finite element model used in the original analysis (see Section 5.3.1) was modified in accordance with the revised designs and used to analyze each one of the design modifications. These revised models for each one of the design modifications are shown in Figures 76 through 85. All other components of the overall model as described in Section 5.3.1 were unchanged from the original analysis.

5.5.3 DETAILED THREAD MODELS

The same detailed thread models as described in Sections 5.3.2 and 5.3.3 were used to calculate the maximum stresses in the threads for the design modifications on the driver vessel inlet end closure.

6.0 RESULTS

Most of the detailed calculations and results are given in the Appendices. These results are summarized and evaluated herein.

6.1 DUCTILE BURSTING ANALYSIS RESULTS

The PVRC ductile bursting pressure formula for thick-walled cylinders development effort is described in Reference 6, 7, and 8. A pressure-expansion relation for an anisotropic thick-walled cylindrical vessel under internal pressure was obtained based on true-strain considerations. The elastic strains were

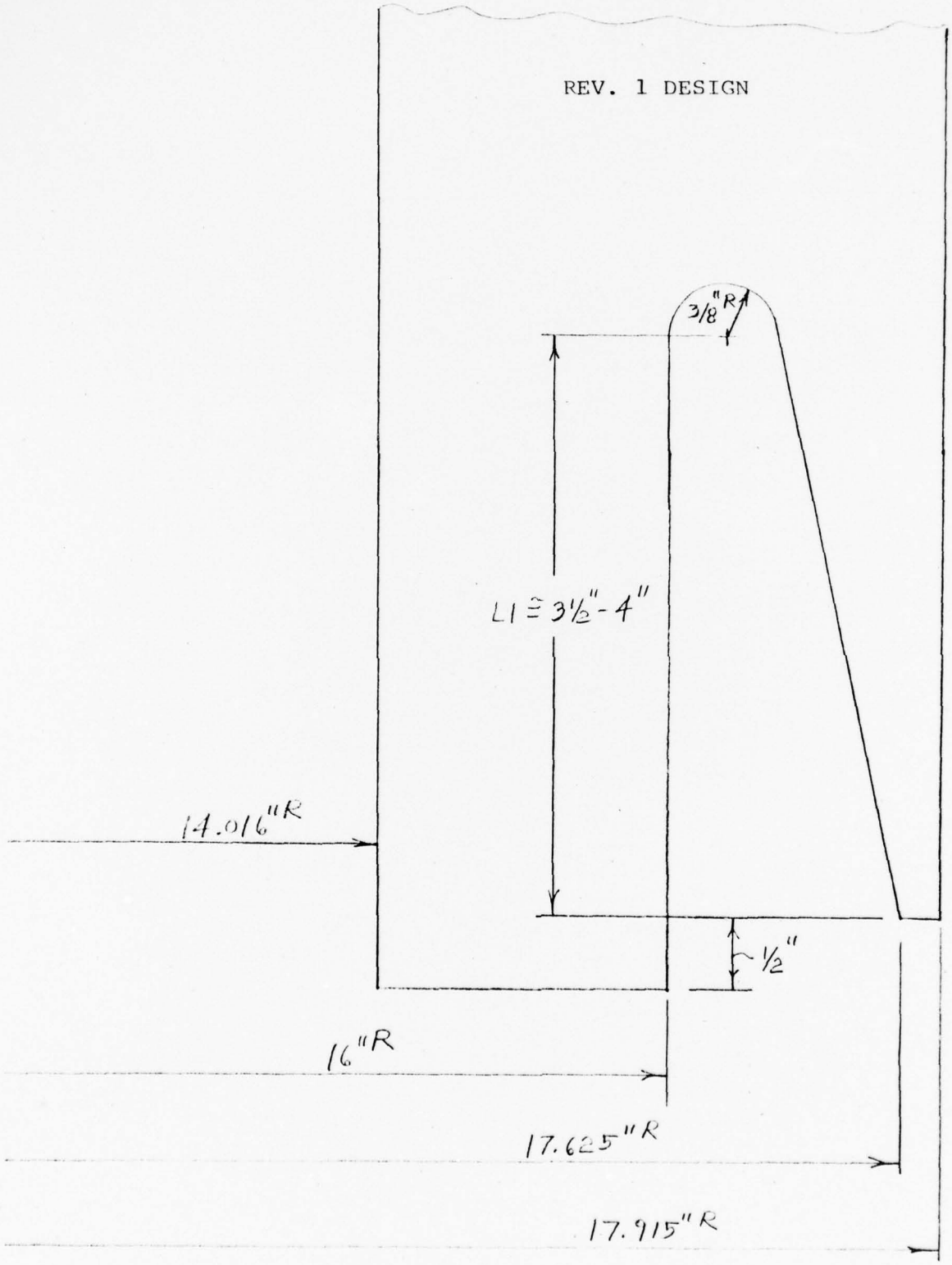

Figure 72
Driver Vessel Rev. 1 Design Modification

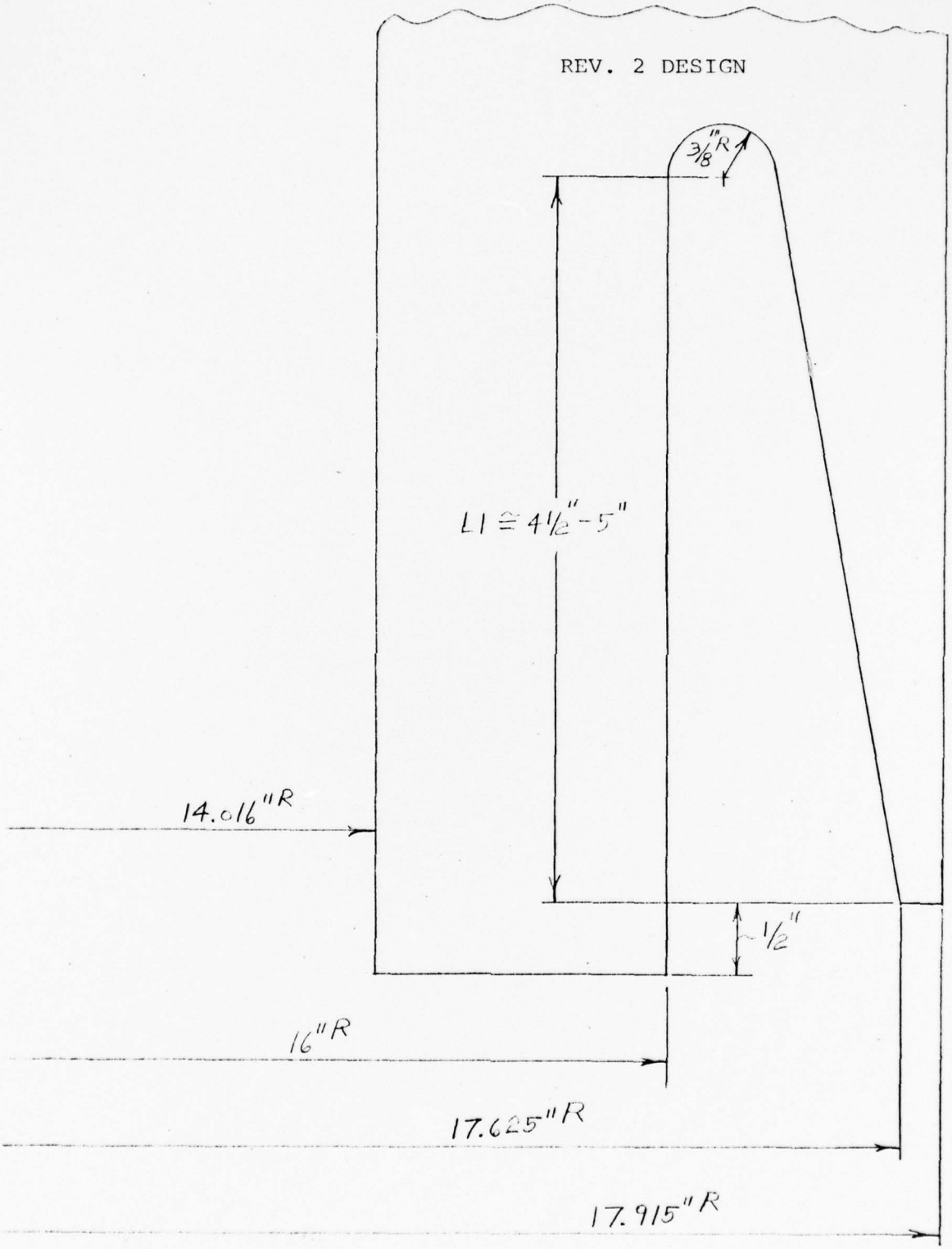

Figure 73
Driver Vessel Rev. 2 Design Modification

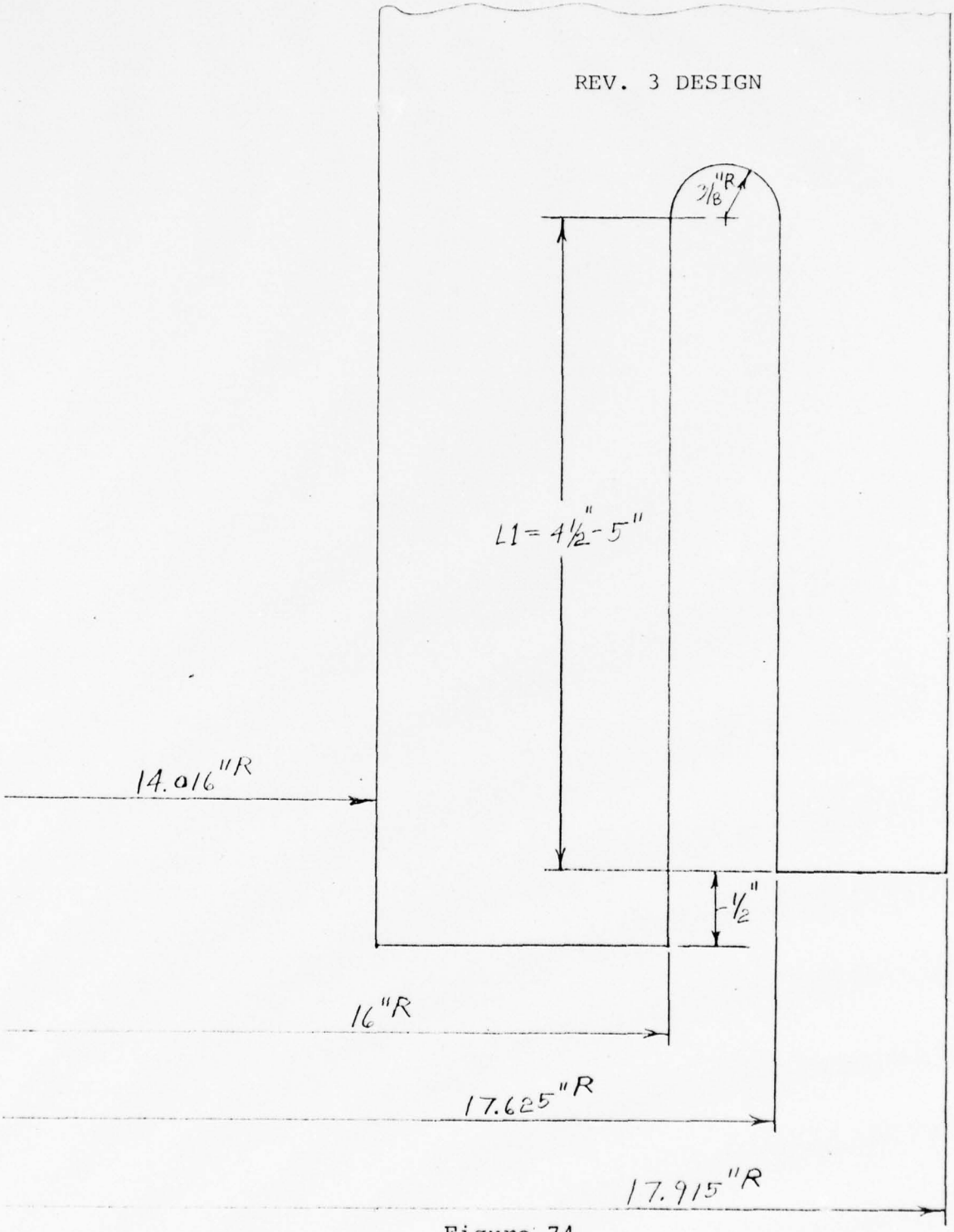

Figure 74
Driver Vessel Rev. 3 Design Modification

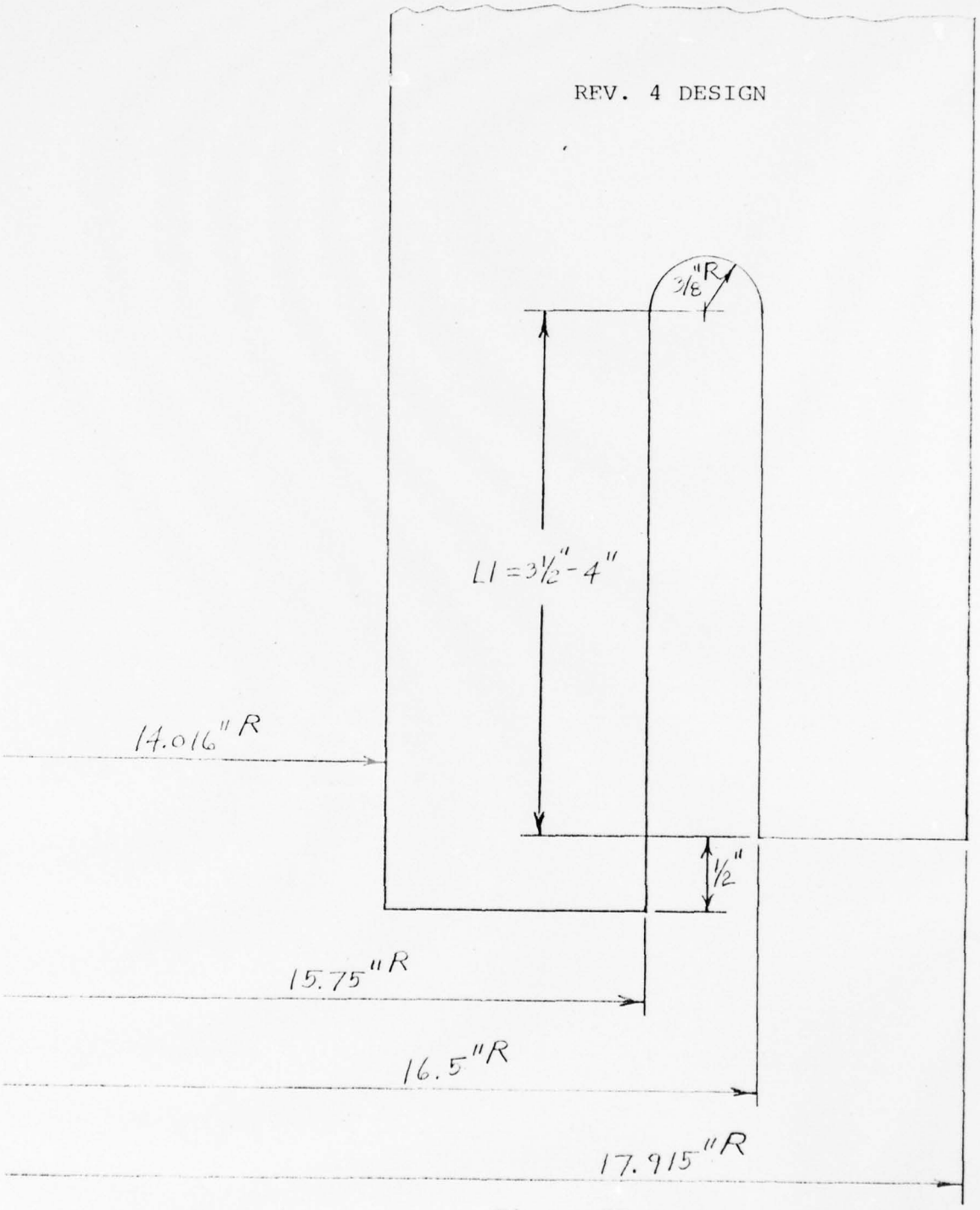

Figure 75
Driver Vessel Rev. 4 Design Modification

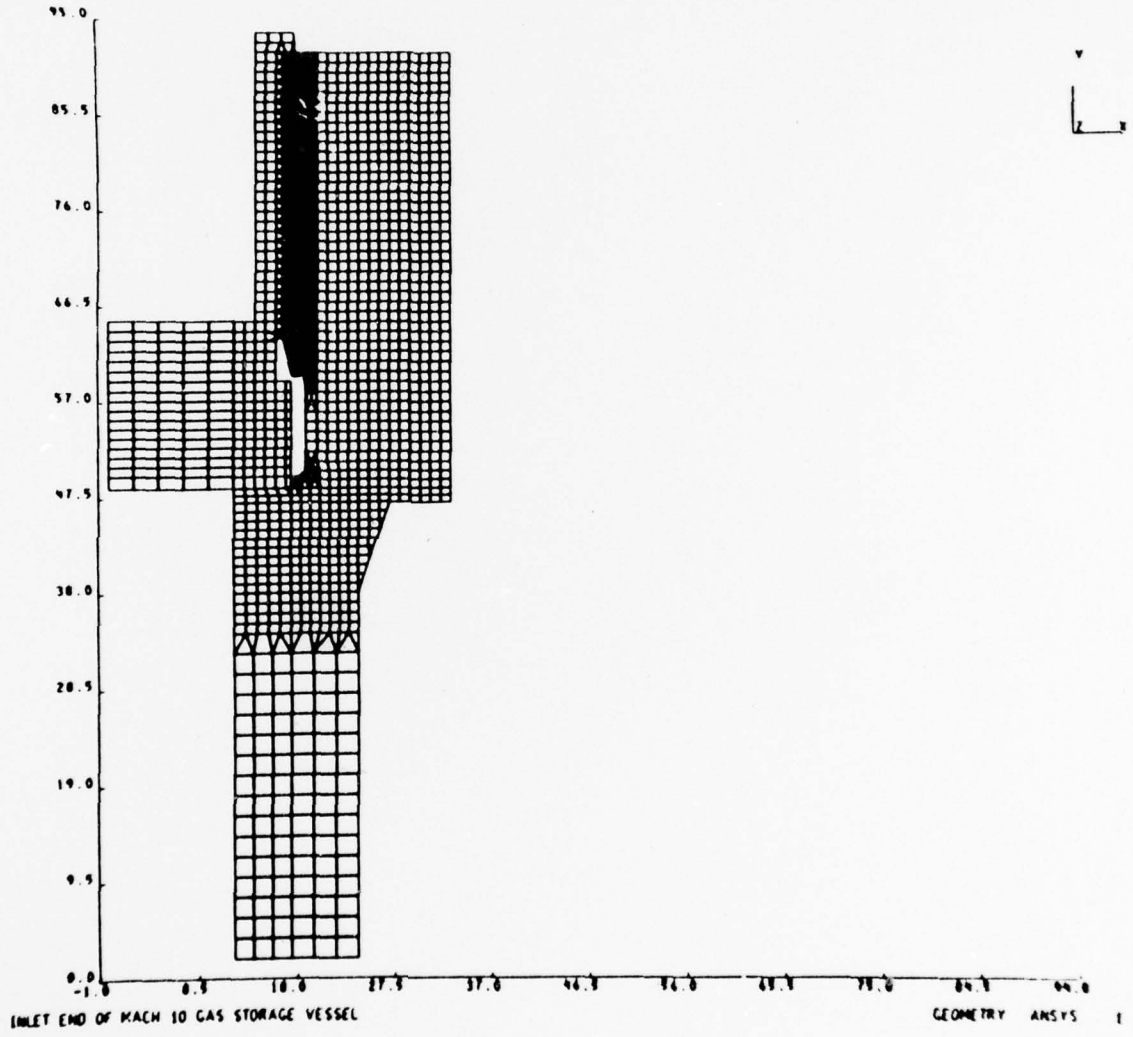

Figure 76
Rev. 1 Design Modification

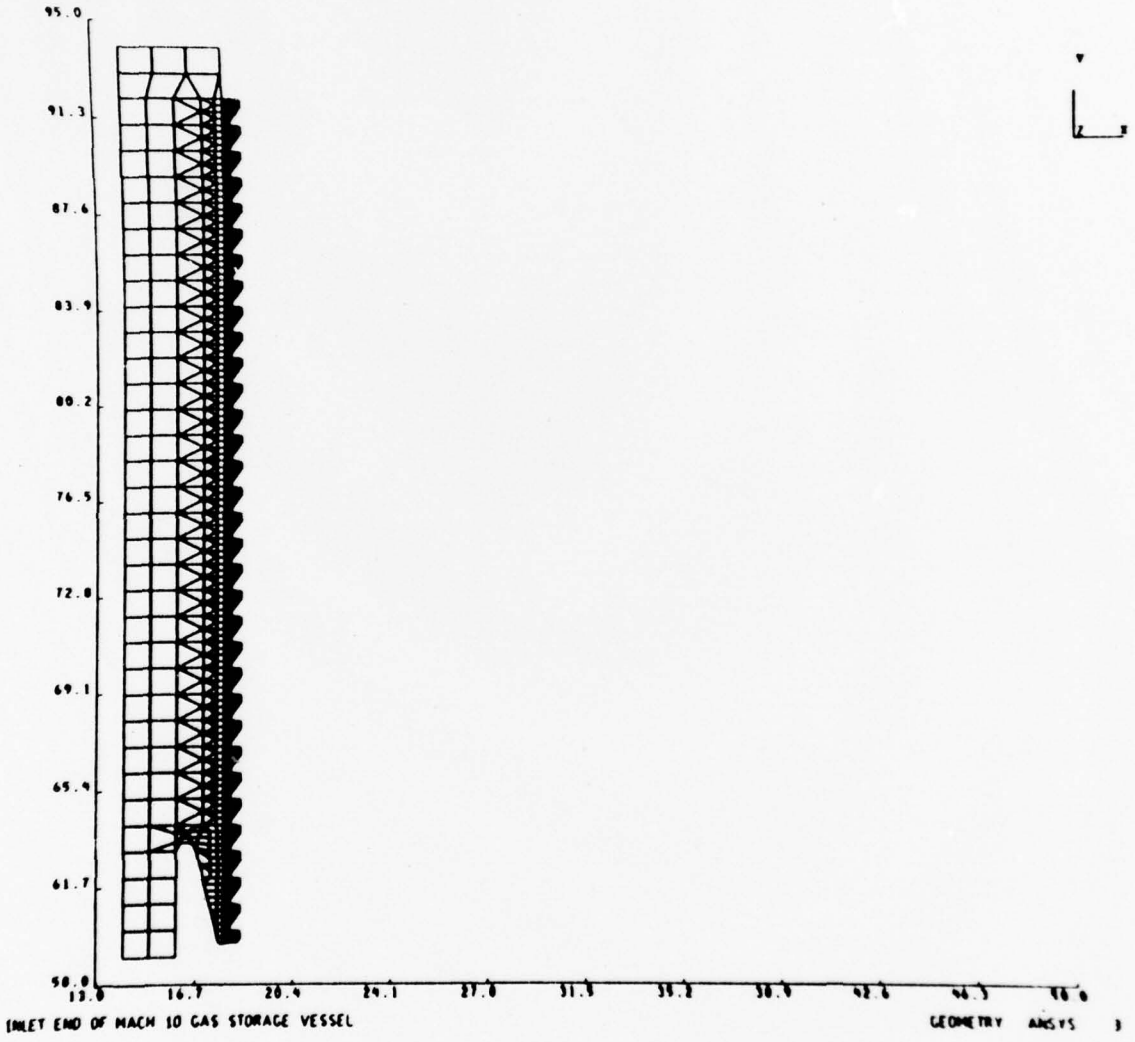

Figure 77
Rev. 1 Design Modification

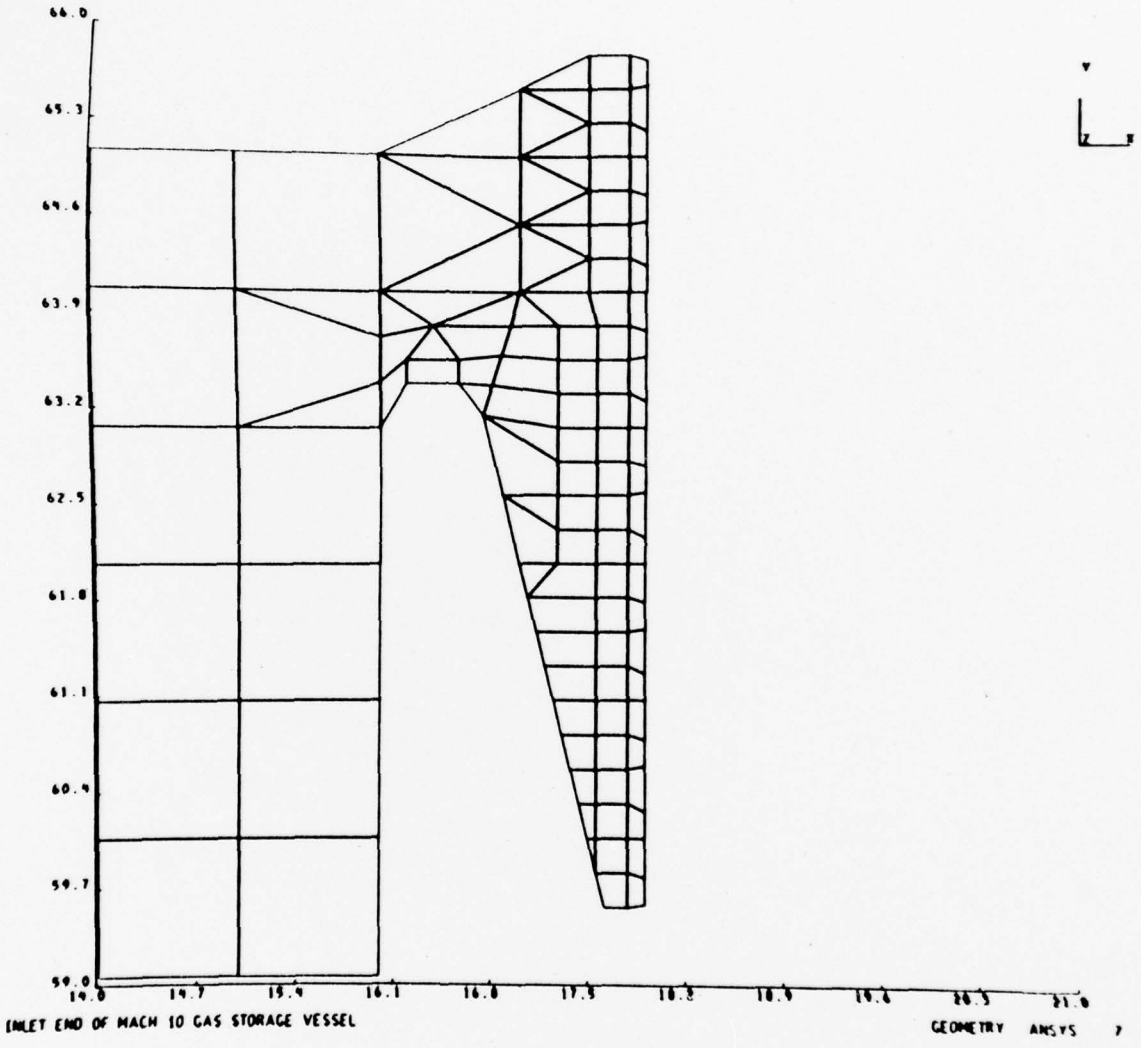

Figure 78
Rev. 1 Design Modification

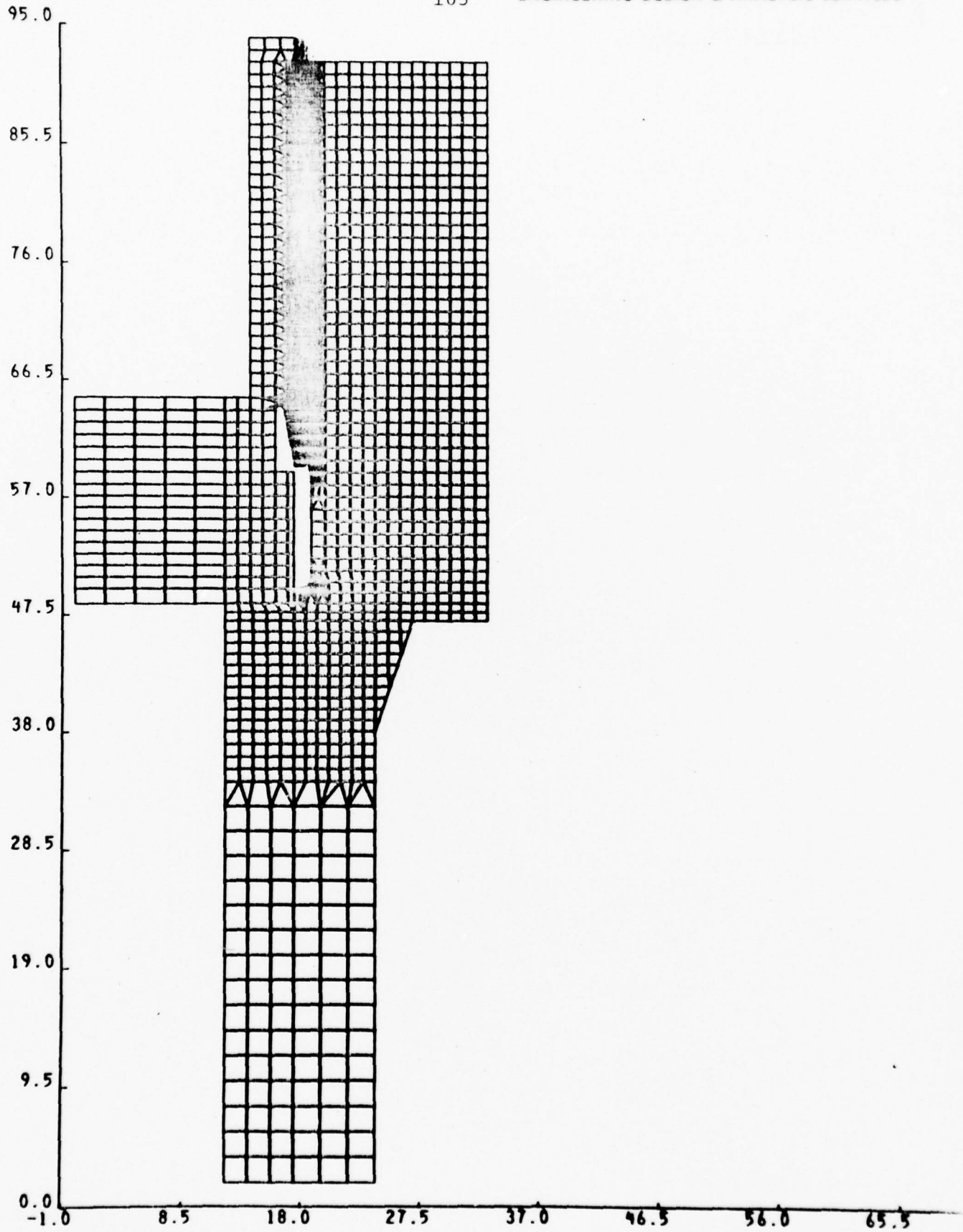

INLET END OF MACH 10 DRIVER VESSEL - REV. 2 DESIGN - THREAD ANGLE CORR.

Figure 79

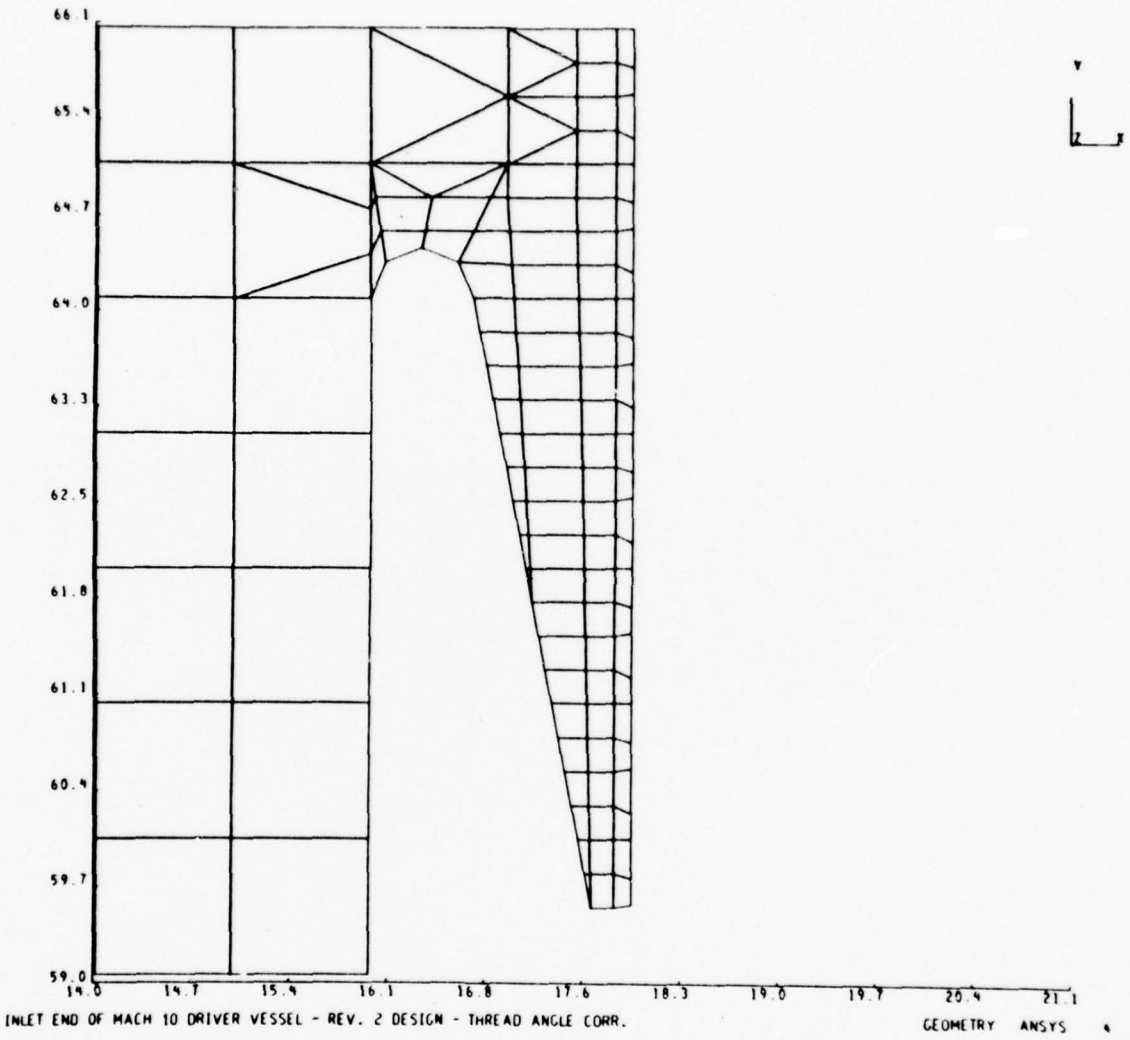
66.1
65.4
64.7
64.0
63.3
62.5
61.8
61.1
60.4
59.7
59.0
14.0
14.7
15.4
16.1
16.8
17.6
18.3
19.0
19.7
20.4
21.1
Y
Z
X
INLET END OF MACH 10 DRIVER VESSEL - REV. 2 DESIGN - THREAD ANGLE CORR.
GEOMETRY ANSYS

Figure 80

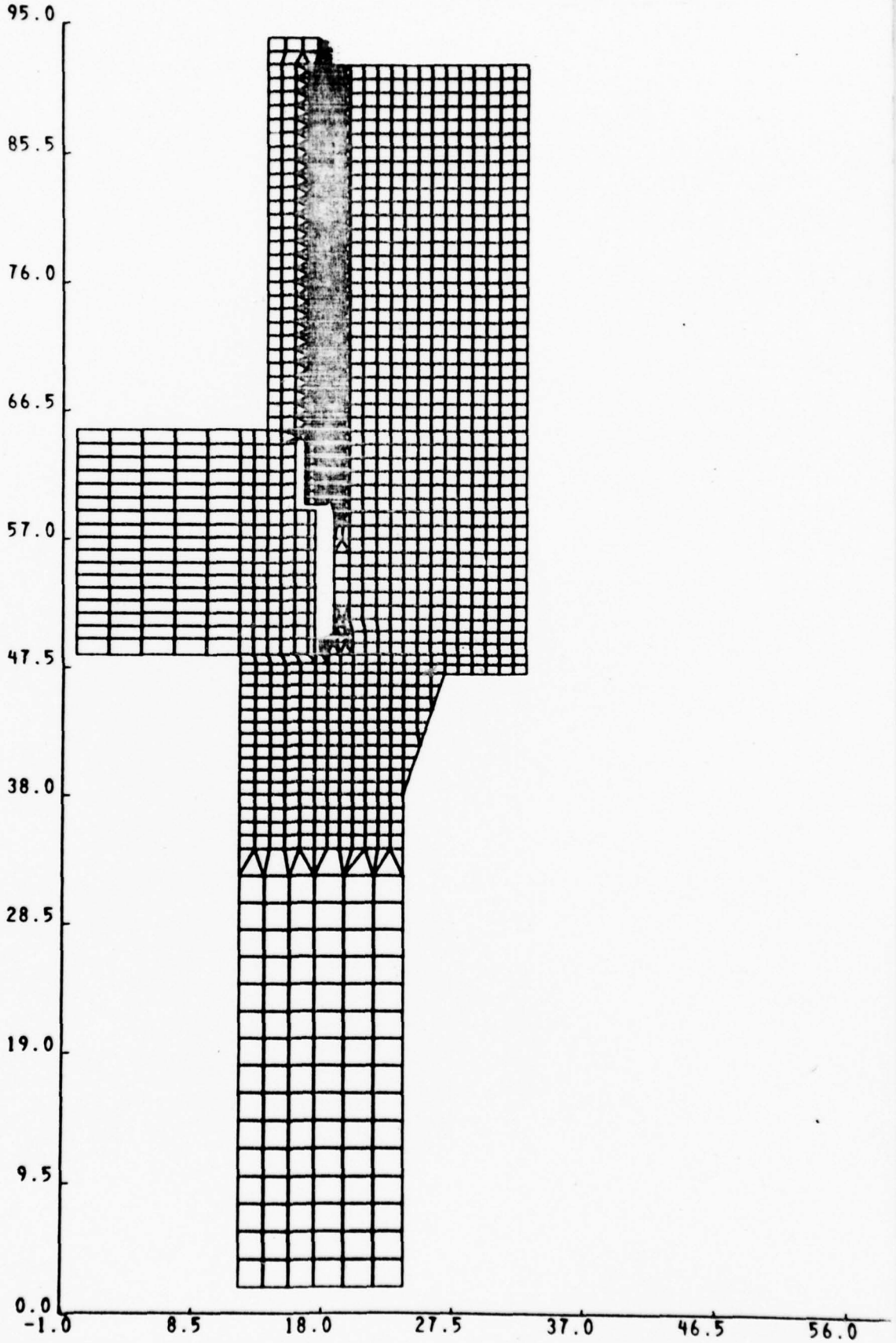

Figure 81

INLET END OF MACH 10 DRIVER VESSEL - REV. 3 DESIGN - THREAD ANGLE CORR.

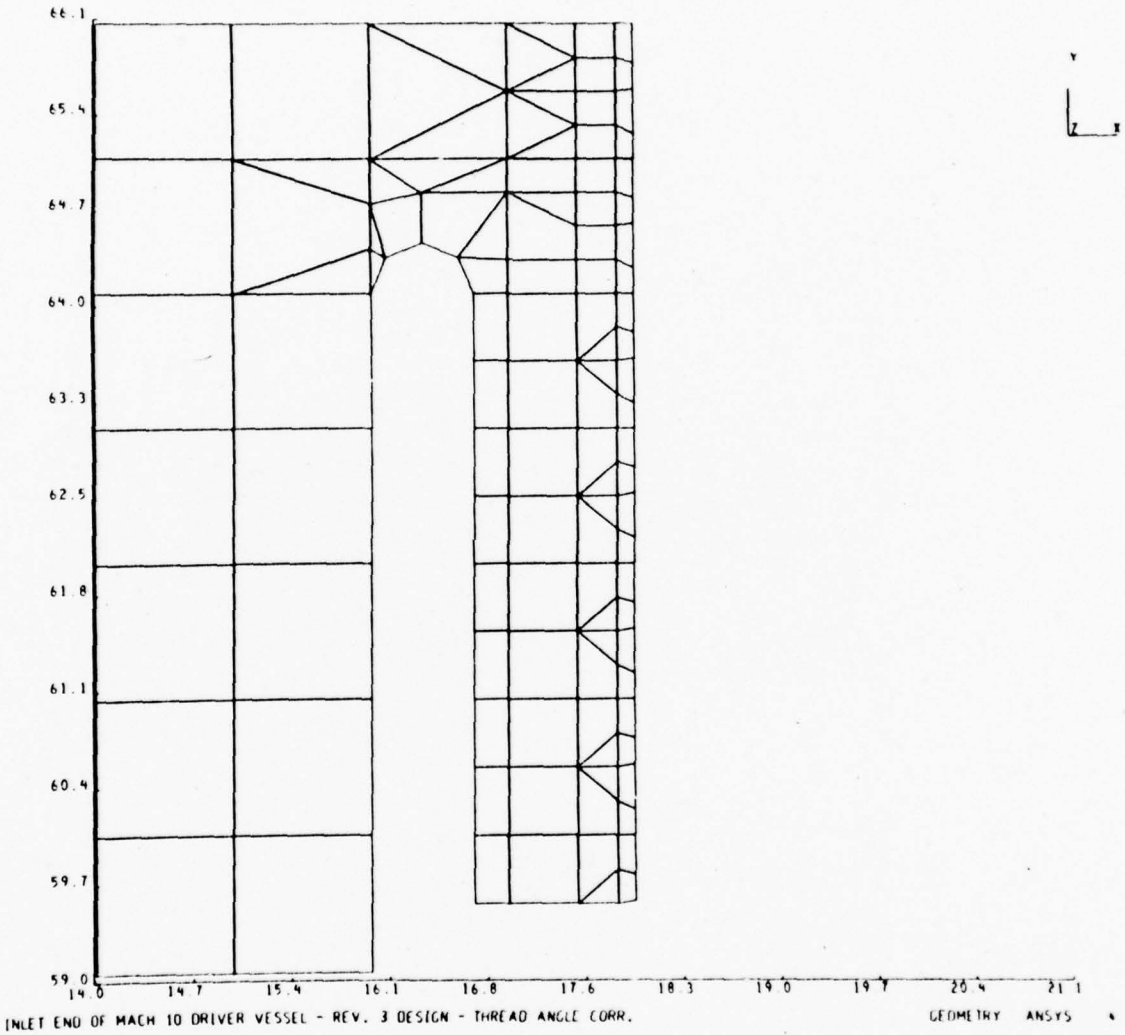
66.1
65.4
64.7
64.0
63.3
62.5
61.8
61.1
60.4
59.7
59.0
14.0
14.7
15.4
16.1
16.8
17.6
18.3
19.0
19.7
20.4
21.1
Y
Z
X
INLET END OF MACH 10 DRIVER VESSEL - REV. 3 DESIGN - THREAD ANGLE CORR.
GEOMETRY ANSYS

Figure 82

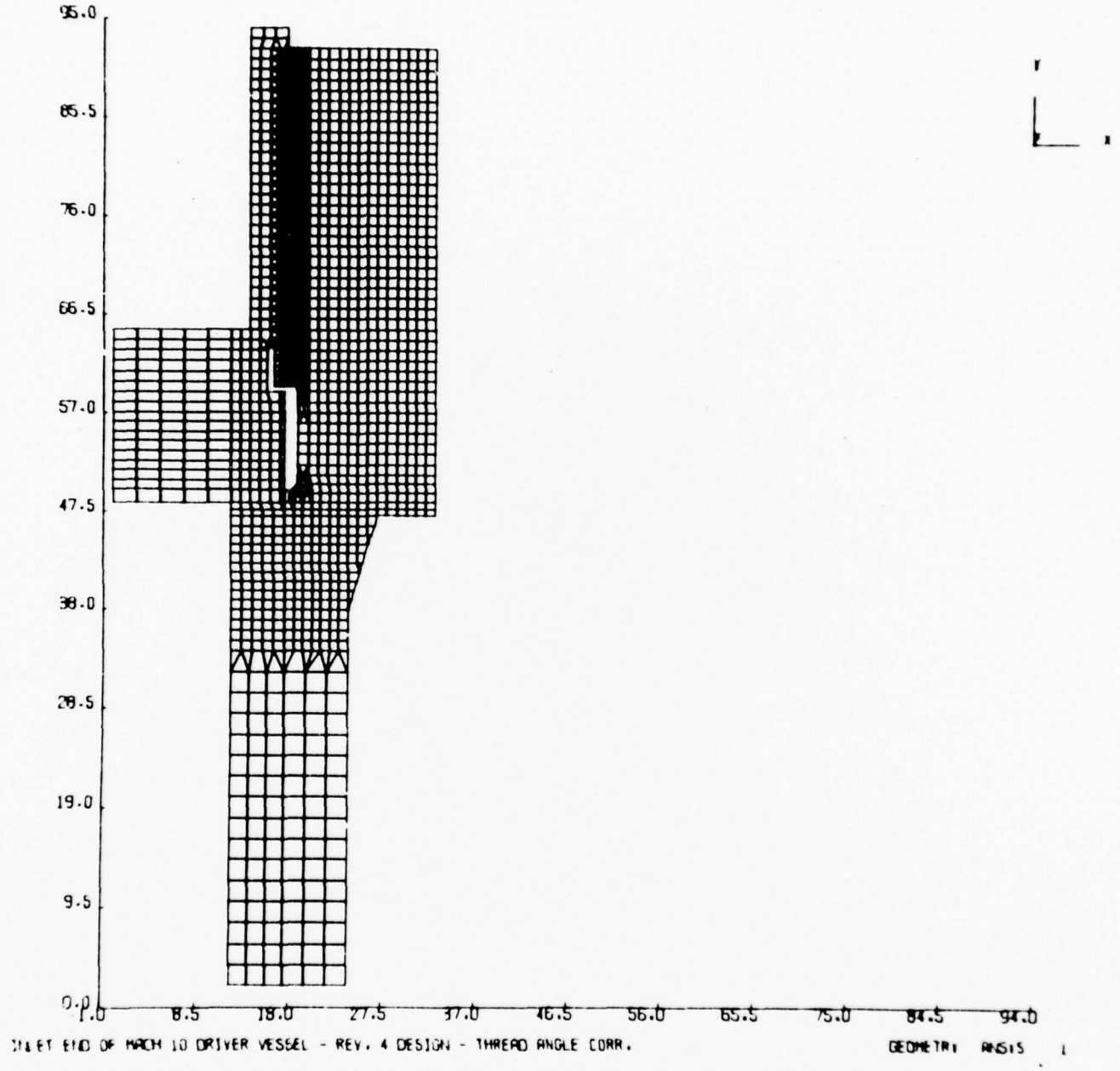
95.0
85.5
76.0
66.5
57.0
47.5
38.0
28.5
19.0
9.5
0.0
1.0
8.5
18.0
27.5
37.0
46.5
56.0
65.5
75.0
84.5
94.0
BULLET END OF MARCH 10 DRIVER VESSEL - REV. 4 DESIGN - THREAD ANGLE CORR.
GEOMETRY ANSYS

Figure 83

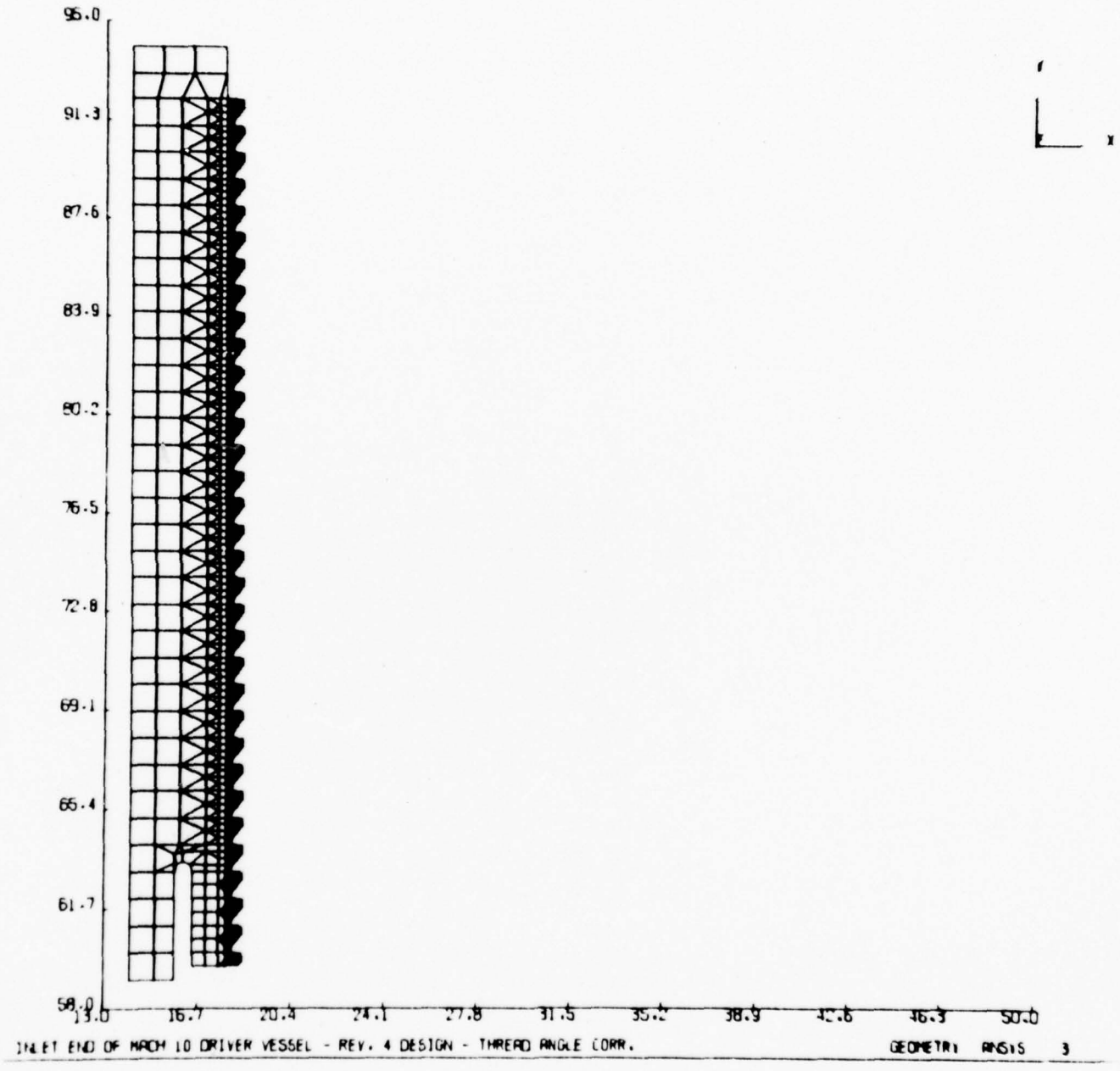
95.0
91.3
87.6
83.9
80.2
76.5
72.8
69.1
65.4
61.7
58.0
13.0
16.7
20.4
24.1
27.8
31.5
35.2
38.9
42.6
46.3
50.0
INLET END OF MACH 10 DRIVER VESSEL - REV. 4 DESIGN - THREAD ANGLE CORR.
GEOMETRY ANSYS 3

Figure 84

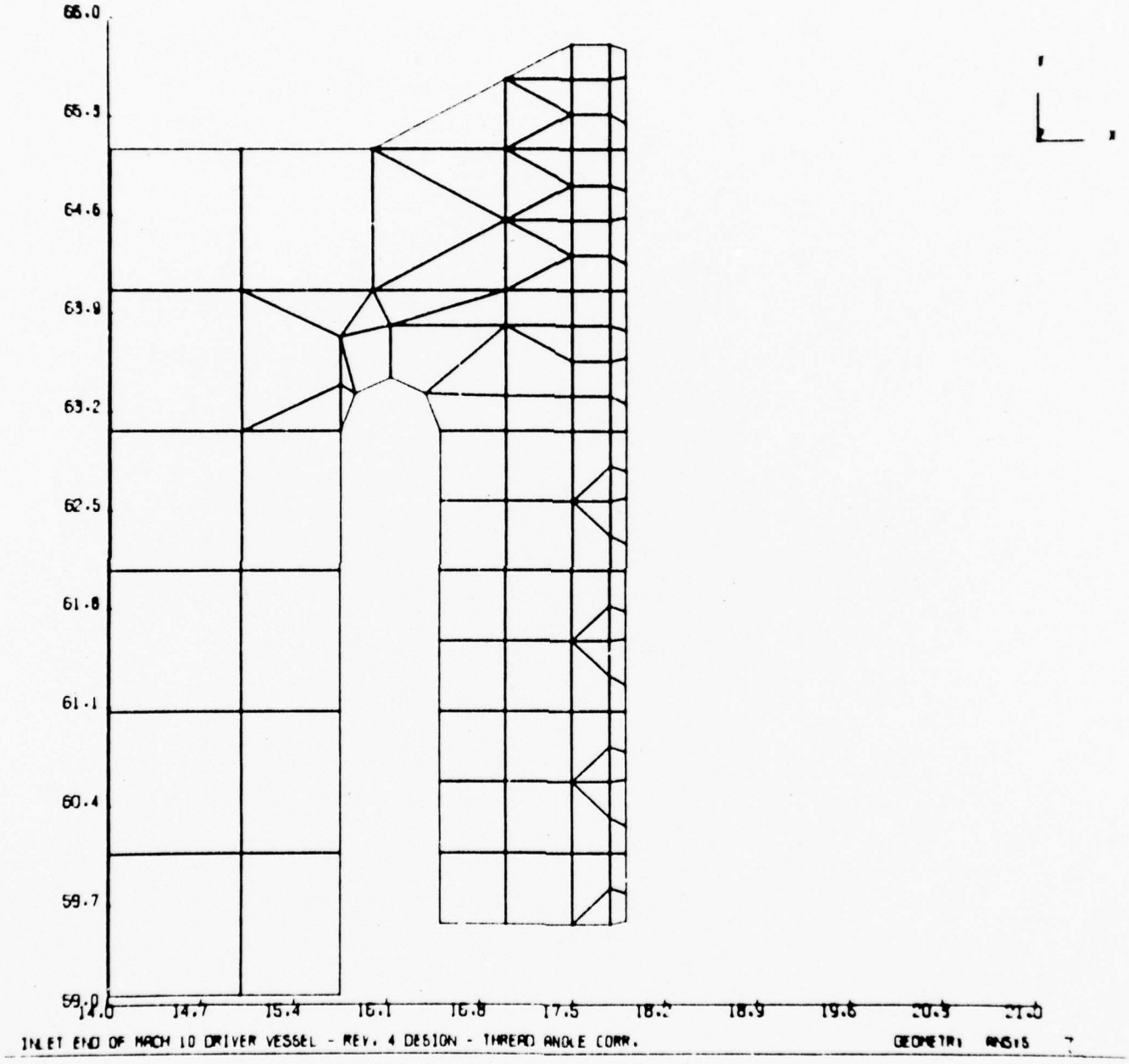
66.0
65.3
64.6
63.9
63.2
62.5
61.8
61.1
60.4
59.7
59.0
14.0
14.7
15.4
16.1
16.8
17.5
18.2
18.9
19.6
20.3
21.0
INLET END OF MACH 10 DRIVER VESSEL - REV. 4 DESIGN - THREAD ANGLE CORR.
GEOMETRY ANSYS

Figure 85

neglected since they were assumed to be small compared to the plastic strains; consequently, all axial strains were neglected. The cylinder was assumed to be of sufficient length so that end effects could be neglected. The true stress-strain relation was assumed to have the form $\sigma = C_1\varepsilon^n + C_2$.

Because of the limited material data available, the material properties are assumed isotropic, and the true stress-strain relationship is assumed to be $\sigma = C_1\varepsilon^n$. A maximum non-conservative error of $\leq$ 10% can be expected by making these simplifications. The PVRC formula reduces to:

$$P_M = \frac{\sigma_u}{2n}\left[\frac{\frac{2}{\sqrt{3}}\log_e W}{W^2 - 1}\right]^n (W^{2n} - 1)$$

where: P_M = bursting pressure (psi
σ_u = ultimate strength (psi)
n = strain hardening exponent
W = wall ratio O.D./I.D.

It can be shown that at the beginning of necking (instability), $n = \varepsilon$. Therefore, the true ultimate strain, ε_u, is an approximation of n. Since $\varepsilon = \log_e(1+\varepsilon')$, it is thus possible to obtain a fair approximation of n from ε_u', the nominal ultimate strain, also called the uniform elongation:

$$n = \log_e(1 + \varepsilon_u')$$

Table 1 contains the ductile bursting data for the MACH 10 components. All safety factors (ratio) exceed 1.0, with the storage vessels having the lowest values (1.6).

6.2 RESULTS FOR MANIFOLDS

The results for the high pressure manifold indicate a fatigue life of 1,350 cycles based upon a peak stress condition at the intersection of the radial and axial penetrations of the

TABLE 1

RESULTS OF DUCTILE BURSTING ANALYSIS - MACH 10

Component	Dwg. No.	σ_u	ε'_u	n	O.D.	I.D.	W	Design Pres	Burst Pres	Ratio
Storage Ves.-001	4-00673, Rev. 1	152,950	0.179	0.165	48	24	2	60,000	95,800	1.60
Storage Ves.-002	4-00673, Rev. 1	162,000	0.172	0.159	48	24	2	60,000	101,850	1.70
Storage Ves.-003	4-00673, Rev. 1	163,000	0.172	0.159	48	24	2	60,000	102,500	1.71
Inlet Manifold	4-01513, Rev. B	143,000	0.197	0.180	17	4	4.25	60,000	178,700	2.98
Exit Manifold	4-01514	142,000	0.203	0.185	17	4.5	3.78	60,000	153,700	2.73
Heater Ves.	B-PV-1409	140,000	0.20	0.182	37	28	1.32	15,000	35,200	2.35
Hous. Particle Sep.	77-D-1139	140,000	0.20	0.182	15.02	7.17	2.10	15,000	92,500	6.16
Separator Body	77-D-1124	140,000	0.20	0.182	13	5.5	2.36	15,000	107,000	7.14
Thermocouple Ring	77-D-1120	140,000	0.20	0.182	13	5.5	2.36	15,000	107,000	7.14

exit manifold body. These results indicate a fatigue life of 900 cycles for the maximum peak stress condition at the intersection of the radial and axial penetrations in the inlet manifold body.

6.3 RESULTS FOR MACH 10 HEATER VESSEL

6.3.1 PRIMARY STRESSES IN CYLINDER

The calculated primary stress intensities in the cylinder due to an internal pressure of 15,000 psi are listed and compared to the allowable stress values in Table 2. As shown in Table 2, the primary stresses satisfy the basic primary stress limits.

Table 2

PRIMARY PRESSURE STRESSES IN CYLINDER
COMPARED TO THE ALLOWABLE STRESSES FOR
MACH 10 HEATER VESSEL

Stress Category	Calculated Stress, psi	Allowable Stress, psi
P_m	53,128	S_m = 67,500
$P_m + P_b$	67,897	1.5 S_m = 101,200

Stresses in cylinder are due to an internal pressure of 15,000 psi.

6.3.2 FATIGUE EVALUATION OF THREADS

The fatigue design life calculated for the highest stressed point for the threads on the right end closure is 640 cycles.

The left end closure (nozzle end) had a fatigue design life of 1900 cycles based upon the peak stress which occurred in the buttress threads.

6.3.3 FRACTURE MECHANICS EVALUATION OF THREADS

A curve of cycles-to-failure versus initial defect size was calculated for the threads on the right end closure. The resulting curve is shown in Figure 86.

In Figure 86, the critical crack depth is 0.048 in., and K_{IC} = 100 ksi $\sqrt{in.}$ These results indicate that even small initial surface defects on the order of 10 mils deep will cause failure in about 400 cycles. Each cycle was assumed to have a pressure range of 15,000 psi.

A curve of cycles-to-failure vs. initial defect size for the nozzle end of Mach 10 Heater is shown in Figure 87. Figure 87 shows that a 10 mil initial defect will cause failure in about 2200 cycles.

6.4 RESULTS FOR MACH 14/18 HEATER VESSEL ORIGINAL DESIGN

6.4.1 PRIMARY STRESSES IN CYLINDER AND LINER

The calculated primary stress intensities in the cylinder and liner of the Mach 14/18 Heater Vessel due to an internal pressure of 46,000 psi, and a shrink fit of 0.017" on the radius between the liner and the cylinder are listed and compared to the allowable stress values in Tables 3 and 4. As shown in these tables, the primary stresses in both the liner and the cylinder exceed the basic primary stress limits.

Table 3

MACH 14/18 HEATER VESSEL LINER STRESSES
COMPARED TO THE ALLOWABLE STRESSES

Stress Category	Calculated Stress, psi	Allowable Stress, psi
P_m	95,568	S_m = 80,000
$P_m + P_b$	121,560	1.5 S_m = 120,000

Stresses in liner are due to internal pressure of 46,000 psi and shrink fit of 0.017" on radius.

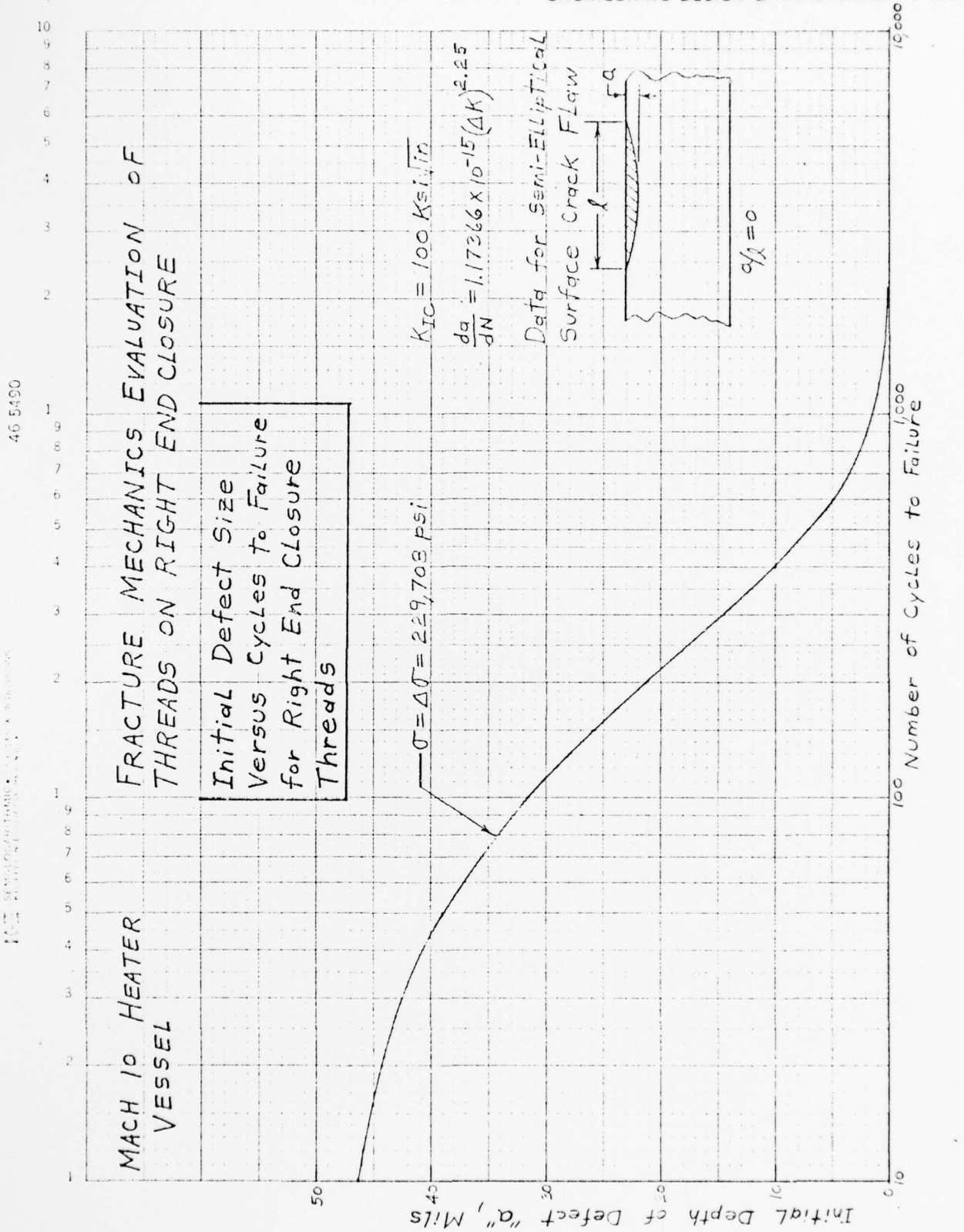

FIGURE 86 - INITIAL DEFECT SIZE VERSUS CYCLES TO FAILURE FOR RIGHT END CLOSURE THREADS

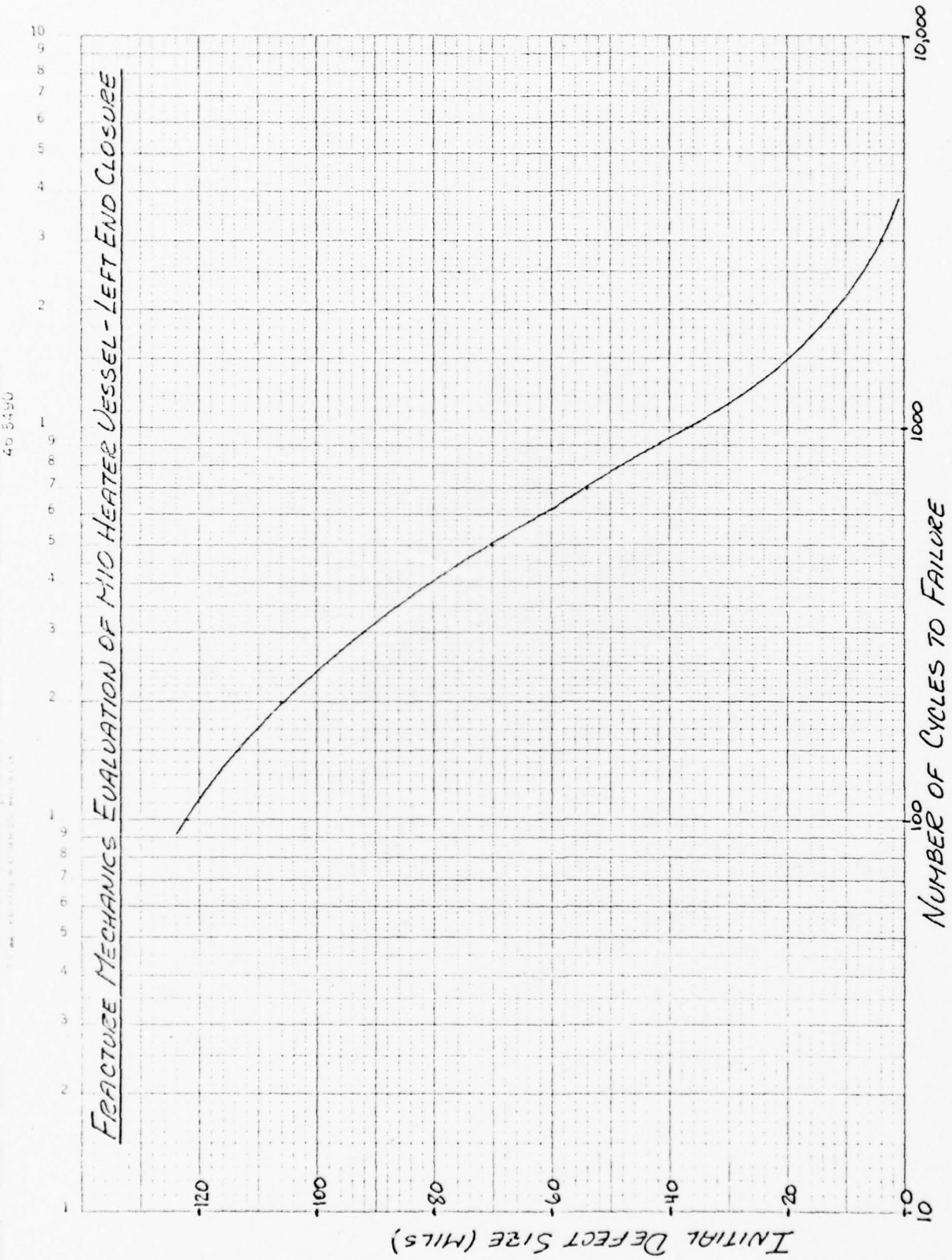

FIGURE 87 FRACTURE MECHANICS EVALUATION OF MACH 10 HEATER VESSEL - LEFT END CLOSURE

Table 4

MACH 14/18 HEATER VESSEL CYLINDER BODY STRESSES
COMPARED TO THE ALLOWABLE STRESSES

Stress Category	Calculated Stress, psi	Allowable Stress, psi
P_m	82,886	S_m = 72,500
$P_m + P_b$	107,086	1.5 S_m = 108,750

Stresses in cylinder body are due to internal pressure of 46,000 psi and shrink fit of 0.017" on radius.

6.4.2 FATIGUE EVALUATION OF THREADS

The fatigue design lives calculated for the threads on the top and bottom ends of the MACH 14/18 Heater Vessel are listed in Table 5. As shown in Table 5, a fatigue design life of 70 cycles was obtained for the threads on the top end, and a fatigue design life of 136 cycles was obtained for the bottom end. These design lives were calculated assuming that in each pressure cycle, the pressure changes from zero to 46,000 psi and back to zero.

Table 5

FATIGUE DESIGN LIFE OF THREADS
ON MACH 14/18 HEATER VESSEL

Location	Stress Range, psi	Calculated Fatigue Design Life, cycles
Top End Inner Plug (1st Thread)	467,501	70
Top End P.V. Wall (1st Thread)	204,127	650
Bottom End P.V. Wall (2nd Thread) Original Design	378,338	136

6.4.3 FRACTURE MECHANICS EVALUATION OF THREADS

Curves of cycles to failure versus initial defect size were calculated for the threads on the top and bottom ends of the MACH 14/18 Heater Vessel.

The resulting curve for the bottom end is shown in Figure 88. In Figure 88, the critical crack depth is 0.01779 in., and K_{IC} = 100 ksi $\sqrt{in}$.

The resulting curve for the top end is shown in Figure 89. In Figure 89, the critical crack depth is .0116 in., and K_{IC} = 100 ksi $\sqrt{in}$.

6.5 RESULTS FOR DRIVER VESSEL ORIGINAL DESIGN

6.5.1 PRIMARY STRESSES IN CYLINDER AND LINER

The calculated primary stress intensities in the cylinder and liner of the Driver Vessel due to an internal pressure of 60,000 psi and a shrink fit of 0.021" on the radius between the liner and the cylinder are listed and compared to the allowable stress values in Tables 6 and 7. As shown in these tables, the primary stresses in both the liner and the cylinder exceed the basic primary stress limits.

Table 6

LINER STRESSES COMPARED
TO THE ALLOWABLE STRESSES

Stress Category	Calculated Stress, psi	Allowable Stress, psi
P_m	94,677	S_m = 80,000
$P_m + P_b$	132,750	1.5 S_m = 120,000

Stresses in liner are due to internal pressure of 60,000 psi and shrink fit of 0.021" on radius.

FIGURE 88

Fracture Mechanics Evaluation of Threads on Bottom End Closure of MACH 14/18 Heater Vessel

$K_{IC} = 100\ Ksi\sqrt{in}$

$\frac{da}{dN} = 1.17366 \times 10^{-15} (\Delta K)^{2.25}$

Data for Semi-Elliptical Crack Flaw with $a/l \cong 0$

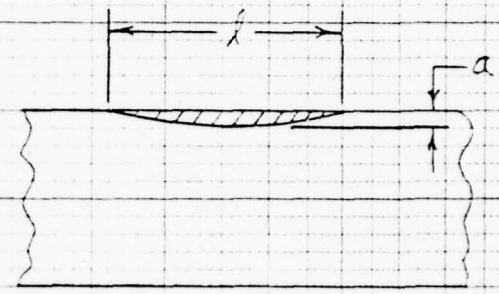

$\sigma = \Delta\sigma = 378,338$ psi

120

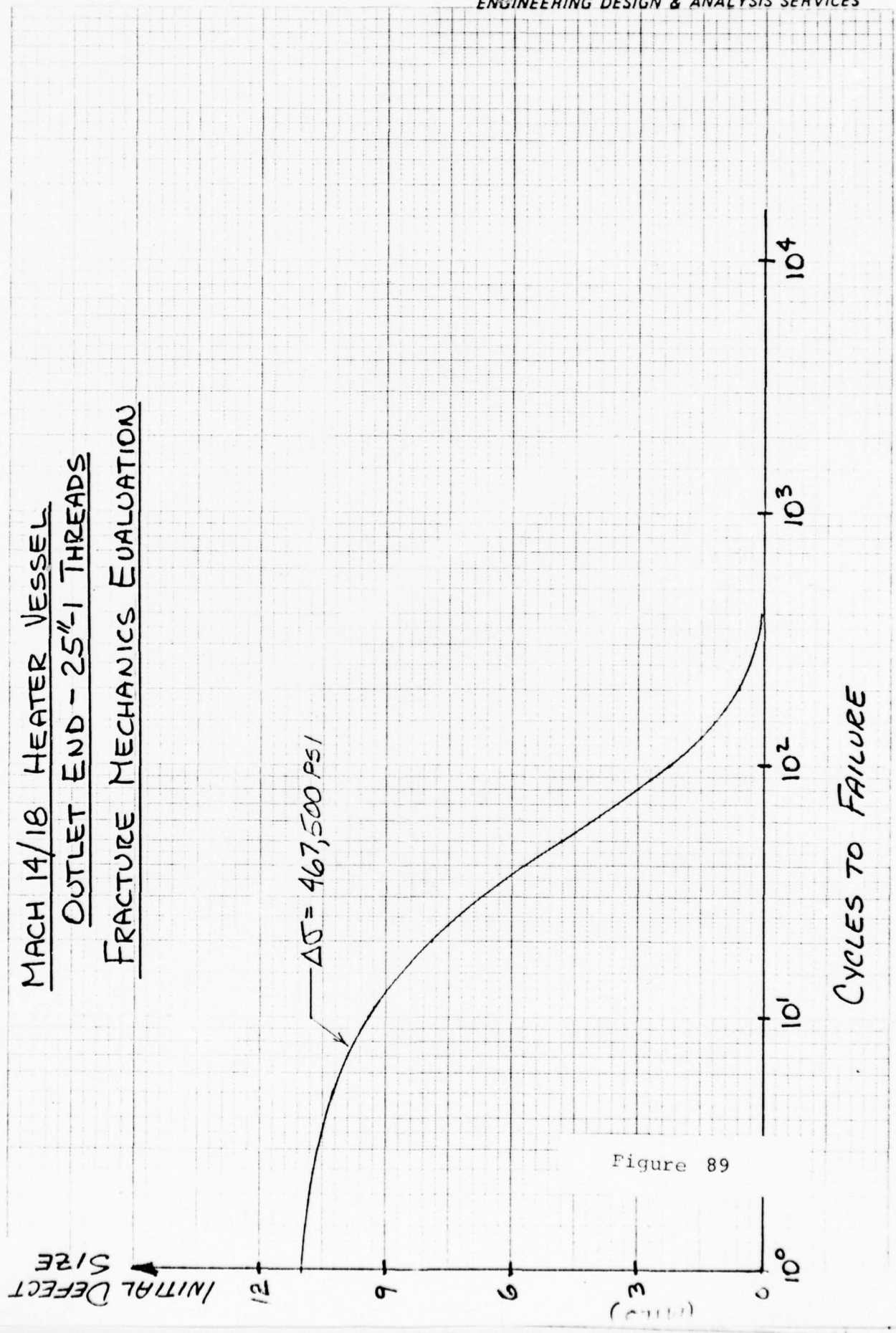
MACH 14/18 HEATER VESSEL
OUTLET END - 25"-1 THREADS
FRACTURE MECHANICS EVALUATION
ΔS = 467,500 PSI
INITIAL DEFECT SIZE
12
9
6
3
0
10⁰
10¹
10²
10³
10⁴
CYCLES TO FAILURE

Figure 89

Table 7

CYLINDER BODY STRESSES COMPARED
TO THE ALLOWABLE STRESSES

Stress Category	Calculated Stress, psi	Allowable Stress, psi
P_m	73,604	S_m = 72,500
$P_m + P_b$	100,363	1.5 S_m = 108,700

Stresses in cylinder body are due to internal pressure of 60,000 psi and shrink fit of 0.021" on radius.

6.5.2 FATIGUE EVALUATION OF THREADS

The fatigue design lives calculated for the threads on the outlet and inlet ends of the driver vessel are listed in Table 8. As shown in Table 8, a fatigue design life of 680 cycles was obtained for the threads on the outlet end, and a fatigue design life of 133 cycles was obtained for the inlet end. These design lives were calculated assuming that in each pressure cycle, the pressure changes from zero to 60,000 psi and back to zero.

Table 8

FATIGUE LIFE OF THREADS IN
DRIVER VESSEL

Location	Stress Range, psi	Calculated Fatigue Design Life, cycles
Outlet End (2nd Thread)	215,192	680
Inlet End (2nd Thread)	380,900	133

Table 9

FATIGUE LIFE OF THREADS ON
UNMODIFIED DRIVER VESSEL FOR
PRESSURE OF 60,000 psi

Location	Stress Range, psi	Fatigue Design Life
Outlet End (No Friction)	215,192	680 Cycles
Outlet End With Friction	238,968	532 Cycles
Inlet End (No Friction)	380,900	133 Cycles
Inlet End With Friction	423,060	100 Cycles

Table 10

FATIGUE LIFE OF THREADS ON
UNMODIFIED DRIVER VESSEL FOR
PRESSURE OF 47,500 psi

Location	Stress Range, psi	Fatigue Design Life
Outlet End (No Friction)	170,360	1,000 Cycles
Outlet End With Friction	189,183	856 Cycles
Inlet End (No Friction)	301,546	270 Cycles
Inlet End With Friction	334,923	195 Cycles

The effect of friction between threads was also investigated. The fatigue design life results for a coefficient of friction equal to Tan (7°), (0.122785), are listed with the results for no friction for pressures of 60,000 psi and 47,500 psi in Tables 9 and 10. These results indicate that friction has a deleterious effect on the fatigue design life of the threads.

A curve of remaining fatigue design life versus applied internal pressure was calculated and plotted for the existing outlet end driver vessel design using a coefficient of friction of 0.122785 (Tan 7°) between the threads. The resulting curve is shown in Figure 90.

6.5.3 FRACTURE MECHANICS EVALUATION OF THREADS

Curves to cycles to failure versus initial defect size were calculated for the threads on the outlet and inlet ends of the driver vessel.

The resulting curve for the outlet end is shown in Figure 91. In Figure 91, the critical crack depth is 0.05499 in., and K_{IC} = 100 ksi $\sqrt{in}$.

The resulting curve for the inlet end is shown in Figure 92. In Figure 92, the critical crack depth is 0.01755 in., and K_{IC} = 100 $\sqrt{in}$.

These results indicate that initial surface defects on the order of 10 mils deep will cause failure in about 500 cycles for the outlet end threads and in about 48 cycles for the inlet end threads. This assumes that the pressure range is 60,000 psi in each cycle.

A curve of cycles to failure versus initial defect size for the existing outlet end driver vessel design based on an internal pressure of 45,000 psi and using a coefficient of friction equal to 0.122785 (Tan 7°) is shown in Figure 93.

Figure 90

Fatigue Life Remaining for Driver Vessel Outlet End Versus Pressure - 2nd Thread With Friction

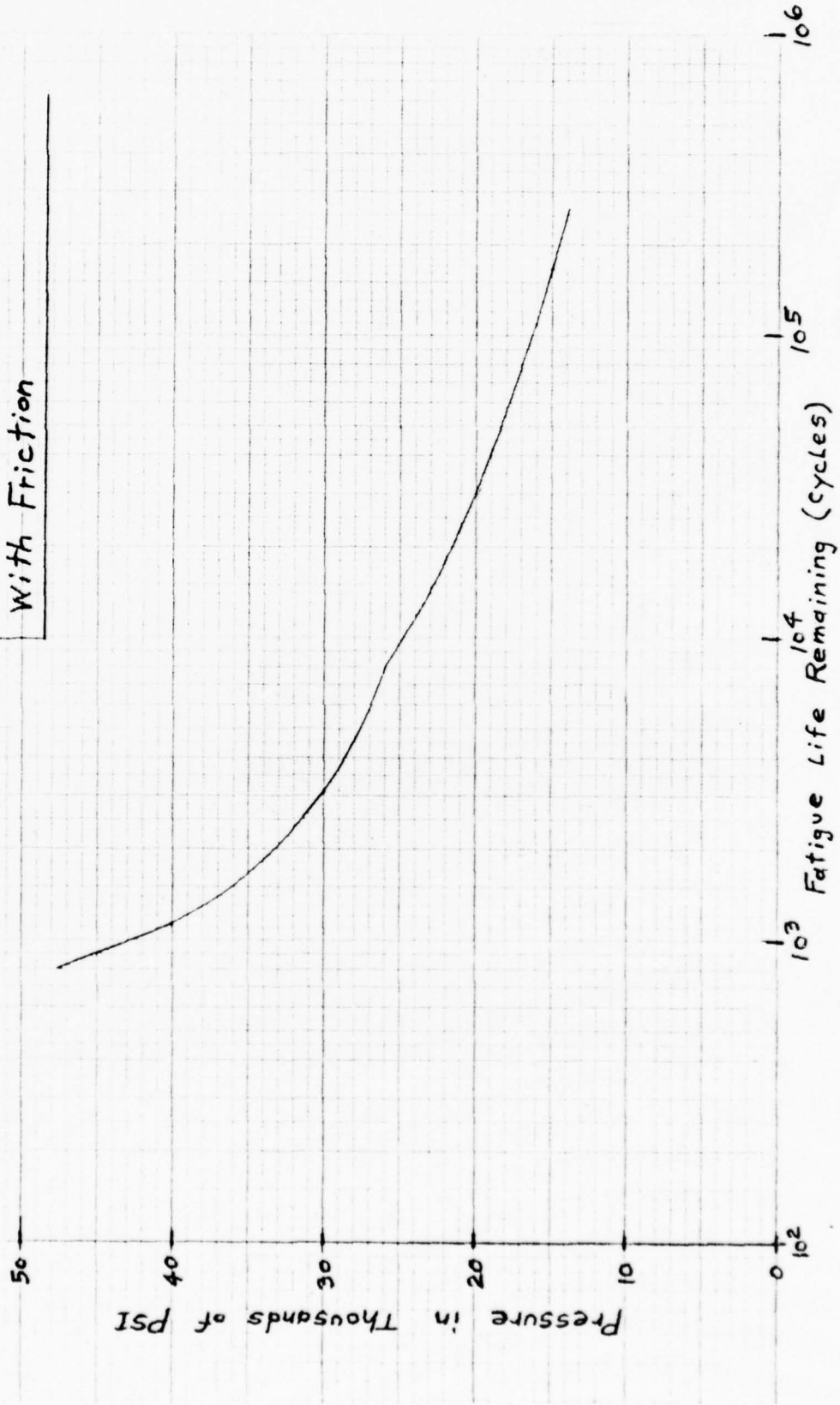

Figure 91 - FRACTURE MECHANICS EVALUATION OF THREADS ON OUTLET END OF Gas Storage Vessel For P = 60,000 psi with No Friction

Initial Defect Size Versus Cycles to Failure for Threads on Oulet End Closure of Gas Storage Vessel

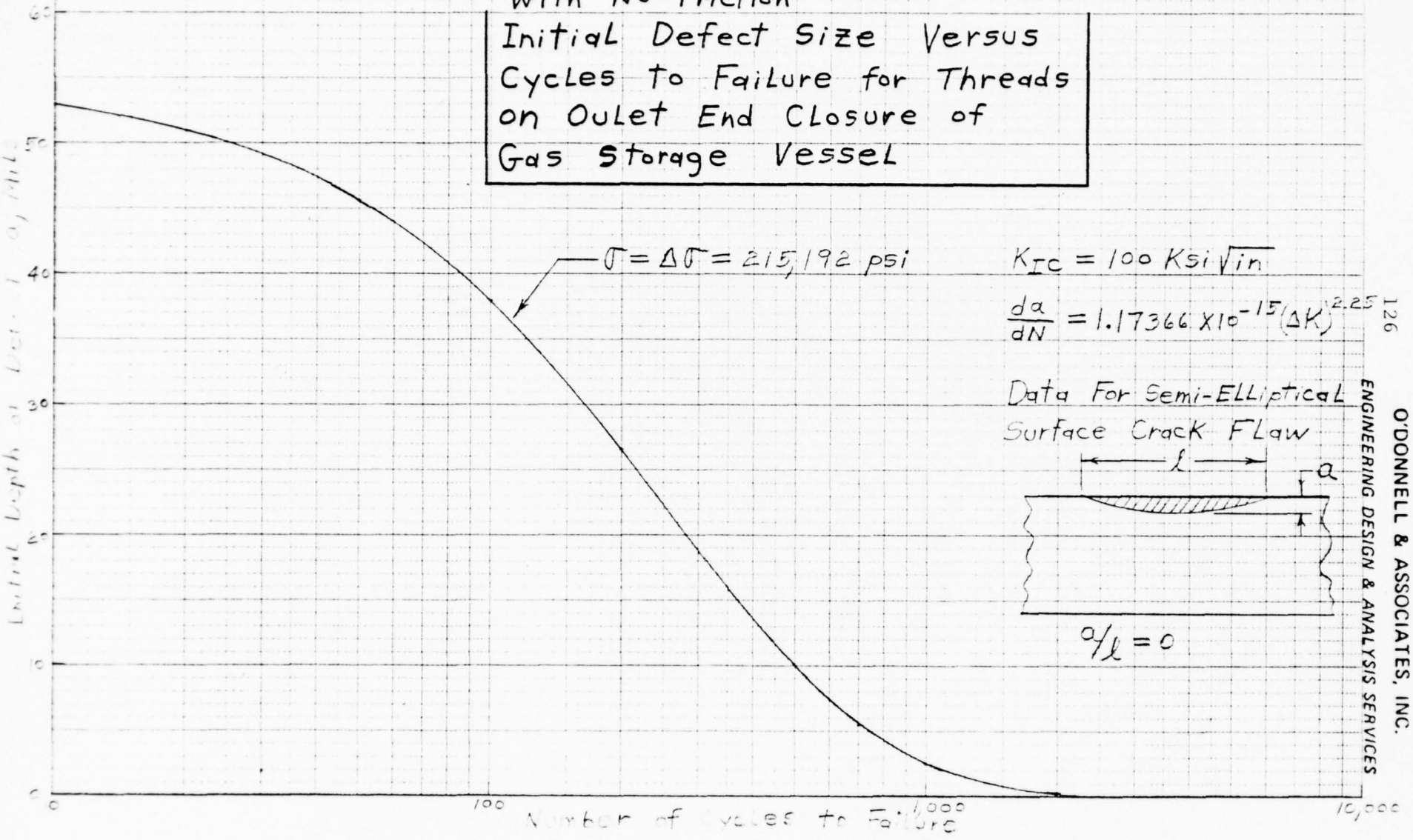

Figure 92 - FRACTURE MECHANICS EVALUATION OF THREADS ON INLET END OF GAS STORAGE VESSEL - original Design with No Friction

Initial Defect Size Versus Cycles to Failure for Threads on Inlet End Closure of Gas Storage Vessel - P = 60,000 psi

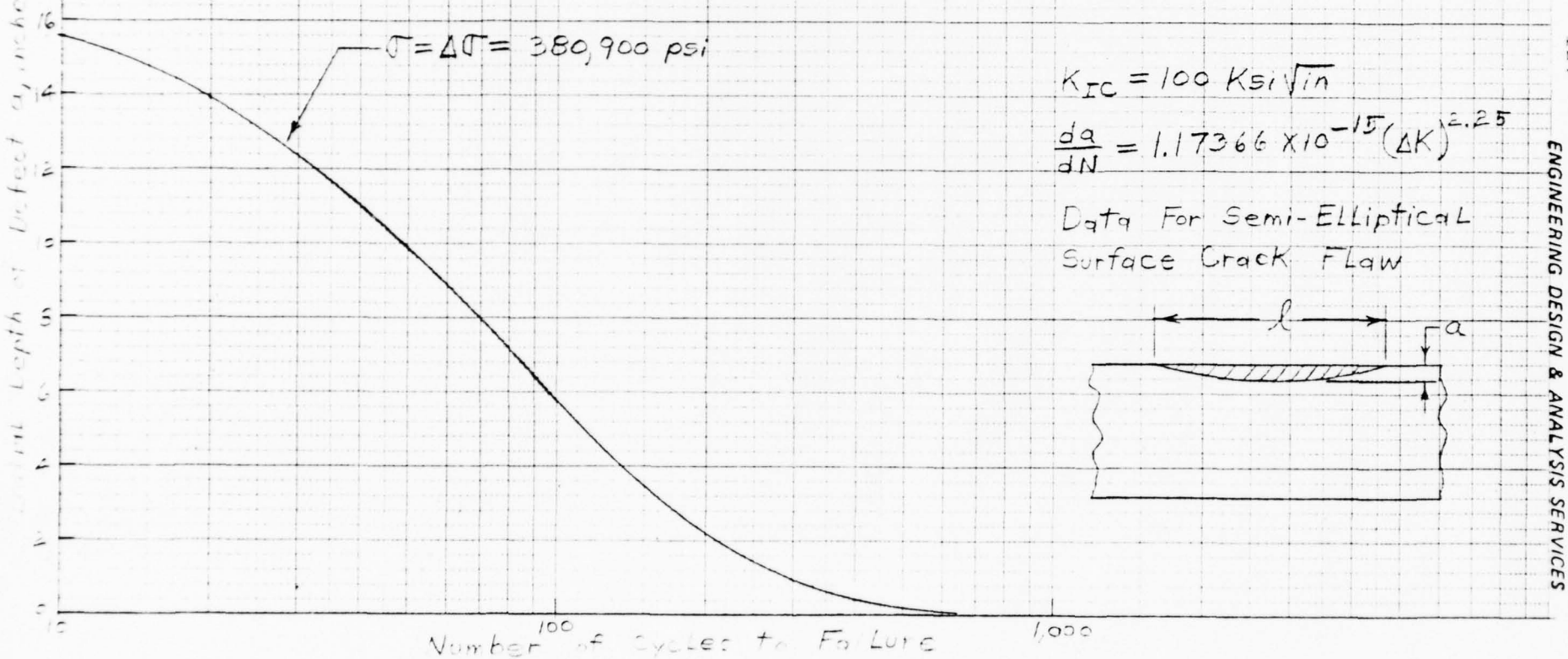

$K_{IC} = 100\ Ksi\sqrt{in}$

$\frac{da}{dN} = 1.17366 \times 10^{-15} (\Delta K)^{2.25}$

Data For Semi-Elliptical Surface Crack Flaw

Figure 93 - FRACTURE MECHANICS EVALUATION OF DRIVER VESSEL OUTLET END

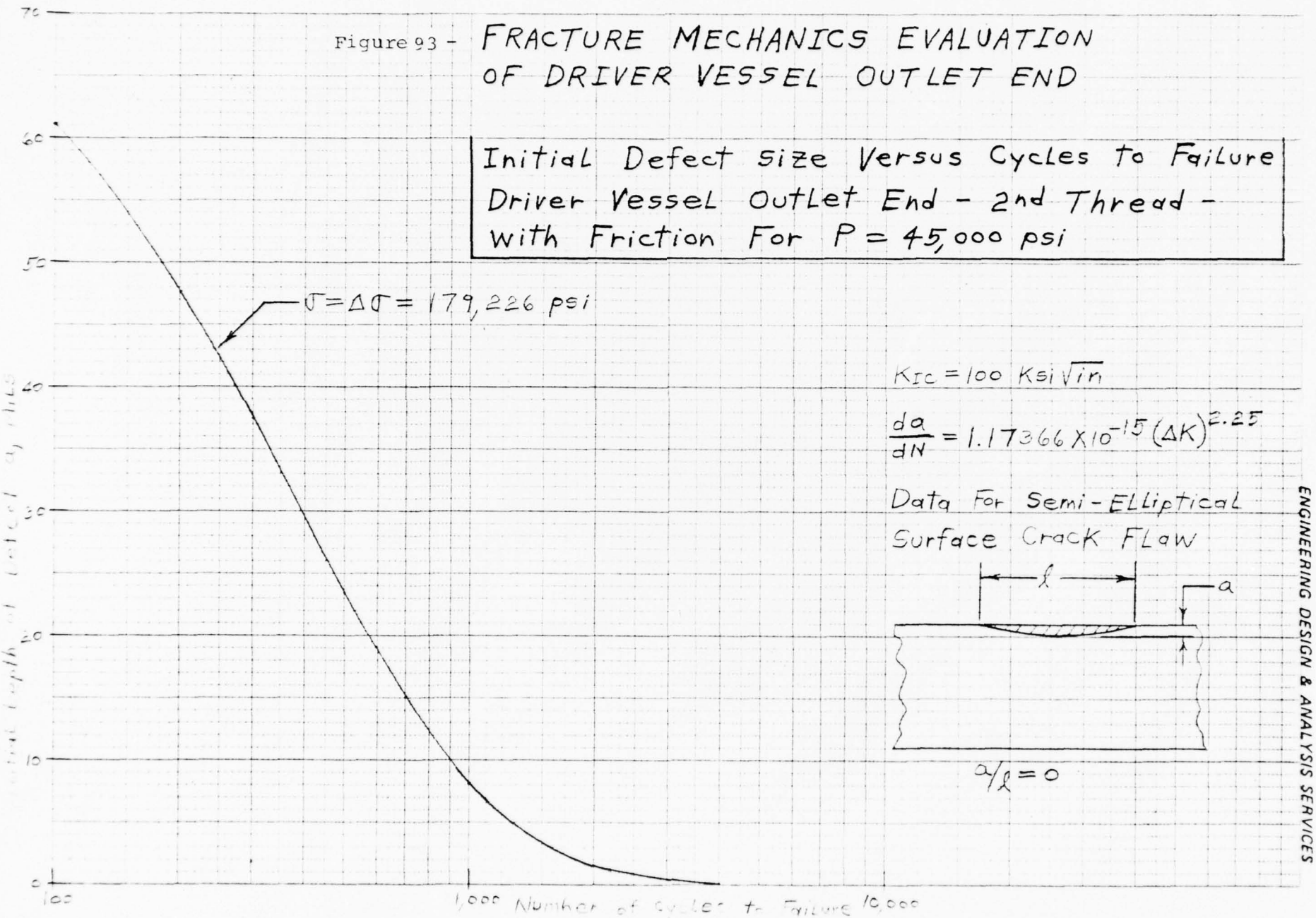

6.6 RESULTS FOR BOTTOM END DESIGN MODIFICATIONS ON MACH 14/18 HEATER VESSEL

Two different design modifications to the bottom end of the MACH 14/18 Heater Vessel were evaluated. The dimensional details of the design modifications, which employed two different undercut configurations on the inside end of the main nut on the bottom end closure, are shown in Figures 59 and 60. In this evaluation, the remaining fatigue design life for each design modification was calculated. This was accomplished by calculating the current usage factor for the critical thread for each design modification. Then, a usage factor of 1.0 minus the current usage factor multiplied by the fatigue design life of the design modification being considered determines the remaining design life for each particular design modification. The current usage factor for each thread was determined from a curve supplied by the Naval Surface Weapons Center.

In the initial evaluation of these design modifications, the same calculation techniques that were used in the original analyses were employed. Fatigue design life predictions were made for the unmodified design and for the two design modifications using the same detailed finite element thread model with geometry typical of the second and subsequent threads. Thus, the elliptical undercut for the first thread was not taken into account in the initial evaluation of these design modifications.

The results obtained from this initial evaluation are shown in Tables 11 through 14. The thread load and maximum stress range for selected threads for each particular design are shown in Tables 11 through 13. The resulting fatigue design life remaining on the MACH 14/18 Heater Vessel Bottom End for each design modification is summarized in Table 14.

Since the results shown in Table 14 indicate that there is no fatigue life remaining in any of these designs due to the high stresses in the first thread, the original design

Table 11

M 14/18 HEATER VESSEL BOTTOM END
ORIGINAL DESIGN - P = 46,000 psi

Thread No.	Thread Load (lbs/Radian)	Stress Range (psi)
1	356,468.	765,532.
2	352,199.	378,338.
4	265,715.	281,467.
7	200,350.	202,242.
10	154,211.	144,921.

Table 12

M 14/18 HEATER VESSEL BOTTOM END
Rev. 1 Design - P = 46,000 psi

Thread No.	Thread Load (lbs/Radian)	Stress Range (psi)
1	61,208.4	568,608.
7	270,307.	312,939.

Table 13

M 14/18 HEATER VESSEL BOTTOM END
Rev. 2 Design - P = 46,000 psi

Thread No.	Thread Load (lbs/Radian)	Stress Range (psi)
1	0	487,929.
4	115,753.2	300,948.
10	270,066.	311,326.

Table 14

SUMMARY OF FATIGUE LIFE REMAINING ON MODIFIED
M 14/18 HEATER VESSEL BOTTOM END BASED ON P = 28,000 psi
(ELLIPTICAL UNDERCUT NOT TAKEN INTO ACCOUNT)

Design	L1 (inches)	L2 (inches)	D1 (inches)	D2 (inches)	Critical Thread No.	Life Remaining No Friction
Original	0	0	-	-	1	0 *
Rev. 1*	3 1/2	1/2	27 1/2	29	1	0 *
Rev. 2*	4	3	27 1/2	29	1	0 *

* R1 = 3/8"
* Elliptical Undercut Not Taken Into Account.

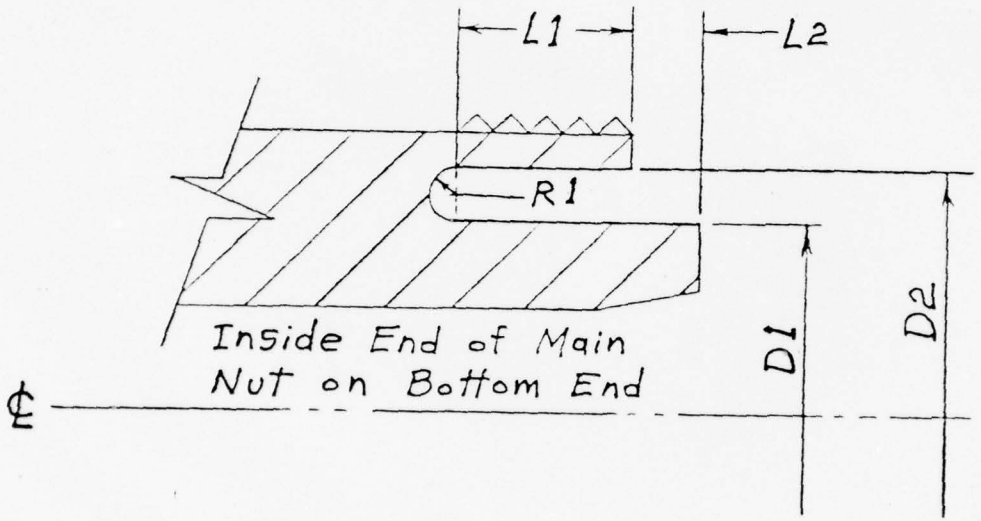

and the Rev. 2 design modification were re-evaluated using a detailed finite element model of the first thread which accounts for the elliptical undercut. The detailed thread model described in Section 5.2.2, which includes the elliptical undercut on the first thread, was used to calculate the maximum stresses in the first thread. The same detailed thread model, which has geometry typical of the second and subsequent threads, was used to calculate the maximum stresses in the threads other than the first thread.

The results obtained from this evaluation procedure are shown in Table 15 through 17. The thread loads and maximum stress ranges for the original design and the Rev. 2 design modification are shown in Tables 15 and 16. The resulting fatigue design life remaining on the MACH 14/18 Heater Vessel Bottom End for these two designs is summarized in Table 17. Comparing these results with those given in Tables 11, 13, and 14 indicates that the maximum calculated stress in the first thread is significantly reduced when the elliptical undercut on the first thread is taken into account. When the effect of the elliptical undercut is included in the stress calculations, the critical stress no longer occurs in the first thread but shifts to the second and fourth threads as shown in Tables 15, 16, and 17.

The effect of friction between threads was evaluated for the Rev. 2 design modification and also for the original design. The effect of friction on these two designs, based on a coefficient of friction of 0.122785 (Tan 7°) is shown in Table 17. As shown in Table 17, this evaluation was based on a pressure of 28,000 psi.

The average bearing stress across the lower face of the Rev. 2 Bottom End Nut design must be less than the yield strength of the nut material. To meet this bearing stress limit, the maximum operating pressure must be reduced to 28,000 psi. For an internal pressure of 28,000 psi, the total pressure load

Table 15

M 14/18 HEATER VESSEL BOTTOM END
Original Design - P = 46,000 psi

Thread No.	Load (lbs/Radian)	Stress Range (psi)
1	356,468.	308,628.*
2	352,199.	378,338.
4	265,715.	281,467.
7	200,350.	202,242.
10	154,211.	144,921.

*Maximum Surface Stress Intensity From Model With Elliptical Undercut

Table 16

M 14/18 HEATER VESSEL BOTTOM END
Rev. 2 Design - P = 46,000 psi

Thread No.	Load (lbs/Radian)	Stress Range (psi)
1	0	119,547.*
2	0	168,191.
4	115,753.2	300,948.
10	270,066.	311,326.

*Maximum Surface Stress Intensity From Model With Elliptical Undercut

Table 17

SUMMARY OF FATIGUE LIFE REMAINING ON MODIFIED
M 14/18 HEATER VESSEL BOTTOM END BASED ON P = 28,000 psi

Design	L1 (inches)	L2 (inches)	D1 (inches)	D2 (inches)	Critical Thread No.	Life Remaining No Friction	Life Remaining With Friction
Original	0	0	-	-	2	422 Cycles	303 Cycles
Rev. 2*	4	3	27 1/2	29	4	775 Cycles	721 Cycles

* R1 = 3/8" Note: With Friction, A Coefficient of Friction, f, of f = 0.12278 was used.

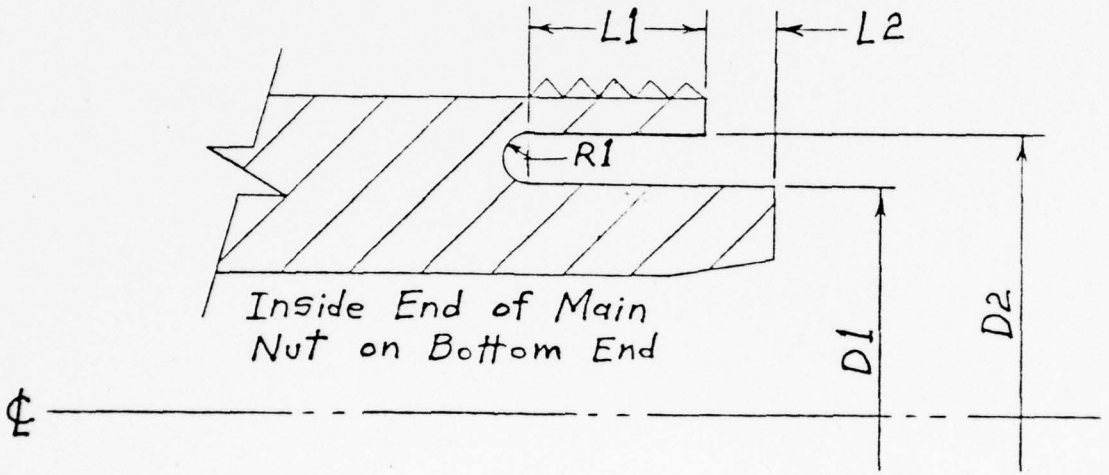

on the lower face of the nut is:

$$F = \frac{\pi}{4}(24)^2(28{,}000) = 12{,}666{,}901.58 \text{ lbs}$$

Therefore, the bearing stress is:

$$\sigma_{bearing} = \frac{12{,}666{,}901.58}{\pi[(13.75)^2 - (12.57)^2]} = 129{,}823. \text{ psi}$$

This is slightly less than the yield strength, S_y:

$$S_y = 130{,}000 \text{ psi}$$

Thus, the maximum operating pressure must be limited to 28,000 psi, to satisfy this bearing stress limit.

Utilizing the modified design stress intensity limits of Section 3.2, the linearized membrane and membrane plus bending stress intensities for Section A-A in Figure 60 for internal pressures of 28,000 psi and 22,000 psi are

PRESSURE

28,000 psi	22,000 psi
P_L = 88,605 psi	69,618 psi < 1.5 S_m^* = 116,250
$P_L + P_b$ = 167,073 psi	131,272 psi > 1.5 S_m

$$*S_m = \frac{UTS}{2} = 77{,}500 \text{ psi}$$

At 22,000 psi internal pressure the combined stresses are always compressive, less than ultimate and about equal to the yield stress. Furthermore, the bending stresses are of a secondary classification. It is concluded that the design is satisfactory for internal pressure not exceeding 22,000 psi.

A fracture mechanics evaluation of the Rev. 2 Bottom End design was performed for the reduced operating pressure of 28,000 psi. The resulting curve of cycles to failure versus initial defect size for this design is shown in Figure 94. The

Figure 94

FRACTURE MECHANICS EVALUATION OF MACH 14/18 HEATER VESSEL BOTTOM END

Initial Defect Size Versus Cycles to Failure For Bottom End - 4th Thread - REV. 2 DESIGN With Friction For P = 28,000 psi

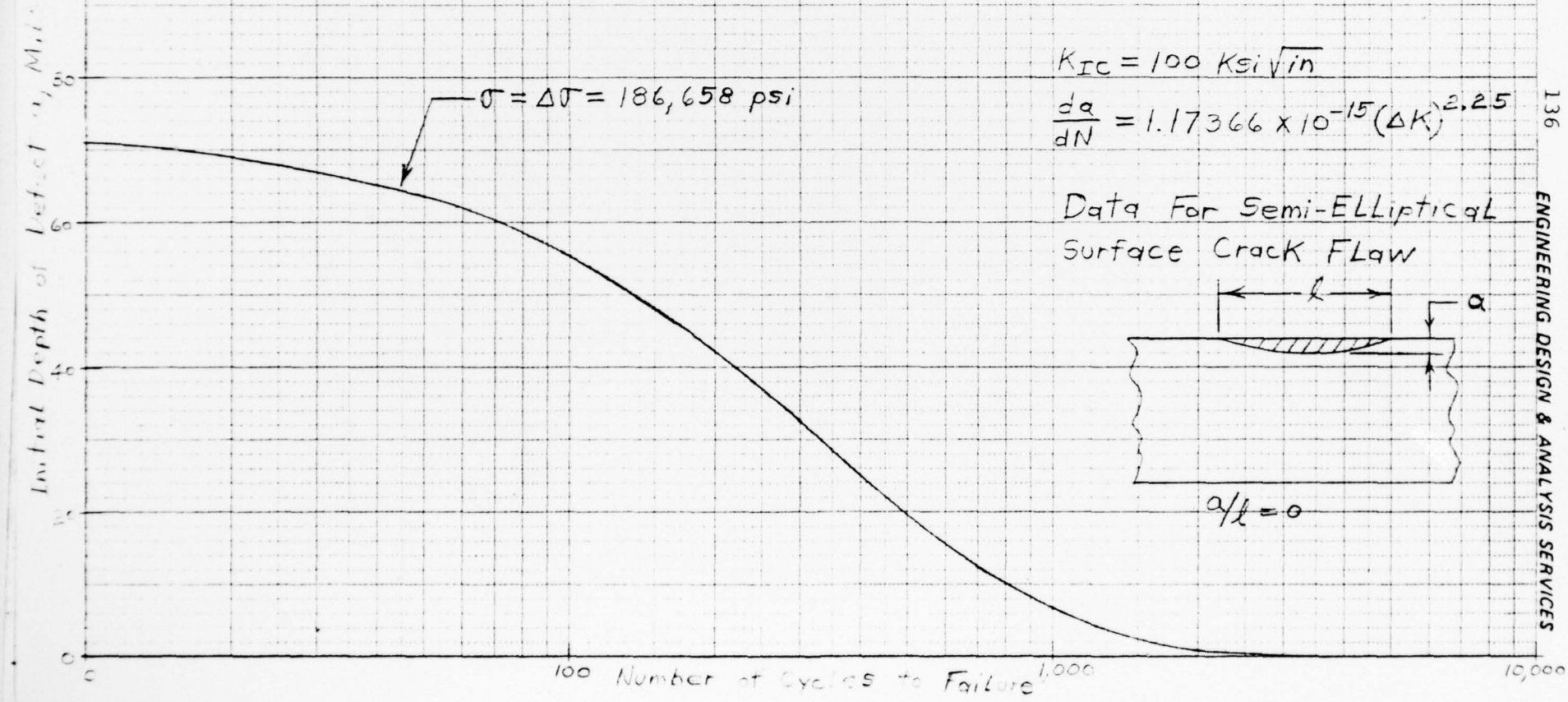

effect of friction using a coefficient of friction equal to 0.122785 (Tan 7°) is included in this curve.

A curve of remaining fatigue design life versus applied internal pressure was calculated and plotted for the Rev. 2 Bottom End design using a coefficient of friction of 0.122785 (Tan 7°) between the threads. The resulting curve is shown in Figure 95.

The detailed calculations and results for the MACH 14/18 Heater Vessel Bottom End design modifications including the resulting thread load distributions for each design are given in Appendix 6A.

6.7 RESULTS FOR INLET END DESIGN MODIFICATIONS ON DRIVER VESSEL

Four different inlet end design modifications, which utilize various undercut configurations on the inside end of the main nut on the inlet end, were evaluated. In this evaluation, the remaining fatigue design life for each design modification was calculated. This was accomplished by calculating the current usage factor for the critical thread for each design modification. Then, a usage factor of 1.0 minus the current usage factor multiplied by the fatigue design life of the design modification being considered determines the remaining design life for each particular design modification. The current usage factor for each thread was determined from a curve supplied by the Naval Surface Weapons Center.

The resulting fatigue design life remaining on the driver vessel inlet end for each design modification is summarized in Table 18. The dimensional details of each design modification are also shown in Table 18. The results given in Table 18 indicate that the Rev. 4 design modification produces the largest increase in the remaining fatigue design life on the driver vessel inlet end. The effect of friction between threads was evaluated for this Rev. 4 design modification and

Figure 95

Fatigue Life Remaining For M 14/18 Heater Vessel Bottom End Versus Pressure - 4th Thread - REV. 2 Design With Friction

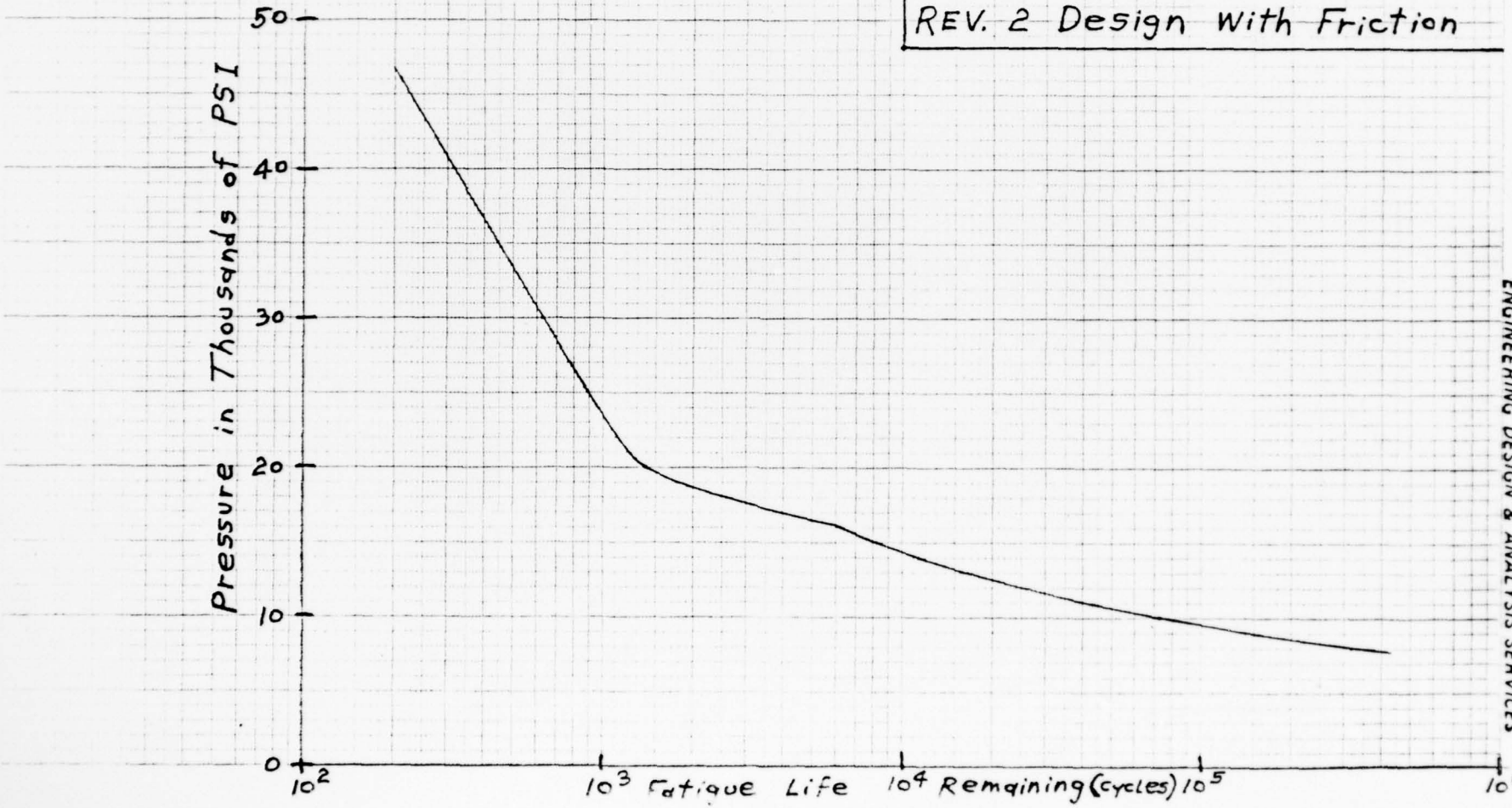

Table 18

Summary of Fatigue Life Remaining on Modified Driver Vessel Inlet End Based on P = 47,500 psi

DESIGN	L1 (inches)	L2 (inches)	D1 (inches)	D2 (inches)	Critical Thread No.	Life Remaining No Friction	Life Remaining with Friction
Original	0	0	—	—	2	222 cycles	152 cycles
REV. 1 *	4	1/2	32	35 1/4	7	423 cycles	—
REV. 2 *	5	1/2	32	35 1/4	8	447 cycles	—
REV. 3 *	5	1/2	32	33 1/2	8	495 cycles	—
REV. 4 *	4	1/2	31 1/2	33	8	515 cycles	389 cycles

* R1 = 3/8"

Note: With Friction, A coefficient of Friction, f, of f = 0.12278 was Used.

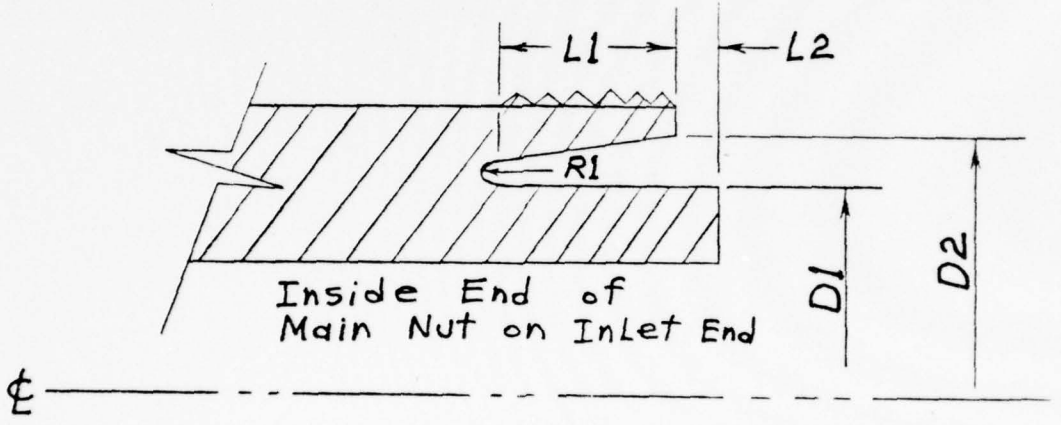

also for the original design. The effect of friction on these two designs, based on a coefficient of friction of 0.122785 (Tan 7°), is shown in Table 18. As shown in Table 18, this evaluation was based on a pressure of 47,500 psi.

For an internal pressure of 60,000 psi, the average bearing stress across the lower face of the Rev. 4 Inlet End nut design exceeds yield. For an internal pressure of 60,000 psi, the total pressure load on this surface is 27,143,360.53 lbs. Therefore, the bearing stress is:

$$\sigma_{bearing} = \frac{27,143,360.53}{\pi(15.75^2 - 14.25^2)} = 192,000 \text{ psi} > S_{Y_{ACT}}$$

where: $S_{Y_{ACT}}$ = 141,570 psi

$S_{Y_{ACT}}$ = Actual Yield Strength of the Nut Material

To meet the bearing stress limit, the maximum operating pressure must be reduced to the following:

$$(P_{design})_{new} = \frac{141,570}{192,000}(60,000) = 44,240.6 \text{ psi}$$

This is almost 45,000 psi. Therefore, the fracture mechanics evaluations of the Rev. 4 Inlet End design was based on an internal pressure of 45,000 psi.

The resulting curve of cycles to failure versus initial defect size for this design is shown in Figure 96. The effect of friction using a coefficient of friction equal to 0.122785 (Tan 7°) is included in this curve.

A curve of remaining fatigue design life versus applied internal pressure was calculated and plotted for the Rev. 4 Inlet End design using a coefficient of friction of 0.122785 (Tan 7°) between the threads. The resulting curve is shown in Figure 97.

The detailed calculations and results for the inlet end design modifications including the resulting thread load distributions for each design are given in Appendix 7A.

Figure 96- FRACTURE MECHANICS EVALUATION OF DRIVER VESSEL INLET END

Initial Defect Size Versus Cycles to Failure For Inlet End - 8th Thread - REV. 4 DESIGN with Friction For P = 45,000 psi

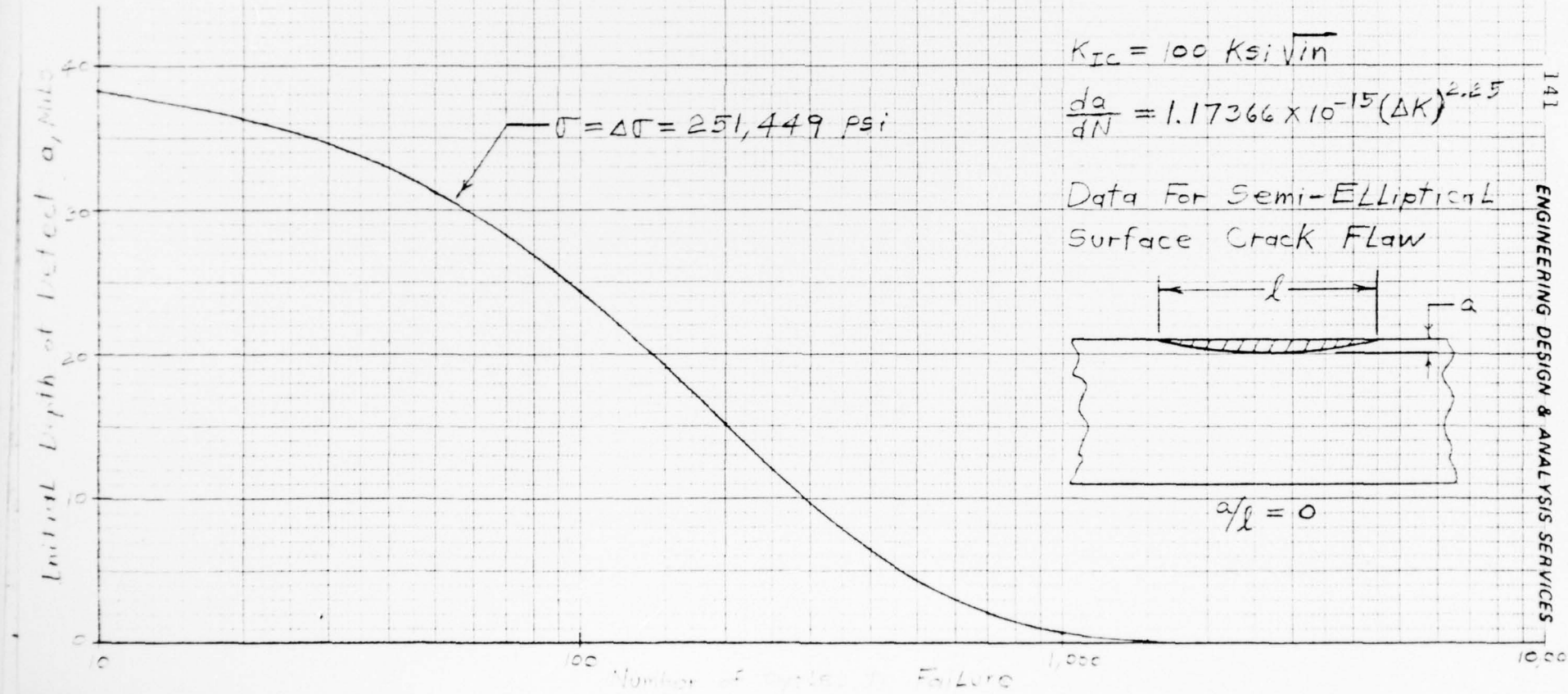

Figure 97

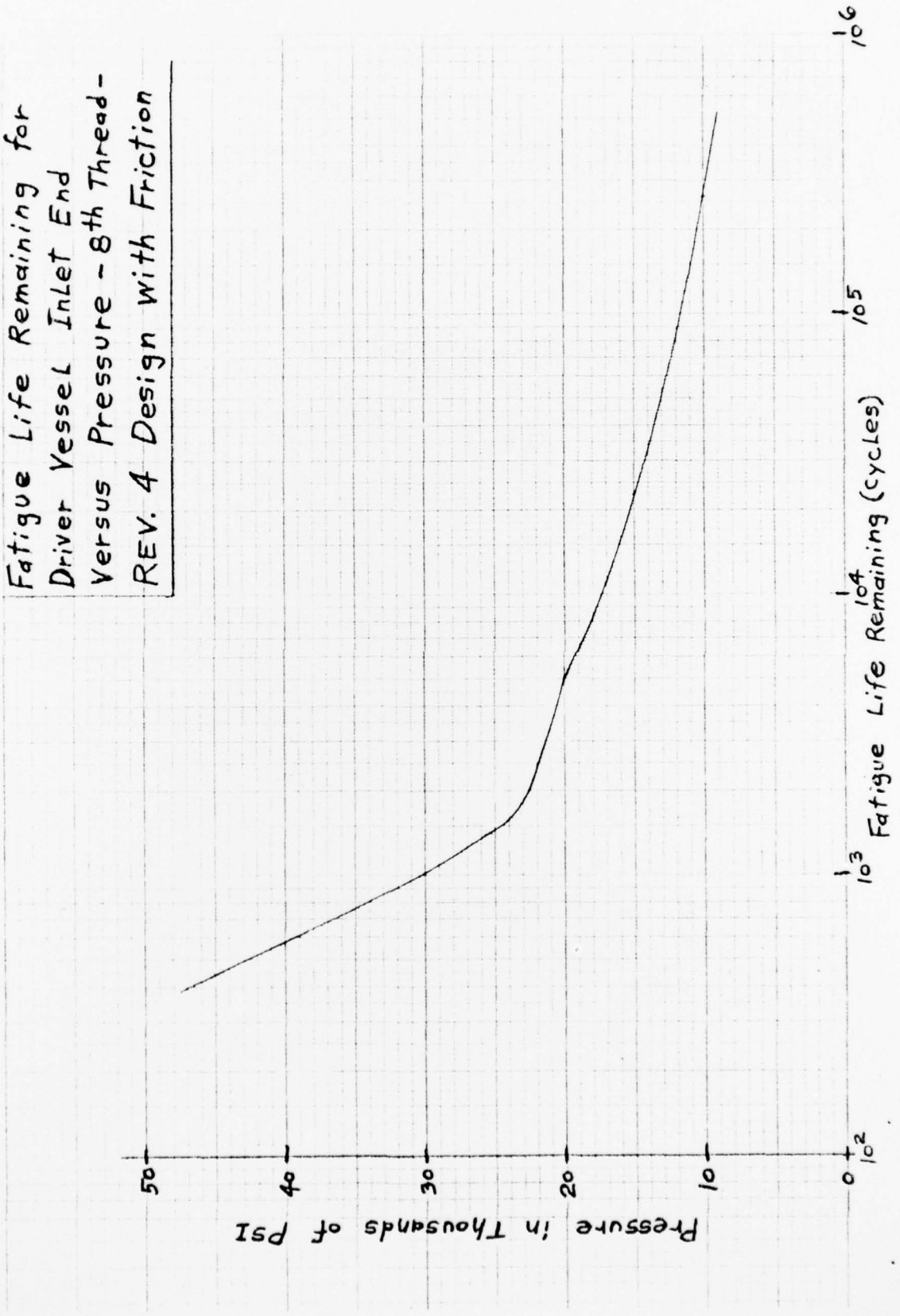
Fatigue Life Remaining for Driver Vessel Inlet End Versus Pressure - 8th Thread - REV. 4 Design with Friction
Pressure in Thousands of PSI
50
40
30
20
10
0
Fatigue Life Remaining (Cycles)
10^2
10^3
10^4
10^5
10^6

6.8 PERIODIC INSPECTION OF CRITICAL AREAS

It is recommended that critical areas of the driver and heater vessels be inspected periodically to increase confidence that no flaws near critical size are present. Based on the assumption that an initial flaw depth of 15 mils is present and that this defect is not found on the first inspection, it is recommended that inspection be performed when

$$\sum \frac{\Delta P_i^{n-0.5} P_{max,i}^{0.5}}{P_{ref}^{n}} = \frac{a_* - a_i}{C_o a_*^{n/2} M^{n/2}} \left(\frac{1}{\sigma_{ref}}\right)^n$$

Table 19 indicates what values are to be used in the above equation. Also shown are the number of full pressure cycles required to extend a 15 mil defect to the critical size. The detailed derivation of the above equation is given in Appendix 8A.

7.0 SUMMARY AND CONCLUSIONS

Based on the results given in Section 6.0 of this report, it is concluded that the threaded pressure vessels in the wind tunnel facility have limited fatigue life due to the high stress concentrations at the root of the thread root radii in the threaded end closures. Design modifications were made to the most critical end closures (Bottom End of MACH 14/18 Heater Vessel and Inlet End of Driver Vessel) which increased the design life of these pressure vessels. To further increase the design life of these threaded pressure vessels, the operating pressure was reduced to the maximum values listed below:

Pressure Vessel	Maximum Internal Operating Pressure, psi
Mach 10 Heater Vessel	12,000
Mach 14/18 Heater Vessel	22,000
Driver Vessel	40,000

Table 19

Vessel	$\frac{\sigma_{ref}}{P_{ref}}$	a_{cr}, in.	a_*, in.	$\Sigma \frac{\Delta P_i^{n-0.5} P_{max}^{0.5}}{P_{ref}^{n}}$	Full Pressure Cycles to Failure*
Driver (Inlet end) Rev. 4 Design	$\frac{223,510}{40,000}$	0.0510	0.0221	87	322
MACH 14/18 Heater (Bottom end) Rev. 2 Design	$\frac{146,660}{22,000}$	0.1184	0.0282	317	1337
MACH 10 Heater (right end)	$\frac{183,766}{12,000}$	0.0754	0.0248	164	646

$a_i = 0.015"$

$C_o = 1.1737(10^{-15})$

$M = 1.25\pi$

$n = 2.25$

*Based on 15 mil initial flaw depth

Using the results for the modified pressure vessel designs operated at the foregoing reduced operating pressures, periodic inspection requirements were established which account for variable pressure cycling and mean stress effects.

The combined effect of the design modifications, reduced operating pressures, and periodic inspection requirements is to increase the design life and confidence in the safety related structural integrity of the threaded pressure vessels in the wind tunnel facility.

8.0 REFERENCES

1. Rules for Construction of Pressure Vessels, Section VIII, Division 2 - Alternative Rules, ASME, 1977.

2. Rules for Construction of Nuclear Power Plant Components, Section III, Division 1, ASME, 1977.

3. Criteria of the ASME Boiler and Pressure Vessel Code for Design by Analysis in Sections III and VIII, Division 2, ASME, 1964.

4. Witkin, D. E. and Mraz, G. J., "Design Philosophy of Pressure Vessels for Service Above 10 ksi," ASME Paper No. 76-PVP-62.

5. "ANSYS - Engineering Analysis System - User's Manual," by J. A. Swanson, Swanson Analysis Systems, Inc., March 1, 1975.

6. J. MARIN, T. WENG, "Strength of Thick-Walled Cylinders Under Pressure for Three Steels," Welding Research Council Bulletin No. 67, 1961.

7. J. MARIN, T. WENG, "A Critical Evaluation of the Strength of Thick-Walled Cylindrical Pressure Vessels," Welding Research Council Bulletin No. 74, 1962.

8. B. F. LANGER, "Interpretive Report of Pressure Vessel Research, Section 1.3 - Bursting Strength," WAPD-T-1482, February 1972.